

AD-A216 016



# ANALYSIS AND DESIGN OF CONNECTIONS, OPENINGS AND ATTACHMENTS FOR PROTECTIVE CONSTRUCTION

T. Krauthammer  
M. A. DeSutter

University of Minnesota  
Department of Civil and Mineral Engineering  
Minneapolis, MN 55455-0220

October 1989

Final Report

Approved for public release; distribution unlimited.

WEAPONS LABORATORY  
Air Force Systems Command  
Kirtland Air Force Base, NM 87117-6008

DTIC  
ELECTE  
DEC 18 1989  
S 9B D

89 12 18 036

This final report was prepared by the Department of Civil and Mineral Engineering at the University of Minnesota, Minneapolis, under contract F29601-87-C-0080, Job Order 21041A36 with the Weapons Laboratory, Kirtland Air Force Base, New Mexico. Aaron Perea (NTESE) was the Laboratory Project Officer-in-Charge.

When Government drawings, specifications, or other data are used for any purpose other than in connection with a definitely Government-related procurement, the United States Government incurs no responsibility or any obligation whatsoever. The fact that the Government may have formulated or in any way supplied the said drawings, specifications, or other data, is not to be regarded by implication, or otherwise in any manner construed, as licensing the holder, or any other person or corporation; or as conveying any rights or permission to manufacture, use, or sell any patented invention that may in any way be related thereto.

This report has been authored by a contractor of the United States Government. Accordingly, the United States Government retains a nonexclusive, royalty-free license to publish or reproduce the material contained herein, or allow others to do so, for the United States Government purposes.

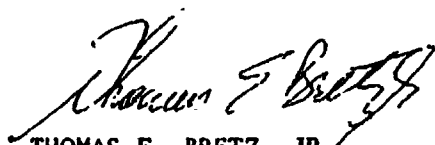
This report has been reviewed by the Public Affairs Office and is releasable to the National Technical Information Service (NTIS). At NTIS, it will be available to the general public, including foreign nationals.

If your address has changed, if you wish to be removed from our mailing list, or if your organization no longer employs the addressee, please notify AFWL/NTESE, Kirtland AFB, NM 87117-6C08 to help us maintain a current mailing list.

This report has been reviewed and is approved for publication.

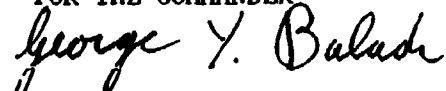


AARON PEREA  
Project Officer



THOMAS F. BRETZ, JR  
Lt Col, USAF  
Chief, Applications Branch

FOR THE COMMANDER



GEORGE Y. BALADI, PhD  
Technical Advisor  
Civil Engineering Research Division

DO NOT RETURN COPIES OF THIS REPORT UNLESS CONTRACTUAL OBLIGATIONS OR NOTICE ON A SPECIFIC DOCUMENT REQUIRES THAT IT BE RETURNED.

UNCLASSIFIED

SECURITY CLASSIFICATION OF THIS PAGE

REPORT DOCUMENTATION PAGE				Form Approved OMB No. 0704-0188	
1a. REPORT SECURITY CLASSIFICATION Unclassified			1b. RESTRICTIVE MARKINGS		
2a. SECURITY CLASSIFICATION AUTHORITY			3. DISTRIBUTION/AVAILABILITY OF REPORT Approved for public release, distribution unlimited.		
2b. DECLASSIFICATION/DOWNGRADING SCHEDULE					
4. PERFORMING ORGANIZATION REPORT NUMBER(S)			5. MONITORING ORGANIZATION REPORT NUMBER(S) WL-TR-89-44		
6a. NAME OF PERFORMING ORGANIZATION University of Minnesota		6b. OFFICE SYMBOL (if applicable)	7a. NAME OF MONITORING ORGANIZATION Weapons Laboratory		
6c. ADDRESS (City, State, and ZIP Code) Department of Civil and Mineral Engineering 500 Pillsbury Drive. SE, Bldg 122 Minneapolis, Minnesota 55455-0220			7b. ADDRESS (City, State, and ZIP Code) Kirtland Air Force Base, New Mexico 87117-6008		
8a. NAME OF FUNDING/SPONSORING ORGANIZATION		8b. OFFICE SYMBOL (if applicable)	9. PROCUREMENT INSTRUMENT IDENTIFICATION NUMBER F29601-87-C-0080		
8c. ADDRESS (City, State, and ZIP Code)			10. SOURCE OF FUNDING NUMBERS		
			PROGRAM ELEMENT NO. 63723F	PROJECT NO. 2104	TASK NO. 1A
11. TITLE (Include Security Classification)  ANALYSIS AND DESIGN OF CONNECTIONS, OPENINGS AND ATTACHMENTS FOR PROTECTIVE CONSTRUCTION					
12. PERSONAL AUTHOR(S) Theodor Krauthammer and Michael A. DeSutter					
13a. TYPE OF REPORT Final		13b. TIME COVERED FROM Sep 87 TO May 89		14. DATE OF REPORT (Year, Month, Day) 1989, October	
15. PAGE COUNT 170					
16. SUPPLEMENTARY NOTATION					
17. COSATI CODES			18. SUBJECT TERMS (Continue on reverse if necessary and identify by block number)		
FIELD	GROUP	SUB-GROUP	Joints, Attachments, Openings, Blast Loading, Connection, Protective Construction, 5/11/89		
13	05				
13	08				
19. ABSTRACT (Continue on reverse if necessary and identify by block number) This report covers the development of some design specifications for connections, openings and attachments in reinforced concrete protective structures that are expected to operate under the effects of modern conventional weapons. The research goals were to investigate the behavior of typical structural details for the above-mentioned items, and to formulate the behavior for implementation into design requirements. Included in the report is an extensive discussion of the known behavior, a complete description of the research, and the design recommendations derived from it. The research was conducted by simulating numerically the response of a wide spectrum of structural details subjected to a loading environment created by "standard" conventional weapons. The observed behavior, obtained from the results, is then evaluated for compliance with the requirements of strength and serviceability determined from the known behavior. The recommended design requirements for the structural systems under consideration are included. K. A. DeSutter					
20. DISTRIBUTION/AVAILABILITY OF ABSTRACT <input type="checkbox"/> UNCLASSIFIED/UNLIMITED <input type="checkbox"/> SAME AS RPT. <input checked="" type="checkbox"/> OTIC USERS			21. ABSTRACT SECURITY CLASSIFICATION Unclassified		
22a. NAME OF RESPONSIBLE INDIVIDUAL Mr Aaron Perea			22b. TELEPHONE (Include Area Code) (505) 846-6467		22c. OFFICE SYMBOL WL/NTESE

UNCLASSIFIED

SECURITY CLASSIFICATION OF THIS PAGE

UNCLASSIFIED

SECURITY CLASSIFICATION OF THIS PAGE

# ACKNOWLEDGEMENT

The investigation described herein was performed under contract for the Weapons Laboratory Civil Engineering Research Division (WL/NTE) under the sponsorship of the Air Force System Command (AFSC) through the Tri-Lab memorandum of understanding. This contract was technically monitored by Mr Aaron Perea under the direct supervision of Col Carl L. Davidson, Chief, Civil Engineering Research Division. The technical advisor to the division was Dr George Y. Baladi.

The study was conducted and the report written by Dr Theodor Krauthammer and Mr Michael A. DeSutter of the Department of Civil and Mineral Engineering, University of Minnesota. The report was reviewed by Capt Raymond Bennett, Dr Rodney Galloway, and Mr Doug Seemann of the Weapons Laboratory.

QUALITY  
INSPECTED  
2

Accession For	
NTIS GRA&I	<input checked="checked" type="checkbox"/>
DTIC TAB	<input type="checkbox"/>
Unannounced	<input type="checkbox"/>
Justification	
By	
Distribution/	
Availability Codes	
Dist	Avail and/or Special
A-1	

## CONTENTS

<u>Section</u>		<u>Page</u>
1.0	INTRODUCTION	1
	1.1 GENERAL	1
	1.2 OBJECTIVES OF THE STUDY	2
	1.3 SCOPE OF THE STUDY	3
2.0	BACKGROUND	4
	2.1 INTRODUCTION	4
	2.2 MATERIAL MODELS	4
	2.3 CONNECTION DETAILING	5
	2.3.1 Knee Joints	5
	2.3.2 Monolithic Tee Joints	17
	2.3.3 Precast Joints	21
	2.3.4 Openings and Attachments	22
	2.4 STRUCTURAL RESPONSE	24
	2.4.1 Flexural Behavior	24
	2.4.2 Shear Behavior	25
	2.4.2.1 Direct Shear	26
	2.4.2.2 Diagonal Shear	26
	2.4.2.3 Joint Shear	27
	2.4.3 Reinforcement Bond	31
	2.4.4 Ductility and Deflections	32
	2.5 DYNAMIC RATE EFFECTS	33
	2.6 THE FINITE ELEMENT METHOD	33
	2.7 SUMMARY	34
	2.7.1 Design Guidelines	35
	2.7.2 Strength and Serviceability Criteria	36
3.0	RESEARCH APPROACH	37
	3.1 METHODOLOGY	37
	3.2 FINITE ELEMENT APPROACH	37
	3.2.1 Code Reliability	37
	3.2.2 Geometry	39
	3.2.3 Element Compatibility	39

## CONTENTS (CONTINUED)

<u>Section</u>		<u>Page</u>
3.3	CONSTITUTIVE MODELS	41
3.3.1	Concrete Modeling	43
3.3.2	SIFCON Modeling	49
3.3.3	Steel Reinforcement Modeling	50
3.3.4	Conclusions	51
3.4	DYNAMIC RATE EFFECTS	51
3.5	LOADING FUNCTIONS	55
3.6	MODEL CALIBRATION	58
4.0	ANALYSIS	72
4.1	DETAIL REQUIREMENTS	72
4.1.1	Design Guidelines	72
4.1.2	Strength and Serviceability Criteria	73
4.2	CONNECTIONS	74
4.2.1	Analysis Procedure	76
4.2.2	Monolithic Knee Joint	78
4.2.3	Monolithic Tee Joint	83
4.2.4	Precast Knee Joint	87
4.2.5	Precast Tee Joint	89
4.3	OPENINGS	92
4.3.1	Openings in Reinforced Concrete Structures	92
4.3.2	Openings in Reinforced SIFCON Structures	96
4.4	ATTACHMENTS	96
4.5	GENERAL TEST RUN INFORMATION	96
4.6	OUTPUT INFORMATION	98

## CONTENTS (CONCLUDED)

<u>Section</u>		<u>Page</u>
5.0	RESULTS AND DISCUSSION	100
5.1	CONNECTIONS	101
5.1.1	Calculated Maximum Allowable Values	101
5.1.2	Monolithic Knee Joints	117
5.1.3	Monolithic Tee Joints	121
5.1.4	Precast Knee Joints	121
5.1.5	Precast Tee Joints	125
5.2	OPENINGS IN REINFORCED CONCRETE STRUCTURES	125
5.2.1	Reinforced Concrete Openings	125
5.2.2	SIFCON Openings	126
5.3	INSERTS FOR ATTACHMENTS	128
6.0	CONCLUSIONS AND RECOMMENDATIONS	128
6.1	INTRODUCTION	128
6.2	CONCLUSIONS	128
6.3	RECOMMENDATIONS	130
6.3.1	General Recommendations	130
6.3.2	Strength and Serviceability Requirements	132
6.3.3	Recommendations for Further Research	133
	BIBLIOGRAPHY	135
APPENDIX	A CONTINUUM DAMAGE/PLASTICITY MODEL FOR CONCRETE	140



## FIGURES

<u>Figure</u>		<u>Page</u>
1.	Acting forces and the calculated stresses on the cross section of a knee joint.	7
2.	Development and location of splitting cracks.	7
3.	Crack pattern and forces acting at failure stage.	10
4.	Diagonal splitting crack with tensile stress distribution.	10
5.	Internal force system in the developed corner reinforcement detail.	12
6.	Suggested details for large opening knee joint.	12
7.	Crack locations at failure on reinforced haunch corner detail.	16
8.	Internal force system in the developed corner with haunch reinforcement detail.	16
9.	Truss idealization of T-joint subjected to bending moment.	19
10.	Exterior column-beam joint: (a) stress resultants (b) crack pattern and bond forces.	19
11.	Connection details for a precast joint.	30
12.	Evaluation of horizontal joint shear.	30
13.	Blast resistant structure with openings.	38
14.	Coarse mesh used for comparison of stress deviation.	42
15.	Fine mesh used for comparison of stress deviation.	42
16.	Uniaxial stress-strain curve for concrete in compression.	44
17.	Uniaxial stress-strain curves for concrete specimens of different height.	44
18.	Uniaxial stress-strain curves for concrete under compressive cyclic loading.	47

# FIGURES (CONTINUED)

<u>Figure</u>		<u>Page</u>
19.	Uniaxial stress-strain curves for concrete in tension.	47
20.	Topical and undamaged material area representation.	48
21.	Prager-Drucker yield surface.	48
22.	Comparison between compression and tension response of SIFCON.	51
23.	Typical stress-strain curves for steel reinforcement.	51
24.	Distribution of peak pressure on a box culvert subjected to blast loading.	56
25.	Typical incident pressure trace.	56
26.	Applied loading function for connection details.	57
27.	Applied loading function for opening details.	57
28.	Geometry and instrumentation of Feldman and Siess beams.	62
29.	Applied midspan load of beam C1.	63
30.	Applied midspan load of beam H1.	63
31.	Applied analytical load of beam C1.	64
32.	Applied analytical load of beam H1.	64
33.	Impact loaded concrete beam H1.	65
34.	Analyticaly loaded model simulation of beam H1.	65
35.	Finite Element mesh model for beams C1 and H1 with concrete and steel elements.	66
36.	Time-history plot depicting the concrete tensile cutoff limit.	67
37.	Deflection vs. time for beam C1.	68

# FIGURES (CONTINUED)

<u>Figure</u>		<u>Page</u>
38.	Deflection vs. time for beam H1.	69
39.	Model simulation of deflection vs. time for beam C1.	70
40.	Model simulation of deflection vs. time for beam H1.	71
41.	Reinforcement detail for a blast resistant box culvert.	77
42.	Connection detail BSL2A with labeled concrete and steel reinforcement elements.	80
43.	Connection detail BL-1A with labeled concrete and steel reinforcement elements.	81
44.	Connection detail BL-6A with labeled concrete and steel reinforcement elements.	84
45.	Connection detail BLS6A with SIFCON material and labeled steel reinforcement elements.	85
46.	Connection detail with diagonal steel reinforcement crossties.	85
47.	Connection detail BT-6A with labeled concrete and steel reinforcement elements.	86
48.	Connection detail BT-9A with labeled concrete and steel reinforcement elements.	88
49.	Connection detail PL-1D with labeled concrete and steel reinforcement elements.	90
50.	Connection detail PL-2S with labeled concrete and steel reinforcement elements.	91
51.	Mesh for opening details with labeled concrete elements.	94
52.	Opening detail STAND with labeled steel reinforcement elements.	94
53.	Opening detail CRUSH with labeled steel reinforcement elements.	95

# FIGURES (CONTINUED)

<u>Figure</u>		<u>Page</u>
54.	Opening detail SIFCO with labeled steel reinforcement elements.	95
55.	Attachment detail with labeled concrete and steel reinforcement elements.	97
56.	Time-history plot of displacement for connection detail BL-6A.	101
57.	Time-history plots of shear for connection detail BL-6A.	102
58.	Time-history plots of y-strain and x-stress for connection detail BL-6A.	103
59.	Time-history plots of uniaxial bar stress for connection detail BL-6A.	104
60.	Time-history plots of uniaxial bar stress for connection detail BL-6A.	105
61.	Time-history plots of uniaxial bar stress for connection detail BL-6A.	106
62.	Picture of shear stress at an early time for connection detail BL-6A.	107
63.	Picture of shear stress at a late time for connection detail BL-6A.	107
64.	Picture of x-direction stress for connection detail BL-6A.	108
65.	Picture of y-direction stress for connection detail BL-6A.	108
66.	Picture of shear stress at an early time for connection detail BL-1A.	109
67.	Picture of x-direction stress for connection detail BL-1A.	109
68.	Picture of shear stress at an early time for connection detail BSL2A.	110
69.	Picture of x-direction stress for connection detail BSL2A.	110

# FIGURES (CONCLUDED)

<u>Figure</u>		<u>Page</u>
70.	Picture of shear stress at an early time for connection detail BL-6B.	111
71.	Picture of x-direction stress for connection detail BL-6B.	111
72.	Picture of x-direction strain for connection detail PL-1D.	112
73.	Picture of x-direction strain for connection detail PL-2S.	113
74.	Picture of shear stress at an early time for connection detail PL-2S.	113
75.	Picture of shear stress for opening detail STAND.	114
76.	Picture of y-direction stress for opening detail STAND.	114
77.	Picture of shear stress for opening detail SIFCO.	115
78.	Picture of y-direction stress for opening detail SIFCO.	115
A-1.	Elastic predictor stress state inside the "wedge".	153

# TABLES

<u>Table</u>		<u>Page</u>
1.	Knee joint test results.	14
2.	Tee joint test results.	20
3.	Modified Prager-Drucker cap model constants.	53
4.	Low strength concrete parameters.	53
5.	Medium strength concrete parameters.	54
6.	High strength concrete parameters.	54
7.	Beam C1 concrete parameters.	59
8.	Beam H1 concrete parameters.	59
9.	Beam C1 steel reinforcement parameters.	60
10.	Beam H1 steel reinforcement parameters.	60
11.	Maximum displacement Beams H1 and C1.	61
12.	Steel reinforcement parameters.	75
13.	SIFCON parameters.	75
14.	Results for monolithic knee joints subjected to opening moments (concrete elements).	119
15.	Results for monolithic knee joints subjected to opening moments (bar elements).	119
16.	Results for diagonal crossties.	120
17.	Results for monolithic knee joints subjected to closing moments (concrete elements).	120
18.	Results for monolithic knee joints subjected to closing moments (bar elements).	120
19.	Results for monolithic tee joints (concrete elements).	122
20.	Results for monolithic tee joints (bar elements).	122

# TABLES (CONCLUDED)

<u>Tables</u>		<u>Page</u>
21.	Results for precast knee joints subjected to opening and closing moments (concrete elements).	123
22.	Results for precast knee joints subjected to opening and closing moments (bar elements).	123
23.	Results for openings in concrete structures (bar elements).	127
24.	Results for openings in concrete structures (concrete elements).	127

## 1.0 INTRODUCTION

### 1.1 GENERAL

One of the most interesting and difficult subjects in structural engineering is the analysis, design and assessment of protective structures. Such structures are expected to resist the effects of severe short duration dynamic loads induced by the detonation of modern weapons systems. The central issue in this area is related to the behavioral characteristics of, primarily, reinforced concrete structures, and extensive research has been conducted since the end of WWII for gaining a better understanding of the relationships between the induced loads and the corresponding behavior. Of special interest is the loading domain produced by conventional weapons which induce localized impulsive forces characterized by sharp time gradients. This is the loading domain considered in the present study.

Previous studies have provided a vast reservoir of information on the general behavior of reinforced concrete structures subjected to conventional weapons effects. However, the design of such facilities is guided by available manuals, such as by Crawford et al. '74, or the U.S. Army '86, which contain specific information on weapons effects but that do not address adequately the advanced topics of structural behavior and response. Furthermore, there are structural details, such as connections, openings, and attachments, that do not receive adequate attention in the literature, and their design aspects are sometimes not very clear.

Structural joints and connections are usually assumed to be capable of resisting the forces transferred from the adjoining members. However, if not designed adequately, they tend to fail before the adjoining members may develop their full load capacity. Recent design requirements in the ACI Code (1986) are



concerned with the application of static loads, and therefore may not be adequate for the severe dynamic environments considered in this study. Openings in reinforced concrete structures are required for allowing the flow of resources into and out of the facility. There are no adequate design procedures that ensure the proper operation of openings following an expected load application. Recent tests on hardened facilities (conducted by the Weapons Laboratory (WL) and by the Air Force Engineering and Services Center) have demonstrated that closures may fail under normal attack conditions, and the entire hardened facility could be lost. Protective structures contain various types of equipment, some of which are attached to the walls. The intensive dynamic responses of the structure induce severe stress conditions to such attachments, and the integrity of the corresponding equipment is of serious concern. Here, too, no specific design requirements have been provided in typical design manuals, and the engineer is left to choose structural details which may not perform as expected.

This study has been aimed at the development of design specifications for connections, openings and attachments in reinforced concrete protective structures. The study was conducted by performing "numerical experiments" on construction details to evaluate their expected performance. An evolution of design approaches subjected to the same loading condition led to the establishment of design requirements which should provide the missing guidelines to the hardened facility designers.

## 1.2 OBJECTIVES OF THE STUDY

This study is concerned with the development of design specifications for connections, openings, and attachments in reinforced concrete structures. The goals set at the initiation of this research were to investigate the behavior of typical structural details, for the above mentioned items, and to

formulate their behavior in a manner that would lend itself for implementation into design requirements. The final report on this study shall contain a complete description of the research, and the design recommendations derived from it.

### 1.3 SCOPE OF THE STUDY

This study will address the behavior of connections, openings, and attachments in reinforced concrete protective structures that are expected to operate under the effects of modern conventional weapons. Although the effects of nuclear weapons will not be considered, the same structural details should introduce significant improvements for that loading domain, also. The study has been conducted by simulating numerically the response of a wide spectrum of structural details under a "standard" conventional weapon's threat. The choice of the loading environment is discussed later in this report, and so are the details of the structural systems that were investigated. This report contains an extensive discussion of the known behavior, and a complete evaluation of the derived results. The conclusions and recommendations include the recommended design requirements for the structural systems under consideration.

## 2.0 BACKGROUND

### 2.1 INTRODUCTION

The purpose of this study is to select structural details of connections, openings, and attachments subjected to blast loads that satisfy acceptable behavior criteria without disrupting the constructability of the structural system. Previous studies on these topics were aimed primarily at static and seismic applications, and here our intent is to evaluate that knowledge and the behavior of these structural details subjected to impulsive blast loadings.

There are significant difficulties in the derivation of accurate and well-understood loading functions which can represent the effects associated with explosions. It is very difficult to measure these effects in a zone close to the source due to the severity of the environment created by a blast. However, recent studies have made great progress in determining accurate load-time histories from which researchers can obtain good estimates as described by Krauthammer '86. Data from research conducted by Coltharp et al. '85 are used extensively in this report for deriving loading functions from conventional blasts to the structural details under investigation.

### 2.2 MATERIAL MODELS

The material under investigation is reinforced concrete. Reinforced concrete consists of two primary elements, a concrete medium inlaid with steel reinforcement. The uniaxial compressive strength ( $f'_c$ ) and density of concrete used in our study are measured in pounds per square inch ( $\text{lb}/\text{in}^2$ ) and pounds per cubic foot ( $\text{lb}/\text{ft}^3$ ), respectively. The grade of steel used is based on the yield strength ( $f_y$ ) of the steel, also measured in pounds per square inch.

A third type of material used as a substitution for concrete is SIFCON. SIFCON differs from concrete in that steel fibers are used in place of the aggregate normally found in concrete. Depending on the type and amount of fibers used, the tensile and compressive strength of SIFCON is approximately 2 to 4 times that of standard concrete respectively, with a modulus of elasticity ( $E_s$ ) softer than concrete by a factor of 4. A more in-depth treatment of these models is discussed in Section 3.3.

### 2.3 CONNECTION DETAILING

The joint size is often limited to the size of the elements framing into it. This restriction along with poor reinforcement detailing may create a connection without sufficient capacity to develop the required strength of adjoining elements. Nilsson '73 has shown that slight changes in a connection detail may have profound effects on the strength and behavior of the joint.

#### 2.3.1 Knee Joints

The knee joint is often the most difficult to design when continuity between the beam and column is required. Methods for analyzing the state of stress at the interior of a joint subjected to external shears and moments have been proposed by Winkler (beams with large curvature) and Paduart's equations proposed in 1940 as discussed in Nilsson '73. These approximations are acceptable in the elastic domain; however, they become increasingly less accurate under nonlinear behavior. Present design philosophy combines the principles of statics with a beam model (similar to that proposed in the American Concrete Institute Code (ACI 318-83)) acting on each face of the joint (Fig. 1 from Nilsson '73). This analysis proves to be fairly accurate in determining regions of tensile stress and crack formation when compared to the results of actual tests on joints subjected to negative and positive (closing and opening) moments.

Under a closing moment, large compression strains in excess of 0.003 can be sustained at the inner corner due to a biaxial state of stress (Park and Paulay '75). This enables the outer bars to reach their full strength before failure occurs. However, there are two conditions which should be addressed when determining the size of these bars and their anchorage in the joint: premature bond loss and failure due to diagonal tension cracks.

Typically the exterior reinforcement is bent at a right angle parallel to the joint and continued through to the opposite element, or is terminated in a standard hook. High bearing stresses at this point will often initiate splitting of the concrete (Fig. 2). Propagation of this splitting crack is directly dependent on the amount of confining pressure on the concrete and the amount of cover above the bar. To minimize the propagation geometric confinement from continuous members such as walls or slabs should be provided. In absence of concrete confinement, stirrups should be placed around the hooks to ensure bond through aggregate interlock and the shear friction mechanism (Park and Paulay '75). The affects of confinement on hooked anchorage have been verified in tests by Hawkins et al. '87, and Soroushian et al. '88. Soroushian also points out the advantage of using smaller diameter bars when developing tension in a hook. The advantages of increased cover for deterring crack propagation near reinforcement bars has been highlighted by the new ACI 318-89 code. Development lengths for reinforcement are now based directly on the amount of cover around the bar.

The ACI-ASCE Joint Committee 352 ('85) also recommends the use of transverse ties for confinement and force transfer within Type Two joints. Type Two joints are defined by Committee 352 as joints that must dissipate energy through inelastic deformations induced by earthquake motions, high winds, or blast effects. The stress multiplier  $\alpha$  (a constant used as an over-strength factor)

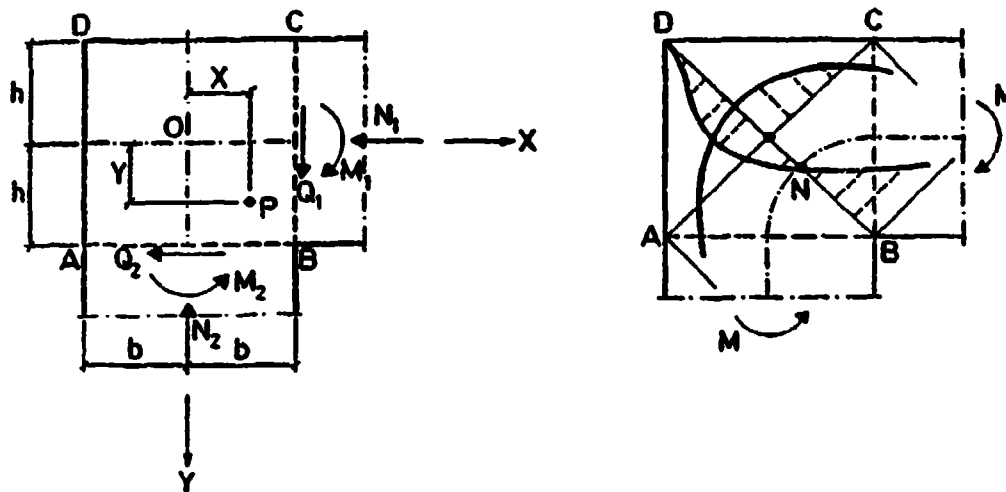


Figure 1. Acting forces and the calculated stresses on the cross section of a knee joint. (Nilsson '73)

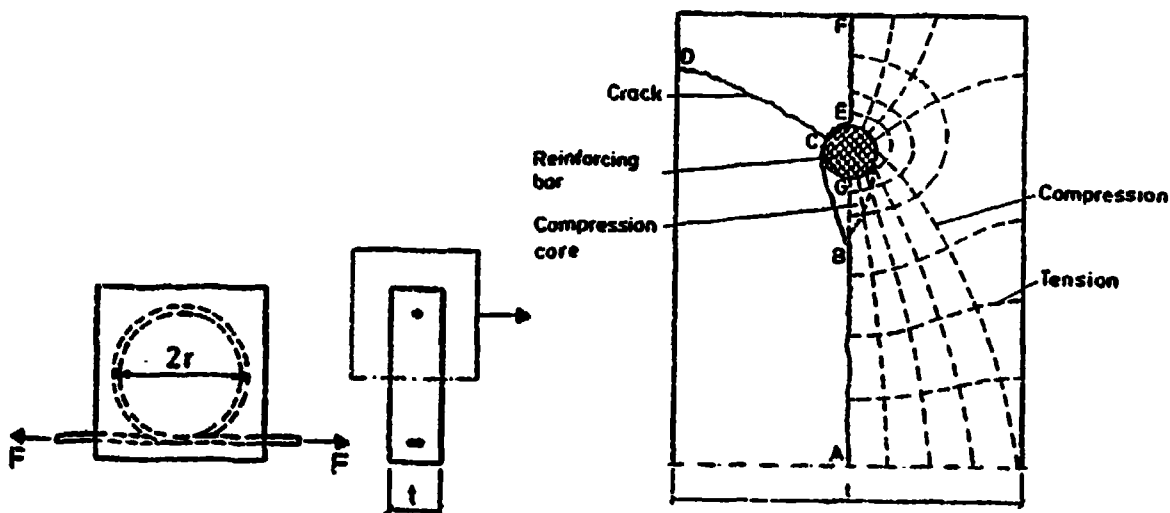


Figure 2. Development and location of splitting cracks. (Nilsson '73)

should be set at 1.25 for Type Two joints. The total cross-sectional area in each direction of transverse steel  $A_{sh}$  should be at least equal to

$$A_{sh} = 0.3 s_h h'' (f'_c/f_{yh}) (A_g/A_c - 1) \quad (1)$$

but not less than

$$A_{sh} = 0.09 s_h h'' (f'_c/f_{yh}) \quad (2)$$

where

- $s_h$  = the maximum distance between ties
- $h''$  = the height of the joint
- $f'_c$  = the concrete compressive strength
- $f_{yh}$  = the yield strength of the ties
- $A_g$  = the gross area of the joint region
- $A_c$  = the confined area of the joint region

The maximum distance between ties  $s_h$  should not exceed the least of one-quarter the minimum column dimension, 6 times the diameter of the longitudinal bars to be restrained, or 6 in.

Another factor to consider in choosing the size of the outer bars is the development of a diagonal tension stress crack originating at the exterior corner and propagating towards the inner corner (from D to B on Figure 1). Kemp and Mukherjee '68, set the limit of this reinforcing on the tensile splitting strength of concrete by setting the steel percentage  $A_s f_y / bd$  equal to  $1.2 * 6 * (f'_c)^{1/2}$ . In their tests, and in tests by Mayfield et al. '71, the full moment capacity was achieved when reinforcement was held to this limit (0.75%). Conversely, tests by Swann '69, on joints with steel ratios equal to 3%, indicated failure at less than 80% of the design strength as discussed also by Park and Paulay '75. If this maximum ratio of steel is exceeded, stirrups should be placed perpendicular to the crack plane to help minimize joint degradation and volumetric increase.

A comprehensive study on the behavior of joints subject to opening moments was completed by Nilsson '73. The objectives of that study were to develop joint details that will provide at least 100% of the moment capacity of the adjoining elements. Results and comparisons on the performance of a portion of the details tested are shown in Table 1 (Nilsson '73). The most common mode of failure in conventionally reinforced joints is due to a combination of cracks. The first cracking appears at the interior corner and propagates towards the center where it branches off in the form of a diagonal tension crack (Fig. 3). This mode is similar to the diagonal shear cracks found in beam behavior. The second mode of cracking or splitting due to internal tension occurs at the interior of the joint (Fig. 4). The value of the internal tensile force is 1.41 times the tension in the main flexural bars (Park and Paulay '75). Also, splitting cracks along the compression reinforcement may cause separation of the outer corner.

According to Nilsson '73, the detail which provides the most strength with the least amount of congestion utilizes a diagonal bar at the interior corner placed at 45 deg from the main flexural steel (Fig. 5). This bar will prevent the migration of the initial flexural crack at the corner. The flexural steel should be bent into a hairpin with the return leg extending from the tensile region into the compression region. This will carry the radial stresses around the perimeter of the bars to help prevent corner separation and diagonal tension failure. Tests completed by Nilsson '73 on connections using this detail (Table 1) show that moment capacities exceed design moments for steel ratios of up to 0.76%. If a large steel ratio (more than 0.76%) is used, then the addition of stirrups placed perpendicular to this bar and around the outer reinforcement is recommended (Fig. 6). These stirrups will cross the diagonal tension crack described above, and the required area of steel ( $a_s$ ) for



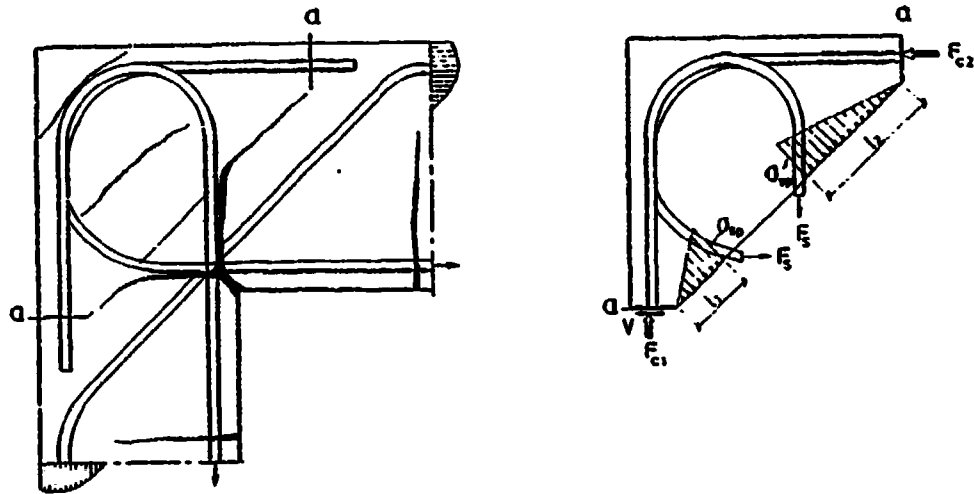


Figure 3. Crack pattern and forces acting at failure stage. (Nilsson '73)

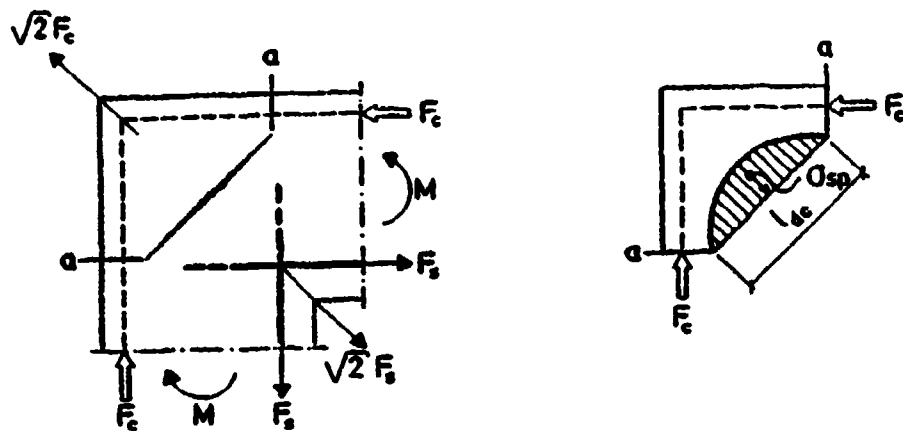


Figure 4. Diagonal splitting crack with tensile stress distribution. (Nilsson '73)

beam/column connections can be estimated according to Park and Paulay '75, as follows

$$a_{sj} = [(\Gamma - 0.005)/\Gamma] (f_y/f_{yj}) [1 + (h_1/h_2)^2]^{1/2} (A_{s1}/n) \quad (3)$$

where

$\Gamma = A_{s1}/bd$  (flexural reinforcement ratio)

$f_y$  = the yield strength of the main reinforcement

$f_{yj}$  = the yield strength of the diagonal ties

$h_1$  = the overall beam height

$h_2$  = the overall column depth

$A_{s1}$  = the area of the main flexural reinforcement

$n$  = number of tie legs crossing the tension crack

Equation 3 is based on a maximum  $\Gamma = 0.5\%$  for connections not requiring ties. As stated earlier, this recommendation is applicable to beam/column details and may be overconservative for wall/slab applications for reasons noted above. Therefore, a slight modification to Eq. 3 is proposed, based on the maximum ratio ( $\Gamma_w = 0.75\%$ ) for wall/slab connections recommended by Nilsson '73.

$$a_{sj} = [(\Gamma_w - 0.0075)/\Gamma_w] (f_y/f_{yj}) [1 + (h_1/h_2)^2]^{1/2} (A_{s1}/n) \quad (4)$$

These stirrups may increase the joint strength by as much as 20%. In addition, these ties will also provide confinement for the outer bars in closing moment situations, as stated earlier.

The use of diagonal stirrups in beam/column connections may be a necessity and can be placed without a great deal of difficulty. However, their placement in slab/wall connections would be very laborious and congestive. For example, poor workmanship and early degeneration are commonplace in European protective structures built in the last decade, as discussed by Naeyaert '89. The cause is linked to the use of excessive

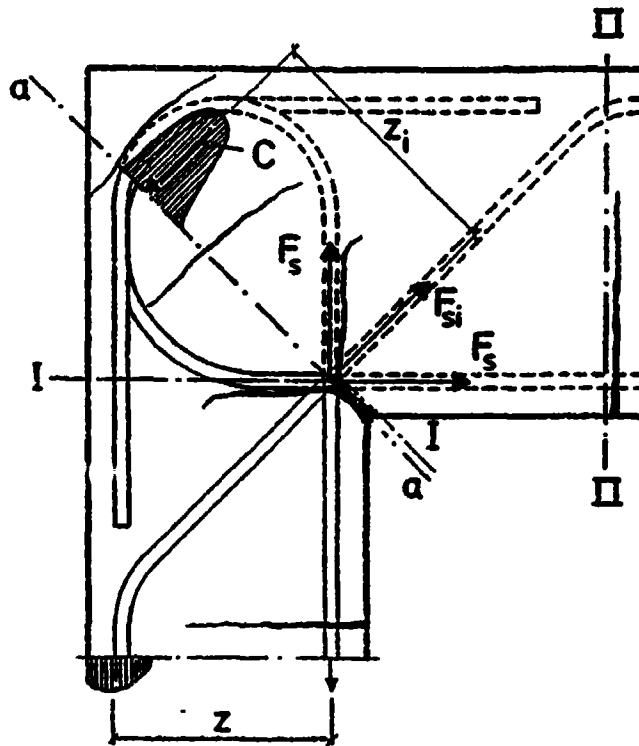


Figure 5. Internal force system in the developed corner reinforcement detail. (Nilsson '73)

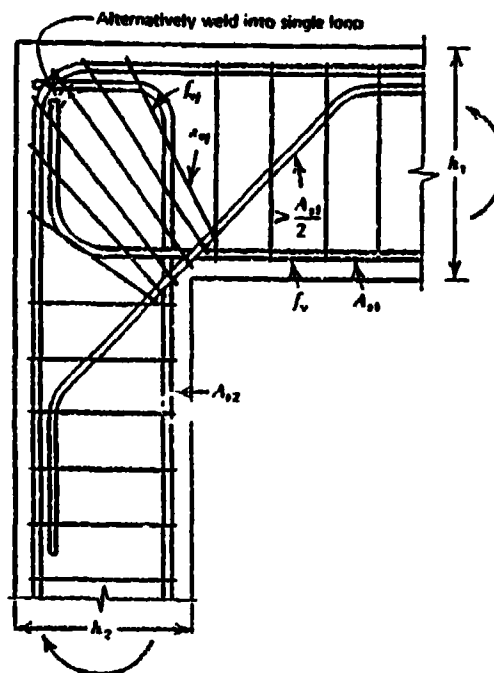
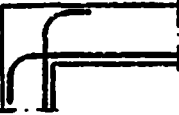
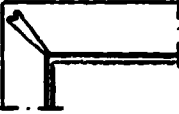
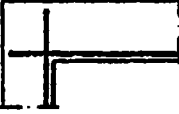



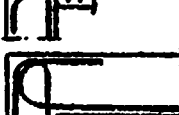








Figure 6. Suggested details for large opening knee joint. (Park and Paulay '75)

amounts of steel tie reinforcement which inhibits proper concrete compaction. Naeyaert '89 recommends substituting steel fibers for the steel bar ties commonly used. Tests by Gefcan and Ramey '89 were completed on connections infiltrated with 2% by volume fiber reinforced concrete (FRC) and subjected to simulated earthquake loading. Their results show that stirrup spacing ( $s_h$ ) in FRC may be increased by a factor of 1.7 over that determined by ACI-ASCE Committee 352 (Eqs. 1 and 2 above) for Type Two joints. Another solution, as mentioned above, would be to set the limit of flexural reinforcement in slabs and walls at 0.75% and increase the overall thickness of the elements when necessary. This would eliminate the need for ties in the joint region. Note that the use of shear ties is recommended in the elements near the joint face. Tests on elements without shear ties, conducted by Coltharp et al. '85, show a definite diagonal shear failure located immediately above the joint region.

The addition of a haunch or splay on the inside corner of the joint is an obvious enhancement. Tests by Balint and Taylor '72 and Nilsson '73 show that efficiencies of 100% are easily attainable for steel ratios of 1.0% when a haunch with 45-deg reinforcement is used. In addition, the space for reinforcement is increased to help alleviate congestion. Nilsson does not recommend the use of a haunch because of the negligible increase in moment capacity of cases UV 3 and 4, which utilize a haunch, over cases UV 5, 6, and 7 which contain identical reinforcement but no haunch (Table 1). However, close inspection of the crack formation after yielding of the reinforcement in the haunch tests clearly shows the failure hinge at the entrance corner or 0.7 times the haunch length from the joint face as shown in Fig. 7. This situation is more desirable than a hinge located at the face for several reasons.

TABLE 1. Knee joint test results. (Nilsson '73)

Specimen number	Haunch size H cm	Concrete strength $\sigma_c$ $\sigma_{sp}$ kgf/cm <sup>2</sup>	Failure moment $M_{ut}$ kgfm	Calculated ultimate mom. $M_{uc}$ kgfm	$\frac{M_{ut}}{M_{uc}}$ %	Inside corner crack width at $M_{uc}/1.8$ mm
 U 21		339 27.3	990	3135	32	Failed
 U 27		277 21.1	1840	2990	61	0.60
 U 15		289 25.6	2227	3290	68	0.70
 U 12		335 31.2	2474	3220	77	0.27
 U 28		272 20.5	2540	3185	79	0.26
 UV 1	15	305 23.7	3160			
 UV 2	5	345 25.2	3120			
 U 24		398 25.9	2804	3240	87	0.34
 UV 3	10	318 24.1	3712			0.08
 UV 4	5	277 22.3	3505			0.06
 UV 5		335 26.2	3629	3180	114	0.11
 UV 6		292 24.3	3505	3040	115	0.13
 UV 7		339 18.4	3773	3070	123	0.13

- 2.3.1.1 A greater distance is available for bonding of the flexural steel in the joint. This distance becomes critical when the connection is subjected to repeating or reversing loads.
- 2.3.1.2 Bond stress profiles on tensile reinforcement is a function of the distance from the crack face with the highest value occurring at the crack (Leon '88). Therefore the bar stress at the interior of the connection will be less, which reduces the likelihood of splitting crack formation.
- 2.3.1.3 Internal tension decreases due to the two reasons noted above, and the moment arm across the diagonal of the joint increases (see Fig. 8). This will delay the failure of the connection due to splitting without adding crossties. The moment capacity for the detail shown in Fig. 6 (no haunch) at section a-a

$$M_{a-a} = (1.41*f_y + f_{yi}) * z_i \quad (5)$$

The moment capacity for the detail shown in Fig. 8 (with haunch) at section a<sub>h</sub>-a<sub>h</sub>

$$M_{a_h-a_h} = (1.41*f_y*z_i) + (f_{yi} * z_{ih}) \quad (6)$$

while the capacity at section I-I

$$M_{I-I} = (f_y + f_{yi}/1.41) * z \quad (7)$$

where  $f_{yi}$  is the yield strength of the diagonal steel,  $z_i$  is the moment arm for section a-a,  $z_{ih}$  is the moment arm for  $f_{yi}$  located in a haunch, and  $z$  is the moment arm for section I-I.

- 2.3.1.4 In Type Two connections, the critical section for development of reinforcing is taken at the face of the confined column core. When haunches are used, this

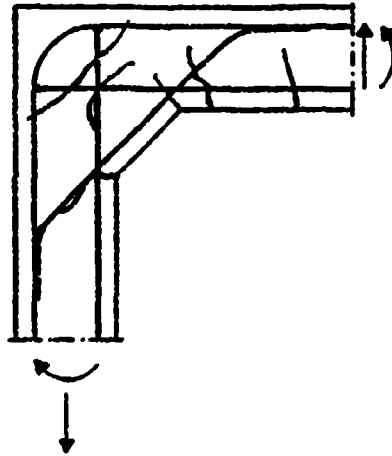


Figure 7. Crack locations at failure on reinforced haunch corner detail. (Balint and Taylor '72)

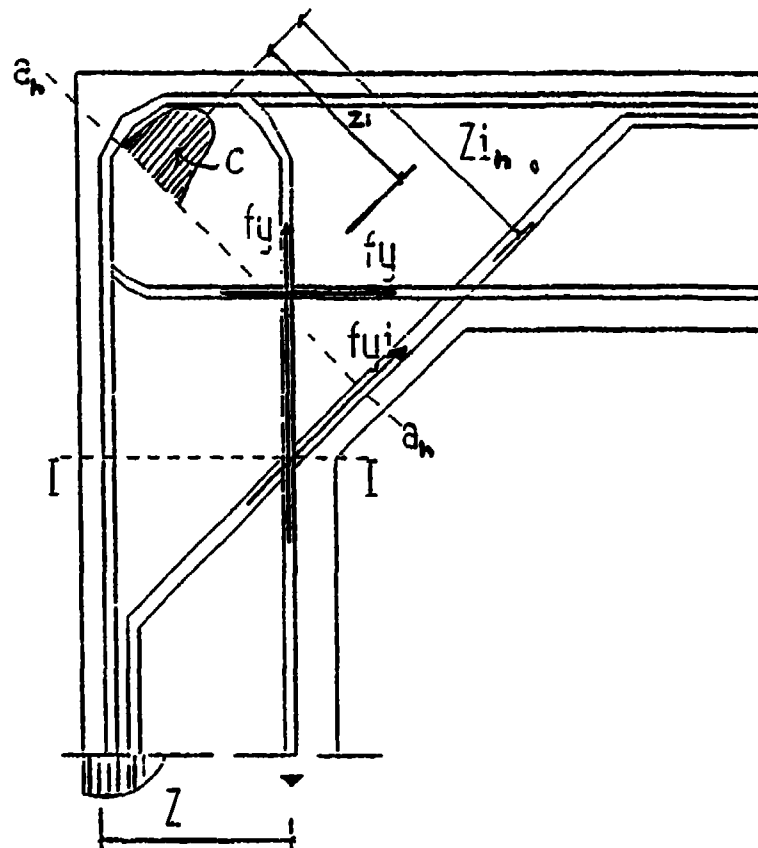


Figure 8. Internal force system in the developed corner with haunch reinforcement detail.

critical section may be taken at the intersection of the diagonal and flexural bars.

2.3.1.5 The formation of splitting cracks near flexural reinforcement has been shown to be directly dependent on the amount of concrete cover around the bar (ACI 318-89). Adding a haunch again will increase this cover at the critical face of the joint.

#### 2.3.2 Tee Joints

Another connection type to consider is the tee joint. Tee joints are typically found at two locations on a structure, the exterior faces and the roof. At the exterior, a beam/slab will frame into a continuous column/wall. At the roof, the column/wall will frame into a continuous beam/slab. In either case, the element terminated at the joint should be connected so that the strength of the joint is equal to or greater than the strength of the connected element. Also, the joint should provide enough confinement and support for the continuous element to prevent its premature failure. Figure 9 depicts a tee joint subjected to shear and bending with the resultant stress distribution.

Nilsson '73 also completed a series of tests on tee joints with several types of reinforcement details subjected to bending moments. Table 2 lists the test results. Nilsson '73 found that the flexural reinforcement terminating in a joint should be developed by a hook turned toward the midheight of the connection. Bond stress at the bend in the hook is transferred to a diagonal compression strut in the joint. Turning the tail of this hook toward the midheight of the joint will direct the concrete compression strut toward the external compression component and assure static equilibrium in the connection. The ACI-ASCE Committee 352 ('85) recommended minimum development length for bars with diameter ( $d_b$ ) terminating in a standard 90-



deg hook,  $l_{dh}$ , from the critical section is

$$l_{dh} = \alpha f_y d_b / 75(f'_c)^{1/2} \quad (\text{lb/in}^2) \quad (8)$$

Park and Paulay '75 recommend ignoring the lead in length on hooked bars due to the early development of splitting cracks along the tensile reinforcement (Fig. 10). Tests completed at the University of Canterbury on exterior tee joints show a crack initiating at the interior corner and propagating towards the hooked end of the bars. Several additional recommendations on the detailing of these connections are based on the results of these tests.

- 2.3.2.1 The ACI 318-83 ('85) code recommendations for shear steel are inadequate when there is little compression on the column. Shear cracks tend to form on a diagonal from the corners of the joint, therefore the 45-deg truss analogy may not be appropriate for shallow columns. Transverse ties should be designed to resist the total shear in the connection with no reliance on concrete.
- 2.3.2.2 Transverse ties are also a necessity for developing confinement of the joint core, and transferring bond forces from the hooked portion of the flexural steel to the column bars through shear friction and aggregate interlock.
- 2.3.2.3 The addition of a stub beam on the back side of the column is recommended for removing the hooked portion of the tensile steel from the shear affected core. This detail greatly increased the stiffness and strength of the joint by reducing the amount of transverse expansion and eliminating bond loss.

The connection advocated in this report uses diagonal struts similar to that outlined in the section on knee joints. This detail should increase the strength of the joint for the same

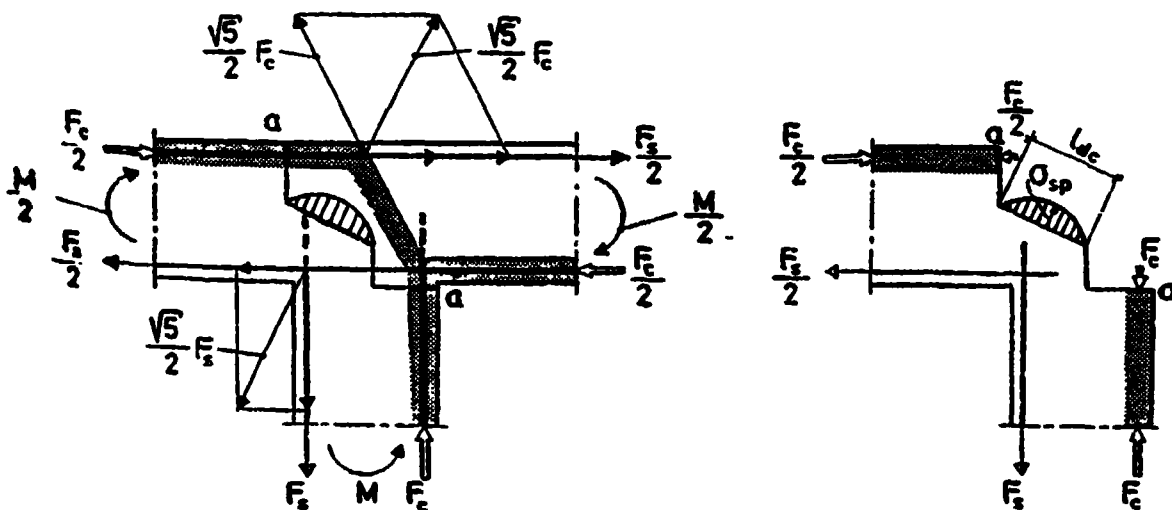


Figure 9. Truss idealization of T-joint subjected to bending moment. (Nilsson '73)

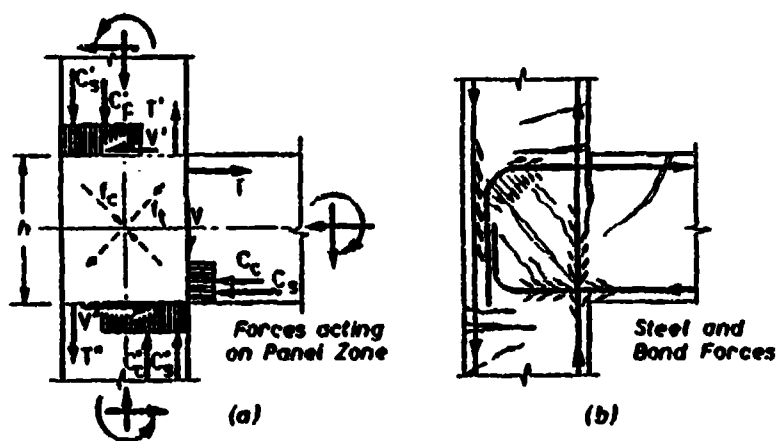





















Figure 10. Exterior column-beam joint: (a) stress resultants (b) crack pattern and bond forces. (Park and Paulay '75)

TABLE 2. Tee joint test results. (Nilsson '73)

Way of loading	Specimen number	Reinforce- ment per- centage in leg $\mu$ %	Concrete strength $\sigma_c$ $\sigma_{sp}$ kgf/cm <sup>2</sup>	$M_{ut}$ test kgfm	$M_{uc}$ calcu- lated kgfm	$\frac{M_{ut}}{M_{uc}}$ %
	 T 1	1.80	308 21.4	1435	3715	39
	 T 15	0.65	378 24.6	1000	2475	40
	 T 11	1.30	370 26.5	1110	4685	24
	 T 14	0.65	319 22.7	1425	2450	58
	 T 13	1.30	386 28.2	3675	4630	79
	 T 2	1.80	238 18.6	4010	3650	110
	 T 12b	1.30	310 24.7	3920	4755	82
	 T 16	0.65	381 26.7	2465	2630	104
	 T 25	1.81	280 22.1	2300	5745	40
	 T 26	1.81	340 24.9	4735	5890	80
	 T 27	1.81	357 26.9	5100	5905	86
	 T 21	1.30	343 20.9	1450	4830	30
	 T 22	1.30	306 28.6	4530	4820	94
	 T 31		388 33.4	1660	1490	111
	 T 32		388 33.4	1610	1510	107

reasons as shown above for the stub beam. Initial cracking will move from the face of the joint to the exterior of the haunch. As stated above, this will reduce the stress on the hooked portion of the bar and the negative effects of splitting cracks. Additional joint area will reduce shear stress and transverse expansion. And the use of diagonal bars will increase the moment capacity of the joint and spread the transfer of bond stress to the column bars over a greater distance.

### 2.3.3 Precast Joints

Connections for precast elements should follow the same basic principles as outlined above. However, inherent in every precast connection detail is a discontinuity between elements. The primary disadvantage encountered at a discontinuity is the inability of the connection to transfer load through shear and flexure. The transfer of direct shear is often resisted by a corbel cast uniformly with the column; and, for blast-loading cases, this corbel will be required to resist loads in opposite directions. Design of corbels should follow standard practice as set fourth by the PCI Design Handbook (1985) based on the shear friction method for resisting direct shear. This type of shear is discussed at length in Section 2.4.2.1. Transfer of flexure, however, is much more difficult, and the subject of moment resistant precast conections has been the object of many studies.

At the University of Minnesota, several precast connection details were subjected to cyclic simulated earthquake loads. The detail which exhibited the best performance, shown in Fig. 11, represents a column connected to a beam through mild beam reinforcement threaded into couplers located in the column (Jayashankar, '87). The couplers were mechanically anchored to the column through steel plates on each face which eliminated many of the bond loss problems encountered in previous tests. This detail is described in full in Section 4.

Another factor important to the serviceability of a precast connection subjected to blast loading is the elimination of gaps which may allow contaminants to enter a structure. This may be accomplished by posttensioning a connection similar to that outlined above. Due to the high magnitude and rate of blast loading, it is not possible to eliminate completely the formation of tension cracks and gap openings in the joint throughout the course of loading. However, by limiting the amount of tensile stress in the posttensioned reinforcement to a value less than yield, the structure will return to a precompressed state and assure a positive seal.

#### 2.3.4 Openings and Attachments

Openings or holes will be placed in a structure for service accommodations. The effects of an opening on a structure will vary depending on its location with respect to the load and supports. Most of the research on openings to date pertains to the disruption caused by an opening on a load-carrying member such as a slab or wall. The path for shear and flexure is altered around the opening and results in a buildup of stress at these locations. A study by Muller et al. '84 points out that a reduction of shear resistance by holes adjacent to a column is mainly dependent on the width of an opening in the tangential direction. Since a study on the optimum placement of an opening in a structural system would pertain more to the actual slab design than on the details immediate to the opening, this subject is not discussed here. The location of an opening will be assumed to occur at the center of the span and the details for connections designed accordingly. What will be investigated in this report is the reinforcement detail at the edge of an opening with a cover (i.e., door or window hatch) subjected to a blast loading.

Covers for these openings (not studied here) will transfer the blast load (Section 3.4) to the edge of the support slab. The object of this study was to determine adequate edge reinforcement required for transferring the load from the edge to the interior of the slab and ultimately to the support via the connections. To accomplish this, the load transferred from the opening cover to the slab must be distributed to a large enough area to keep compressive stresses within a tolerable range and an adequate amount of reinforcement supplied for shear and tension requirements. The basis for design follows the behavior requirements outlined in the next section on structural response.

Attachments on a structure typically consist of inserts or ties connected to the slab or wall elements. Usually these items are fastened to the structure by casting them directly into the concrete, or they are drilled in and secured through expansion wedges or epoxy grout. For normal gravity loads this procedure is very reliable. However, when the structure is subjected to high accelerations typical of blast loads (accelerations of 20 g were reported by Coltharp et al '85; one g is equivalent to the acceleration due to gravity), the attachment may fail prematurely for the following reasons.

- 2.3.4.1 The load on the attachment increases in proportion to the amount of acceleration increase.
- 2.3.4.2 Inserts embedded in concrete are dependent on the tensile strength of the surrounding cone pullout (PCI Design Handbook 3rd Edition). Also, the back side of a wall subjected to blast loads experiences high magnitudes of tensile stress due to the refraction of shock waves (which often spalls the concrete cover). This will severely limit the load-carrying capacity of the concrete cone.

Consequently, it is recommended that all attachments be directly connected to the slab/wall reinforcement. This type of detail will assure ductility and prevent premature failure.

## 2.4 STRUCTURAL RESPONSE

Several parameters measured in the joint region are used to determine adequate connection behavior in relation to structural response. These parameters consist of direct shear, diagonal shear, concrete tension and compression, reinforcement tension and compression, bond slippage, deflections, and rotations. Often these parameters reach maximum stress values at one location in a connection which greatly complicates the design procedure. Member analysis, on the other hand, will deal primarily with one or two parameters at each given point. The following subsections discuss each of these parameters, their effect on joint strength, and how they are influenced by different connection details.

### 2.4.1 Flexural behavior

Behavior of reinforced concrete in flexure has been the subject of numerous investigations and reports. The basics of flexural design are outlined in the ACI 318-83 code, which follows the assumptions proposed by Whitney (Whitney stress block). This procedure assumes that the stress in the concrete above the neutral axis is uniform over the compression region. A couple created between this compressive zone and the tensile stresses in the reinforcement below the neutral axis resists the external moment. This method is acceptable for design. However, when accurate behavioral analysis is required, a more general theory as shown in Park and Paulay '75 is suitable. Through the use of rational constitutive models of steel and concrete, a reliable method is shown for determining moment-curvature relationships. Average compressive stress due to flexure in the

concrete immediately above the compression reinforcement should not exceed  $0.45 * f'_c$ . This seemingly arbitrary value is taken from actual working stress design and is approximately equal to the maximum compressive stress in concrete where elasticity is the governing model for behavior. Limiting the compressive stress to this value should ensure the survivability of a structure when subjected to repeated blast loading situations.

#### 2.4.2 Shear Behavior

Failure in reinforced concrete elements due to shear may be represented by three major modes: diagonal shear, direct shear, and punching shear. Diagonal shear failure is characterized by the formation of diagonal cracks (usually curved) normal to the principal tensile stresses, and is associated with flexural response. Direct shear is characterized by a sliding type of failure along a well-defined plane in which the vertical slip occurs due to compressive and rotational deformation of small concrete struts (Park and Paulay '75, Ross '83, Assadi and Krauthammer '88). The phenomenon of direct shear usually occurs at points of force or geometrical discontinuities (for example, at the edges of loaded regions or supports). Punching shear is characterized by a concrete cone pushed out of a slab by its supporting column, and is probably a transition mechanism between direct and flexural shear. The cracks are usually less curved than flexural cracks.

From shear time-history plots obtained in the present study observed at different points in the structure, one can notice these two principal types of shear. These plots typically will show a high peak value with a very short time duration similar to that of the load, and then a reverse trend which leads into a plateau region (refer to Section 5 for examples). The initial shear stress resultant represents direct shear, with the remaining portion showing diagonal or flexural shear.



2.4.2.1 Direct Shear. The direct shear resultant will travel along the length of the structure as the load is transferred from element to element as the shock wave propagates along the structure (i.e., the point of discontinuity travels with the shock wave). The value of this direct shear at each point will decrease rapidly and is negligible at the onset of flexural response. For this reason it is acceptable to uncouple the response of direct shear failure with the effects of flexural behavior. Data from tests conducted by Kiger '84 and Slawson '84 on shallow buried flat roof structures support this contention. When direct shear was the resultant mode of failure, the structure was not allowed sufficient time to develop any meaningful flexural response as outlined by Krauthammer '86, and Assadi Lamouki and Krauthammer '88.

Recent studies by Mattock and Hawkins '72; Hawkins '74 and '81; and Mattock '74, '76, and '77, have shown a direct relationship between shear stress and shear slip on a vertical plane. This relationship will also predict the maximum direct shear stress that can be obtained at a section known as the Hawkins shear limit ( $\tau_m$ , Eq. 9) as set forth by Murtha and Holland '82. This shear limit should not be exceeded and the detail should be designed accordingly.

$$\tau_m = 8 (f'_c)^{1/2} + 0.8 \Gamma_{vt} f_y < 0.35 f'_c \quad (9)$$

where  $\Gamma_{vt}$  is the ratio of total reinforcement area to the area of the plane which it crosses. For design,  $\tau_m$  should be multiplied by a factor of 0.8 to ensure structural integrity under multiple loading situations.

2.4.2.2 Diagonal Shear. Under flexural response, diagonal shear failure will be the controlling mode of behavior. After cracking, shear stresses are resisted by the combined action of

concrete struts in compression and tension in the transverse and longitudinal reinforcements (the truss mechanism analogy). Present design procedures typically assume the compression struts to act at a 45-deg angle; however, this prediction is very conservative when determining the tensile forces in the transverse reinforcement (Park and Paulay '75). To account for this overdesign, the ACI 318-83 code adds an empirical correction factor  $V_c$  called the 'concrete contribution' to the shear capacity of the transverse steel.

Flexural shear capacity will be controlled by the capacity of the structure at a hinge location. Yield of flexural reinforcement can decrease the shear capacity due to the loss of in-plane restraint. Shear capacity at this section should be decreased to 75% of the capacity shown above.

A more rational approach for the design of diagonal shear has been proposed by researchers at the University of Toronto (Mitchell and Collins '74, Collins '78; Vecchio and Collins '86; Mitchell and Collins '87) and is commonly known as the 'Compression Field Theory'. This approach resembles the Tension Field Theory composed by Wagner '29 in the analysis of post-buckling shear resistance of thin webs. In the analysis of reinforced concrete, it is assumed that no tension is resisted by cracked concrete and that shear is carried by a field of diagonal compression and tension in the vertical ties and longitudinal bars. The value of this tension is directly proportional to the angle of inclination in the compression struts. These unknowns are determined by simultaneously solving the strain compatibility equations, equilibrium equations, and constitutive relationships.

**2.4.2.3 Joint Shear.** Another type of shear phenomenon which must be analyzed is joint shear. Joint shear is a term used to describe diagonal shear at the interior of the connection. Traditionally, two types of methods, panel truss and compression

strut, have been used to quantify this shear and determine its effects on the joint.

In the elastic domain, a compression strut mechanism occurs across the diagonal of the joint subjected to opening or closing moments. The strut is required to resist vertical and horizontal reactions imposed on the joint at the intersection of the column and beam flexural steel. At the onset of flexural yield under cyclical loading, crack sizes at the face of the joint increase and reinforcement bond begins to break down. Compressive forces initially transferred at the face of the column are now transmitted through high intensity bond forces at the interior of the joint. Consequently, compression struts initiating at the interior of the joint will extend to the face of the joint before reaching the bottom flexural steel. Several cracks will have propagated along the initial compression struts at the interior of the joint, eliminating any tensile capacity of the concrete. To prevent total failure of the joint, stirrups placed normal to the column reinforcement are required to resist the forces created by the shortened struts.

Experimental studies noted in Park and Paulay '75, and Leon '88, have shown the compression strut method to be the dominant mechanism if adequate reinforcement development is maintained over the life of the loading cycles. However, the resultant compressive and tensile stresses will cause extensive cracking parallel to the compression strut. Stirrups similar to the shear ties required for the panel truss mechanism should be placed in this region to ensure (1) the integrity of the overall section under reversed loading, and (2) sufficient bond of flexural reinforcement through confinement.

The standard procedure for calculating joint shear according to ACI-ASCE Committee 352 is shown in Fig. 12. Note that the value of  $\alpha$  used should correlate with that used for Type Two

joints (1.25 when the strength of materials is known). This value must be less than the nominal joint shear strength  $\phi V_n$ , where  $\phi = 0.85$  and  $V_n$  is determined by Equation 10.

$$V_n = r (f'c)^{1/2} b_j h \quad (10)$$

where  $r$  is equal to 20, 15, and 12 for interior, exterior, and corner Type Two beam/column joints. The thickness of the column in the direction of the load is  $h$ , and the effective joint width is  $b_j$ , determined from Eq. 11, where  $b_b$  is the average width of beams framing into the joint and  $b_c$  is the width of the column.

$$b_j = (b_b + b_c)/2 \quad (11)$$

This equation is based on the fact that transverse ties have been placed in the joint in conformance with the discussion on confinement noted earlier.

For wall/slab connections, the shear capacity of concrete is increased due to the confinement obtained through geometric continuity. The value of diagonal shear allowed in the ACI 318-83 code for plain concrete is

$$\phi V_n = 0.85 (4) (f'_c)^{1/2} \quad (12)$$

If this value is exceeded, stirrups for shear should be added to the joint in accordance with the analysis for beam/columns. As stated earlier the addition of stirrups in wall/slab connections will create congestion problems; therefore, an increase in the overall connection dimension may be warranted. The addition of stirrups in the slab portion near the face of the connection is highly recommended.

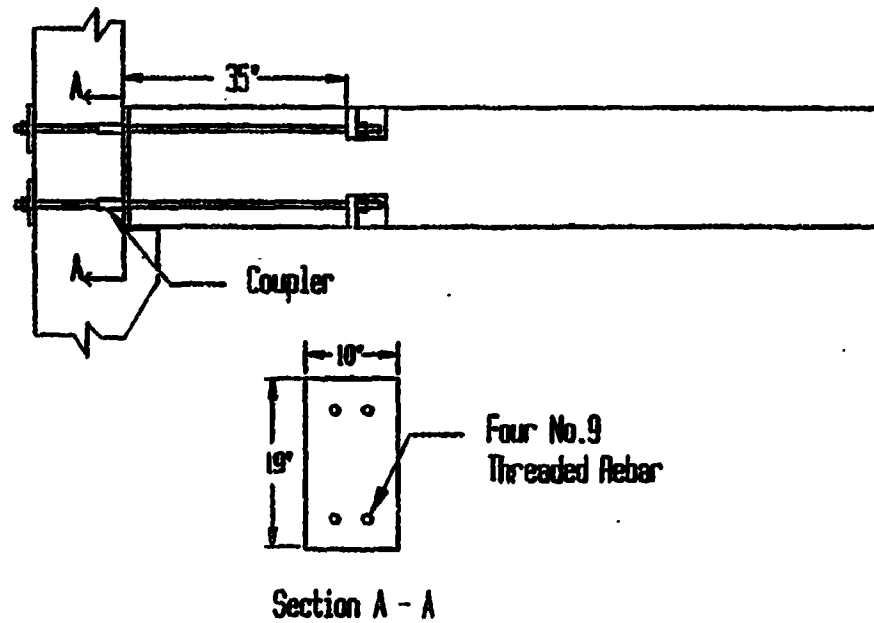


Figure 11. Connection details for a precast joint.  
(Jayashankar '87)

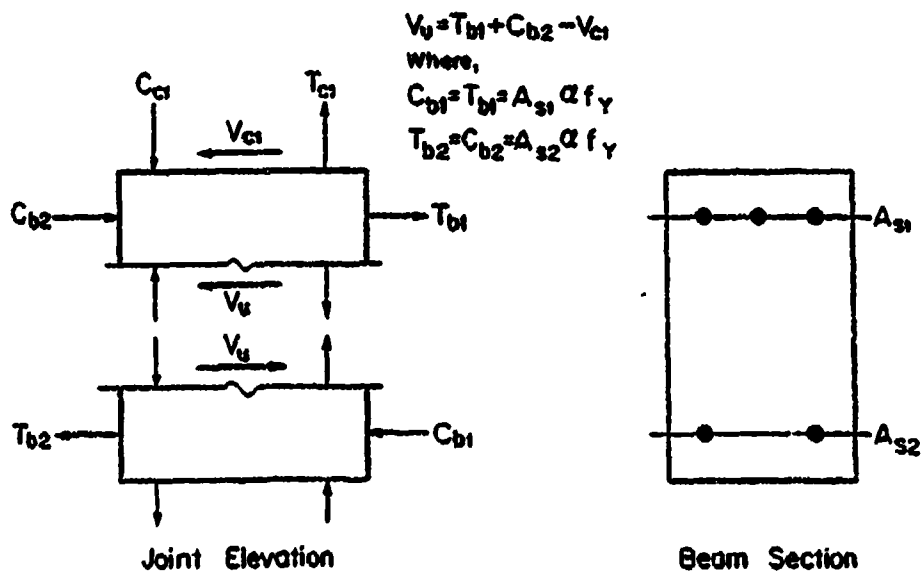


Figure 12. Evaluation of horizontal joint shear.  
(ACI-ASCE Committee 352 '85)

### 2.4.3 Reinforcement Bond

For interior joints, the ACI-ASCE Committee 352 recommends 20 bar diameters for the development of flexural bars in Type Two interior joints. Presently there is much discussion on the acceptable values of joint shear shown above and its interaction with the requirements for anchorage of reinforcement in the joint region. Recent studies have shown that the effects of shear stress on a joint depends on the length of development available for bonding the flexural reinforcement (Leon '88). If adequate bond of the reinforcement is provided well into the postyield range, the level of shear stress in the joint will have little effect on the strength or behavior of the joint. For interior joints, the recommended length for adequate bond development is 28 bar diameters with 24 specified as a minimum. Shear stress levels near  $15(f'_c)^{1/2}$  under cyclic loading will not produce substantial damage to the joint if these lengths are provided. These results can be interpolated to exterior joints with the use of hooked bars. As stated in the section on connection details, it is recommended that hooked bars be turned toward the midheight of the connection. According to Nilsson '73, the hook in a knee joint should consist of a 180-deg bend with the return leg embedded in the opposing force region.

Reinforcement bond slippage and loss are also dependent on the amount of development available. Initial slip is due to the loss of adhesive bond. This will not affect the strength of the bar; however, stiffness will decrease and crack propagation will begin. Slippage will occur earlier in bars with relatively short development lengths. Bars with  $24d_b$  and less development experienced significant bond deterioration under cyclic loading in the elastic domain, with most of the damage occurring in the initial cycle of loading (Leon '88). Bars with  $28d_b$  development were able to withstand the loading with no appreciable loss in bond. As mentioned earlier, bond loss and failure may also

initiate from the uncontrolled propagation of splitting cracks around the bar. To avoid this type of failure, the ACI 318-89 code requires a minimum cover of  $2d_b$  for a development length cover factor of one.

To assure bond integrity at the interior of the joint, a limit should be set on the maximum amount of bar stress at that point. For this study a maximum of  $1/3 f_y$  will be used as a criterion for acceptable bond behavior in critical regions. For less critical areas of the structure or possible hinge locations, a value of  $2/3 f_y$  will be acceptable. Maintaining these values for bar stresses will give ample confidence that the connection will not fail due to bond loss.

#### 2.4.4 Ductility and Deflections

Structural ductility is measured by comparing the amount of allowable plastic strain a member can sustain before failure, to the maximum amount of strain experienced under elastic conditions. This value is quantified by a "ductility factor" ( $\mu$ ) equal to the ratio of ultimate strain to elastic strain. For connections in protective structures, a ductility of  $\mu = 1$  (i.e., elastic connection) is advisable, and to allow for energy dissipation in the adjoining members. ACI-ASCE Committee 352 also recommends this method for providing ductility in a structure subjected to seismic loads. The ductility of the adjoining members should be determined based on the maximum allowable deflections for serviceability and operational requirements of the facility.

There are no special limits set for the maximum allowable deflection of a structure subjected to blast loading in the ACI 318-83 code. For design purposes, the maximum deflection ( $d_{max}$ ) will be based on the assumption that attached nonstructural

elements will not be damaged. The governing equation for this case as set by the ACI 318-83 code is

$$d_{\max} = L / 240 \quad (13)$$

where L is the total length of the span in inches. This rational limit will be used as a reference point for comparison purposes between the details tested and is not intended to be a design parameter.

## 2.5 DYNAMIC RATE EFFECTS

Rate effects of dynamic loading have been shown to alter the behavior of a structure significantly. Materials generally show increased stiffness and strength with an increase in strain rate (Newmark and Rosenblueth '71). When modelling linear material, a dynamic enhancement factor (DEF) relating stress to strain rate may be applied to the equations of equilibrium. However, the modelling of nonlinear materials such as reinforced concrete is much more complicated (Assadi-Lamouki and Krauthammer '88). They suggest using a DEF which is a function of loading rate based on the discussion by Ross '83. This approach may be practical for simple member analysis, but it does not approximate the complicated phenomena experienced by concrete under high rates of loading (Stevens and Krauthammer '88). Due to the limited amount of data available on this subject, Stevens and Krauthammer '88 have not included rate effects in their constitutive concrete model (discussed in Section 3) which is used extensively in the analysis portion of this report.

## 2.6 THE FINITE ELEMENT METHOD

The geometric discontinuities and material nonlinearity (which limit closed form solutions in connection regions), coupled with the high strain rates associated with blast loading,



severely limit classical mathematic analysis of behavior in the joint. Therefore, the use of numerical procedures in approximating stresses and strains for these applications is widely accepted. By far the most common tool used today for the numerical analysis of structural mechanics problems is the Finite Element approach (Bathe '82 and Cook '81). In its simplest form, a structure is partitioned into a finite number of discrete elements, which are defined by their relative geometric orientation, and behavioral stiffness in variational or weighted residual form. The governing equations of equilibrium are discretized spatially over the structure, and the solution is expressed in the particular field of interest (displacements, strains, and stresses). The procedures used above are easily performed on a digital computer, which is largely responsible for the popularity of the method.

## 2.7 SUMMARY

As stated earlier, there are many complicated parameters which must be analyzed in a connection or opening detail to determine its strength and serviceability. An attempt has been made to introduce these parameters to the reader and give reasonable guidelines for their use in designing details for protective structures. Conclusions from each area of interest are assembled into two different groups: guidelines for design, and criteria for strength and serviceability. The guidelines were assembled from Section 2.2 and will be used for picking an acceptable detail to test. The results of the test will then be compared with the criteria discussed in Section 2.3 and a determination made on the performance of the particular detail.

## **2.7.1 Design Guidelines**

**2.7.1.1** Reinforcement ratios  $A_s/bd$  should be limited to a range of 0.5% to 0.75% for slab/wall connections. This ratio may be increased for beam/column applications; however, crossties in the joint region should be designed accordingly.

**2.7.1.2** Stirrups for diagonal shear are required in all beam/column joints in accordance with;

- ACI 318-83 Type Two connections for shear and confinement (Eqs. 1 and 2), and
- Park and Paulay '75, requirements for diagonal splitting (Eqs. 3 and 4).

**2.7.1.3** Reinforcement terminating in a knee joint should be developed in a 180-deg bend with the return leg embedded in the opposing force region.

**2.7.1.4** Reinforcement terminating in a tee joint should be developed in a 90-deg hook with the legs extending through the midheight of the connection (Eq. 8).

**2.7.1.5** Minimum clear cover for reinforcement should exceed  $2d_b$  and the minimum bar spacing should exceed  $3d_b$  for limiting the effects of splitting cracks as set forth in the ACI 318-89 code.

**2.7.1.6** Diagonal haunches or splays should be added to all inside corners.

**2.7.1.7** Diagonal reinforcement equal to half the area of the main flexural steel is required at all inside corners.

**2.7.1.8** A hinge should not occur in the joint region.

2.7.1.9 Precast connections should be posttensioned to eliminate the formation of gaps which could allow the contamination of the facility.

## 2.7.2 Strength and Serviceability Criteria

2.7.2.1 The "ductility factor" ( $\mu$ ) should not exceed 1, and deflections should not exceed approximately  $L/240$  at midspan. The value for deflections may be altered by the designer depending on the structures requirements.

2.7.2.2 Average compressive stress due to flexure in the concrete immediately above the compression reinforcement should not exceed  $0.45 * f'_c$ .

2.7.2.3 Tensile and compressive stress in the reinforcement located in the elements should not exceed  $2/3 f_y$ .

2.7.2.4 Tensile and compressive stress in the reinforcement located in the joint region should not exceed  $1/3 f_y$ .

2.7.2.5 Direct shear at any point in the structure should not exceed the Hawkins shear limit  $\tau_u * 0.8$  (Eq. 9).

2.7.2.6 Diagonal shear in slab/walls should not exceed  $[0.85(4)(f'_c)^{1/2}]/\alpha$ . For values of shear higher than this, stirrups must be added in accordance with ACI 318-83 Type Two connections.

### 3.0 RESEARCH APPROACH

#### 3.1 METHODOLOGY

The approach adopted for this study incorporates the finite element method for simulating and studying the structural response for connections, openings, and attachments. The simulation will use structural details (selected from previous research) which provide the desired behavioral characteristics under static and seismic loads and subject them to a conventional blast load. From the results of the numerical tests, candidates for these details will be chosen based on their behavioral performance. The detailing concepts of each structural candidate can then be subjected to physical testing under actual impulsive loads.

#### 3.2 FINITE ELEMENT APPROACH

The accuracy and reliability of addressing structural problems with a finite element method depends on four factors:

- A code that has the capacity to treat the numerical simulations with a high degree of precision,
- The correctness of the overall geometry of the model with boundary conditions and loading functions,
- Compatibility of individual element mesh size and type with the problem configuration,
- Reliable constitutive models that represent the physical properties of the materials used in the structure.

##### 3.2.1 Code Reliability

The first factor can be achieved by using a code with proven reliability in the area of analysis similar to the problem in

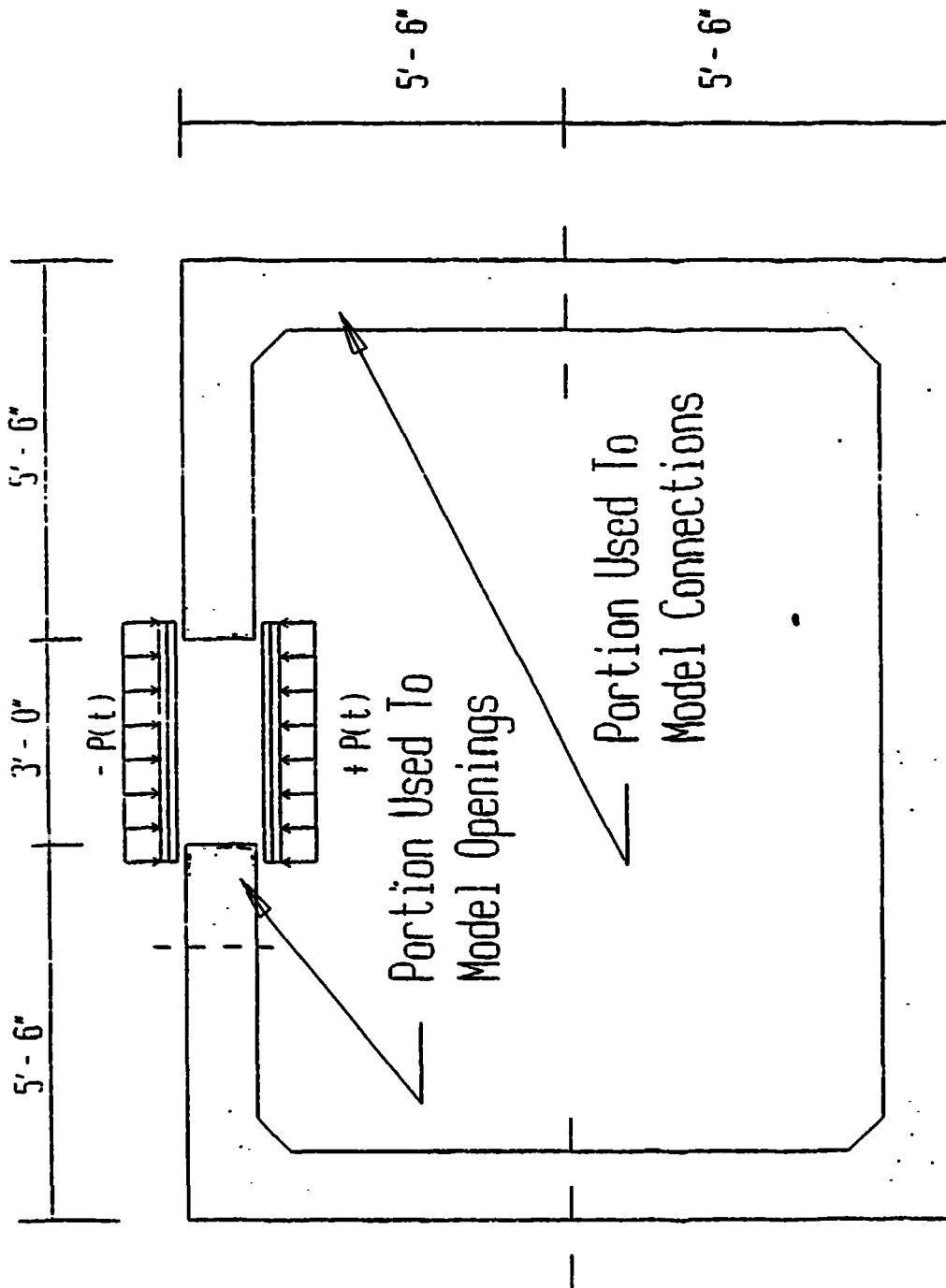


Figure 13. Blast resistant structure with openings.

question. The finite element code used in the present study is SAMSON2 (Schreyer, et al. '84). SAMSON2 has been written explicitly for studying structures subjected to high rates of loading. Various researchers have used SAMSON2 successfully for these types of analyses. Two of the three factors are discussed in the following subsections, and the last factor will be treated in a separate section due to the amount of material covered.

### 3.2.2 Geometry

The geometrical approach used to model beam/column connection behavior is similar to that used by Nilsson '73. The column is rigidly attached at its base (mid-height between stories), and the beam is cantilevered approximately one-third of a typical span length. This method was chosen in order to predict a worst-case scenario (i.e., beam/slab discontinuity due to openings or localized failure) (Fig. 13). A concentrated blast load (as discussed in Section 3.4) was then applied to the end of the cantilever. Although the details represent beam/column configurations, the actual simulation could also model wall/slab structures by analyzing a slice through the structure and assuming that each such section is subjected to worst-case loadings. This approach does not consider three-dimensional load distributions in the slab for two reasons. The blast load under consideration is somewhat uniform over the width of the structure and the susceptibility to repeated loading is likely. Typically a continuous slab/wall structure modelled in two dimensions would utilize plane strain analysis; however, due to the observations noted above, plane stress analyses have been performed.

### 3.2.3 Element Compatibility

The concrete was modeled with a mesh composed of quadratic 8-node parabolic and 6-node triangular elements. The cost of

using parabolic elements is greater than that of 4-node rectangular elements. However, this cost is offset by the fact that parabolic elements are capable of modeling exactly a constant bending moment (Bathe '82). The additional reliability of the elements will allow the use of a coarser mesh while yielding accurate predictions.

A  $(3 \times 3)$  order of integration is required for evaluating exactly the stiffness matrix of a parabolic element (Bathe '82). However, this integration order would overestimate the system stiffness due to a finite element displacement formulation based on a lower bound of the exact strain energy of the system. For this reason, a  $(2 \times 2)$  order of integration will be implemented to reduce the system stiffness and improve the stress and strain predictions. The drawback of using a reduced integration scheme is the creation of one or more spurious zero energy modes, which may give unstable solutions. This problem can be averted if the directionality of the elements is controlled with the expected deformations (Bathe '82).

The element mesh size was refined until a change in stress of 5% or less was observed between adjacent elements. This procedure was completed by recording the principal stresses at an integration point near the area of interest. These stresses are then compared to the stresses recorded at the neighboring integration point of an adjacent element. The deviation of 5% was chosen as a reasonable upper bound based on a loading function known to be inaccurate to 5%. The data provided by Coltharp et al. '85 exhibited significant scatter of peak pressures, and in general the loads corresponding to High Explosive (HE) detonations cannot be predicted accurately. This mesh was then compared to a further refined mesh with a stress deviation of less than 5% recorded at identical points. This final check assures that the solution is converging with mesh refinement and therefore the solution is not mesh dependent.

See Figures 14 and 15 for an example of the final coarse mesh model used in the report, with the fine mesh used in the comparison of stress deviation.

Steel reinforcement was modeled using bar elements connected to the midline nodes of the concrete elements. By using discrete reinforcement, stresses in the bars can be measured directly. From these data determinations can be made on the efficiency of the detail under investigation. For example, bars that are highly overstressed may be increased in size or relocated for better performance. Provisions for bond slip and bond failure are not implemented directly in the connection of the bar elements with the concrete. However, when a bar element is stressed to near yield conditions, the concrete elements directly connected to the bar will probably be highly damaged and offer little resistance to deformation. The high strains exhibited should correspond well to slippage experienced during actual bond loss. For this reason, the resulting bar behavior simulated very well the physical properties of reinforcement bond with accurate stress and strain contours (see background on reinforcement bond discussed earlier in Section 2.4.3).

### 3.3 CONSTITUTIVE MODELS

The use of reliable material models is the most predominant factor in obtaining accurate solutions from a finite element analysis. The two major materials under investigation in this report are concrete and steel, the latter being a fairly easy material to model due to its accurate representation by the theories of elasticity and plasticity in the static domain and viscoplasticity for dynamic response. Concrete, however is a much more difficult material to model due to its highly complex behavior under postelastic loading.



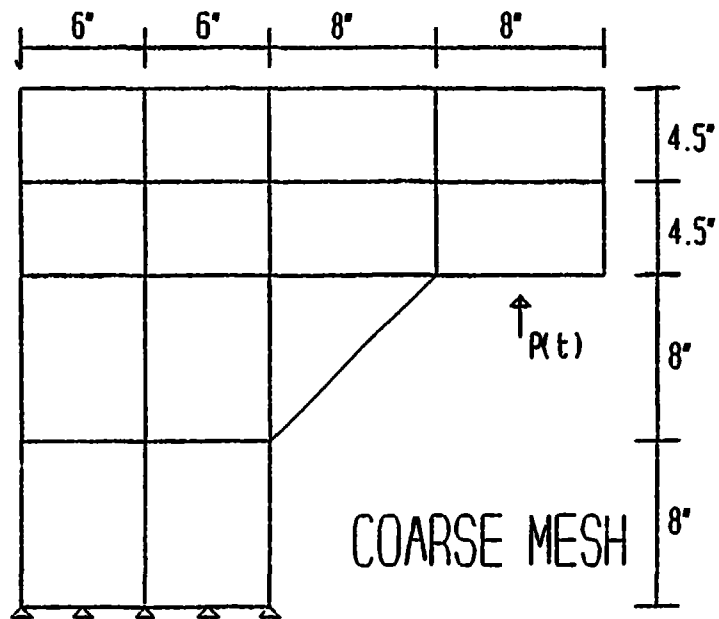


Figure 14. Coarse mesh used for comparison of stress deviation.

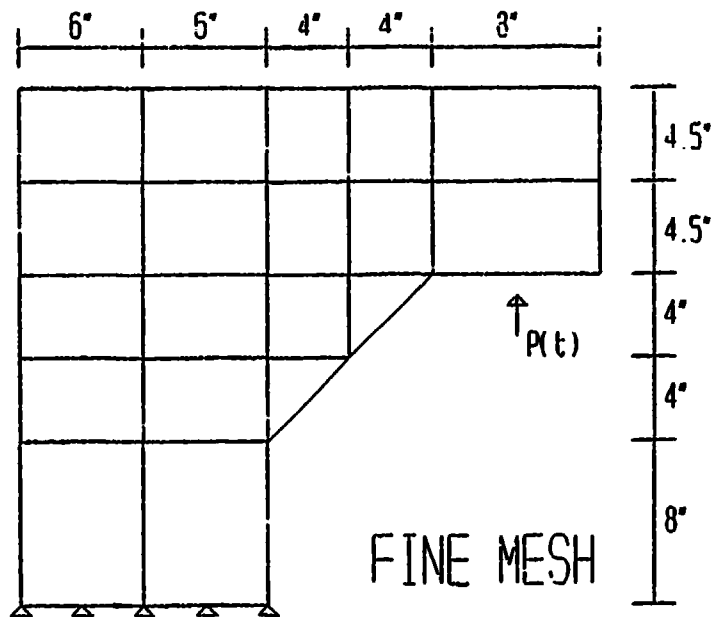


Figure 15. Fine mesh used for comparison of stress deviation.

### 3.3.1 Concrete Modeling

The subject of modeling concrete has been the topic of numerous research reports, with many different types of constitutive models proposed over the last 20 years. For this study, the finite element code SAMSON2 (Schreyer, et al. '84) has been modified with a constitutive nonlocal damage plasticity model by Stevens and Krauthammer '88 developed at the University of Minnesota. The following discussion on concrete behavior and constitutive modeling is based primarily on the above report, on Schreyer and Bean '87, and on Park and Paulay '75.

Microcracking is common to all types of concrete, caused primarily by strain incompatibilities produced in the hydration process of the cement paste (Hsu et al. '63). Up to about 30% of  $f'_c$  in compression these cracks do not appear to grow and the resulting stress-strain response is nearly linear elastic as shown in Figure 16. Between 30 to 50% of  $f'_c$ , these cracks will increase to a stable final length if the load remains constant. This portion of the stress-strain curve becomes increasingly nonlinear with a decreasing positive slope. At about 75% of  $f'_c$ , these microcracks will again begin to grow along with cracks between the aggregate and mortar. Locations where both of these cracks are present are defined as "zones of damage," and the cracks are usually accompanied with the increase of volumetric strain (Schreyer and Bean '87). After the peak stress  $f'_c$  is reached, a descending curve known as the strain-softening portion develops. Unloading of the concrete in this region is accompanied with permanent deformation, and the slope of this curve decreases as the point of unloading moves to the right. Furthermore, softening in concrete is a result of damage accumulation (Read and Hegemier '84) and should be accounted for in the analysis.

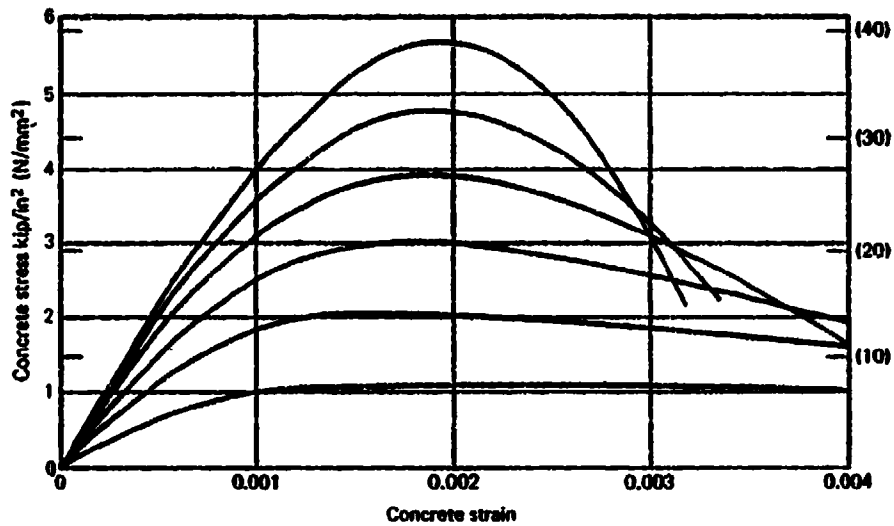


Figure 16. Uniaxial stress-strain curve for concrete in compression. (Park and Paulay '75)

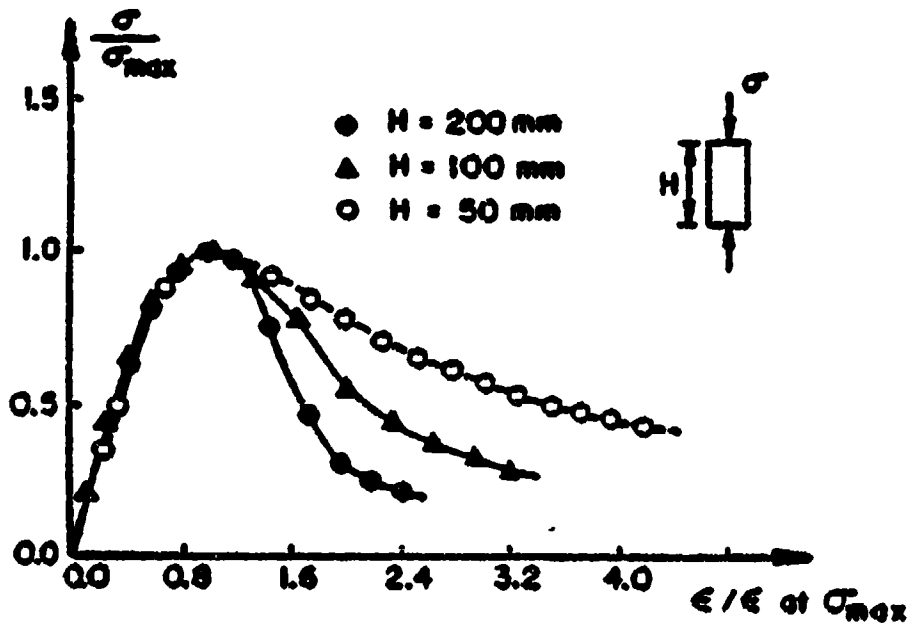


Figure 17. Uniaxial stress-strain curves for concrete specimens of different height. (Chen '82)

Plots of stress-strain curves shown in Figure 17 indicate that strain softening is a function of specimen size and therefore not a true continuum material property. The phenomenon of strain softening is primarily due to an increase of inhomogeneity in the material caused by extensive cracking in the mortar. In this phase the internal frictional resistance at the crack interfaces is the main load resisting mechanism (Read and Hegemier '84). This friction is also responsible for the accumulation of permanent deformation during unloading (Fig. 18).

Concrete in tension will exhibit behavior similar to that of compression, but to a much smaller ultimate capacity; usually the splitting tensile strength of concrete ( $f'_t$ ) is approximately equal to 10% of the compressive strength ( $f'_c$ ) (Fig. 19). Under careful displacement controlled tensile loading, concrete will show a surprising amount of ductility with a strain softening region. For analysis, a linear elastic curve is commonly used up to the point of rupture, with a modulus similar to that of concrete in the early stages of compression.

Formulation of Stevens and Krauthammer's ('88) constitutive nonlocal damage plasticity model is shown Appendix A and is taken directly from their report. In the compression domain, the model utilizes a combination of plasticity and continuum damage mechanics theories with a nonlocal definition of a scalar damage variable to model strain softening. Figure 20 illustrates the transformation of topical material ( $A_t$ ) to damaged material ( $A_d$ ), and the respective internal acting force vectors ( $F^t$ ) and ( $F^d$ ).

The use of a nonlocal damage approach allows the successful inclusion of strain softening effects without the shortcomings (mesh dependency, unrealistic energy dissipation, etc.) that occur in a typical unstabilized strain softening calculation. Stevens and Krauthammer '88 combined this model with a Timoshenko beam element which requires the use of a nonlocal definition.

The cross section of their beam is modeled with one element. If the strain softening is not averaged to the adjacent integration points, failure will commence immediately upon initiation of the damage - a situation which is highly unstable and unrealistic. The mesh used in the present report eliminates the effects of local instability through two different methods. (1) The continuum elements are divided into small regions through each cross section, which enables the structure to retain load-carrying capacity after a particular element has been completely damaged. (2) Steel bar elements located in a damaged zone will continue to carry load in a manner similar to that of reinforced concrete.

The plasticity portion of the model uses a modified Drucker-Prager failure surface which incorporates a curved cap closure of the surface as it opens out along the compressive hydrostatic axis (Fig. 21). This model, developed by Schreyer and Bean '87, has been called a Prager-Drucker model to distinguish it from the previous one. The general flow rule for this model is associative; however, under low compressive or tensile hydrostatic applications, a nonassociated flow rule will provide more reasonable results as shown in Appendix A.

This model is assumed to be isotropic with respect to damage. However, since concrete reaches the strain-softening region in tension at about 10% of that in compression, an artificial restraint has been applied in order to assure an accurate amount of energy dissipation. The normal tensile stresses are reduced by a factor of 10. Since the overall behavior of a concrete structure is not significantly affected by the tensile strength of concrete, this modification is not viewed as a severe limitation.

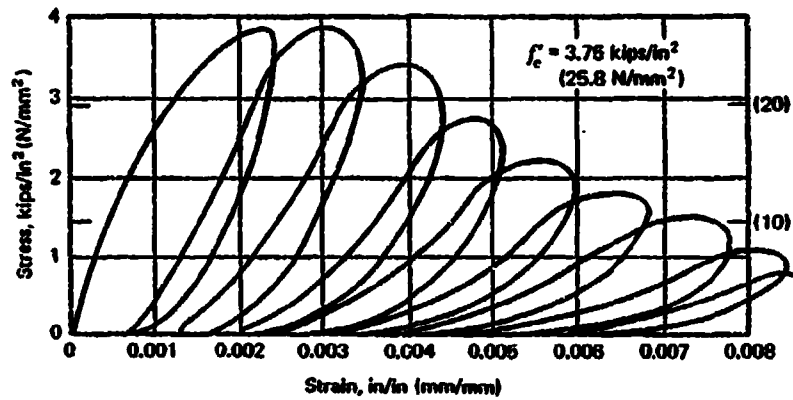


Figure 18. Uniaxial stress-strain curves for concrete under compressive cyclic loading. (Park and Paulay '75)

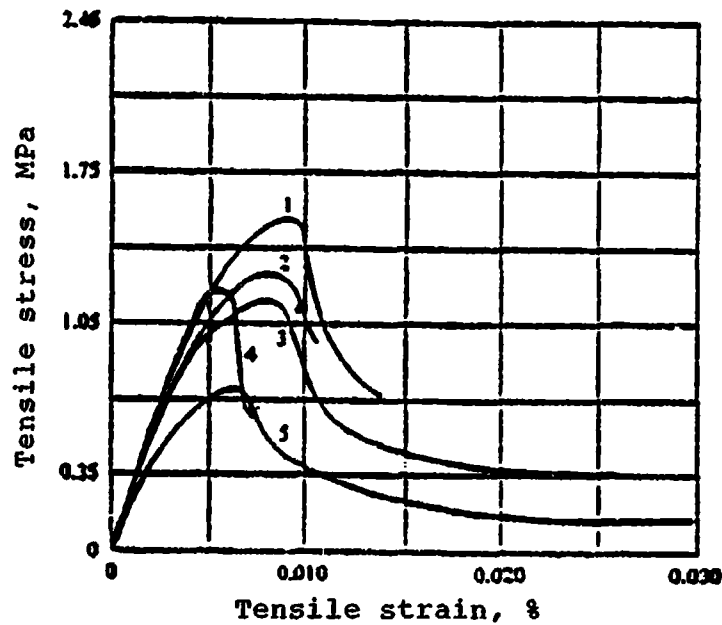


Figure 19. Uniaxial stress-strain curves for concrete in tension. (Chen '82)

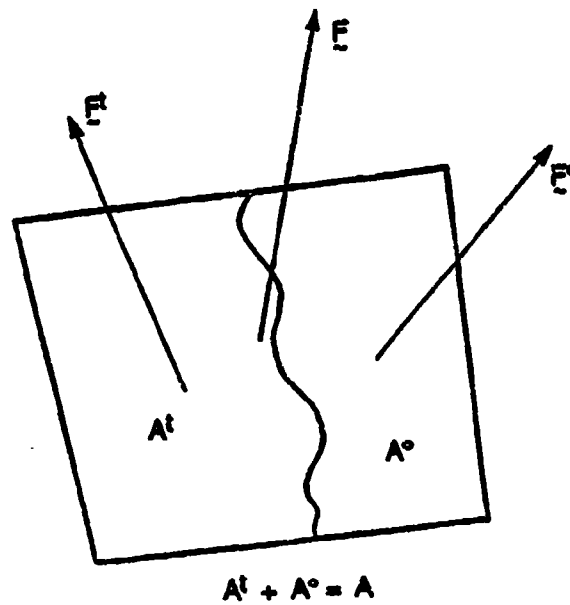


Figure 20. Topical and undamaged material area representation.  
(Stevens and Krauthammer '88)

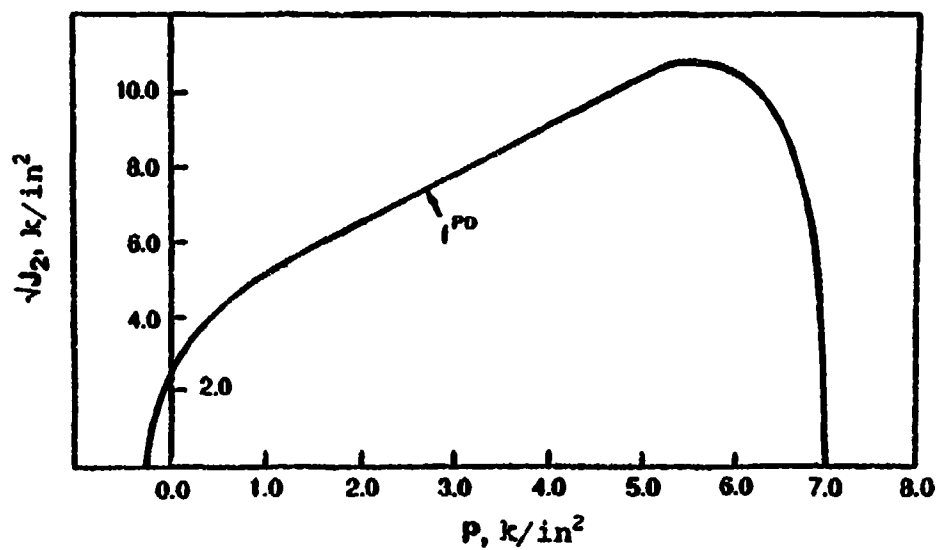


Figure 21. Prager-Drucker yield surface.  
(Stevens and Krauthammer '88)

### 3.3.2 SIFCON Modeling

SIFCON (Slurry Infiltrated Fiber Concrete) is a relatively new construction material and consequently there is very little known about its mechanical properties. A comprehensive study completed by Homrich and Naaman '88 deals directly with these properties and will be used extensively in this discussion. SIFCON composites are similar to standard concrete in that the mortar portion of the matrix is developed from the hydration of cement and water. The main difference between the two is related to the material bonded together by the mortar. Instead of rock aggregate, SIFCON uses a large volume (from 8% to 20%) of small steel fibers. To produce a SIFCON element, these fibers are placed into a mold filling it to capacity. The remaining fiber network is infiltrated with a cement-based slurry or fine mortar. The resulting stress-transferring behavior involves frictional and mechanical interlock between fibers along with the usual bond of the matrix.

Three types of fibers (crimped, hooked, and deformed) were tested by Homrich and Naaman '88. Of these fibers, deformed wires (length = 30 mm, and width = 0.5 mm) performed the best in both the compressive and tensile regions. Another factor in the behavior of SIFCON is the orientation of the fibers with the direction of loading. Stress-strain curves for wires placed normal, perpendicular, and random to this direction are available for comparison. For analysis purposes, the mechanical properties of SIFCON (using 12% by volume deformed wires averaged in proportion to directionality) will be used in the present study.

Based on data by Homrich and Naaman '88 (Fig. 22), the peak compressive stress  $f'_c$  is set at 12,000 lb/in<sup>2</sup>; the peak tensile stress  $f'_t$  is set at 1800 lb/in<sup>2</sup>; and the modulus of elasticity  $E_c$  is set at 1,200,000 lb/in<sup>2</sup>.



The ascending branch of a stress-strain curve for SIFCON in compression and tension (Fig. 22) is very similar to that of standard concrete, with the differences located in the peak values and slopes. For this reason, the constitutive model shown above (concrete coupled with the adjusted values for  $f'_c$ ,  $f'_t$ , and  $E_c$  of SIFCON) should give reliable results. However, the descending portion of the curve shows a behavior slightly different than that for concrete in the strain-softening region. SIFCON will tend to show a slowly decaying shape in the postpeak stress-strain region, indicating a higher degree of ductility than concrete. Absi and Naaman '86 have proposed an equation to model this behavior; however, the incorporation of such a model into a finite element code is beyond the scope of this report, and was not performed here. The method is not compatible with the strain softening damage model, but the damage model will give results that are a reasonable lower bound on the behavioral stiffness of a SIFCON structure subjected to blast loading.

### 3.3.3 Steel Reinforcement Modeling

The behavior of steel used as reinforcement for concrete is well documented and easily modeled. Typical stress-strain curves developed from uniaxial tensile tests show clearly the response of steel in the elastic and plastic ranges (the lower curve Fig. 23). The initial ascending portion of the curve will follow a linear pattern until the strain reaches approximately 0.002, defined as the upper yield point. After this point the curve will drop slightly to the true characteristic yield point. Beyond yielding, the curve will become linear again with a much smaller slope than the initial. This is referred to as the plastic range. Unloading from this range will follow a descending curve parallel with the initial elastic curve. For higher grades (grade is based on the stress at yield) of steel, hardening will commence immediately after yield. The yield stress for steels in this range will typically correspond with a

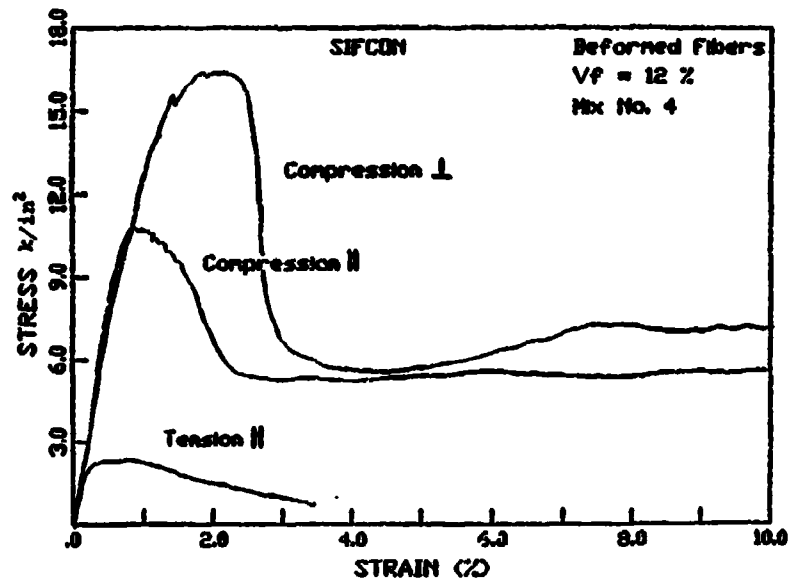


Figure 22. Comparison between compression and tension response of SIFCON. (Homrich and Naaman '88)

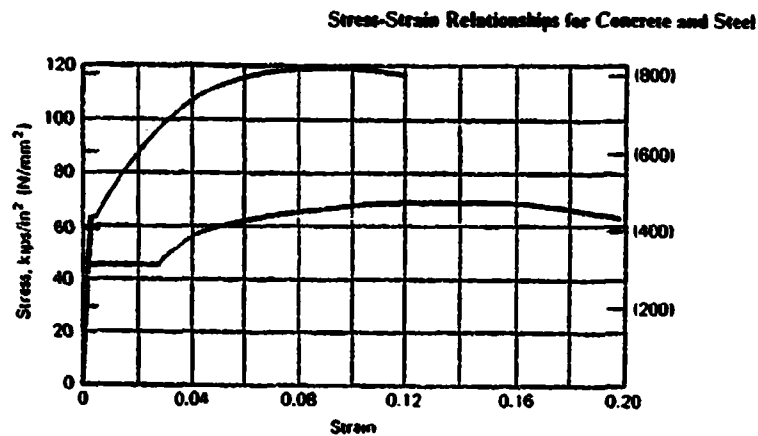


Figure 23. Typical stress-strain curves for steel reinforcement. (Park and Paulay '75)

strain of 0.005 (Park and Paulay '75) (the upper curve in Fig. 23). Strain rate effects on the material properties of steel are minimal for grades over 50 k/in<sup>2</sup>; therefore, they have not been included in the constitutive model.

#### 3.3.4 Conclusions

The proposed model shown in Appendix A accurately predicts the significant material responses of plain concrete for stress paths that remain in the compressive hydrostatic regions. Most importantly, it provides a unified, consistent approach to concrete modelling in both the tensile and compressive hydrostatic regions. The number of material constants required is large and could possibly be simplified. Constants for a modified "Prager-Drucker" cap model are listed in Table 3. If extensive multiaxial test data are available, the material constants may be found with a trial and error approach or a parameter estimation technique; if laboratory test data are not available, then adequate material values for typical low-, medium-, and high-strength concretes may be taken from Tables 4, 5, and 6, respectively.

#### 3.4 DYNAMIC RATE EFFECTS

As outlined in Section 2, rate effects of dynamic loading have been shown to alter the behavior of a structure. Various factors have been proposed for modifying material models subjected to high rate loadings. This approach may be practical for simple member analysis, but in no way does it approximate the complicated phenomena experienced by concrete under high rates of loading (Stevens & Krauthammer '88). Due to the limited amount of data available on this subject, Stevens and Krauthammer '88 have not included rate effects in the concrete model. This may appear to be a large assumption; however, based on the results shown in Section 3.6, it appears to be an adequate one.

TABLE 3. Modified Prager-Drucker cap model constants.  
(Stevens and Krauthammer '88)

Prager-Drucker Cap Model			
$f'_c = 7000. \text{ lb/in}^2$	$E = 6400. \text{ k/in}^2$	$\nu = 0.20$	$a_f^p = 0.0030$
$\alpha = 0.60$	$\beta = 1.25$	$n = 0.50$	$h_o = 0.60$
$P_c = -250. \text{ lb/in}^2$	$m = 0.65$	$S_m = 25. f'_c$	$q = 0.35$
$c_1 = 0.40$	$c_2 = 1.0$	$c_3 = 1.0$	$c_{cap} = 0.70$
$P_o = 7000. \text{ lb/in}^2$	$P_{co} = 7000. \text{ lb/in}^2$		

TABLE 4. Low-strength concrete parameters.  
(Stevens and Krauthammer '88)

Prager-Drucker Cap Model			
$f'_c = 3000. \text{ lb/in}^2$	$E = 4350. \text{ k/in}^2$	$\nu = 0.25$	$n = 0.50$
$a_f^p = 0.0032$	$\alpha = 0.60$	$\beta = 1.25$	$h_o = 0.50$
$P_c = -145. \text{ lb/in}^2$	$m = 0.75$	$S_m = 25. f'_c$	$q = 0.50$
$c_1 = 0.50$	$c_2 = 1.0$	$c_3 = 1.0$	$c_{cap} = 0.70$
$P_o = 11600. \text{ lb/in}^2$	$P_{co} = 4741. \text{ lb/in}^2$		
Continuum Damage Mechanics Model			
$d_u = 0.875$	$r_o = 0.0038$	$B = 1.30$	$A_{te} = 600.$
$\eta = 0.001 \text{ lb/in}^2$	$C = 8.0$	$D = 10.0$	$A_{co} = 50.$
Nonassociated Flow Rule			
$\phi = 0.10$	$\theta = 0.001$	$\Omega = 0.003$	$\omega = 2.0$

TABLE 5. Medium-strength concrete parameters.  
(Stevens and Krauthammer '88)

Prager-Drucker Cap Model			
$f'_c = 7000. \text{ lb/in}^2$	$E = 4240. \text{ k/in}^2$	$\nu = 0.19$	$n = 0.27$
$\epsilon'_c = 0.0027$	$\alpha = 0.50$	$\beta = 1.50$	$h_o = 0.50$
$P_c = -200. \text{ lb/in}^2$	$m = 0.75$	$S_m = 25.f'_c$	$q = 0.30$
$c_1 = 3.60$	$c_2 = 0.50$	$c_3 = 5.0$	$c_{cap} = 0.98$
$P_o = 4000. \text{ lb/in}^2$	$P_{co} = 3000. \text{ lb/in}^2$		
Continuum Damage Mechanics Model			
$d_u = 0.875$	$r_o = 0.0035$	$B = 1.30$	$A_{to} = 700.$
$\eta = 0.0005 \text{ lb/in}^2^{-1}$	$C = 8.0$	$D = 10.0$	$A_{co} = 50.$
Nonassociated Flow Rule			
$\phi = 0.10$	$\theta = 0.001$	$\Omega = 0.003$	$\omega = 2.0$

TABLE 6. High-strength concrete parameters.  
(Stevens and Krauthammer '88)

Prager-Drucker Cap Model			
$f'_c = 10700. \text{ lb/in}^2$	$E = 4300. \text{ k/in}^2$	$\nu = 0.20$	$n = 0.40$
$\epsilon'_c = 0.0025$	$\alpha = 0.60$	$\beta = 1.25$	$h_o = 0.70$
$P_c = -500. \text{ lb/in}^2$	$m = 0.75$	$S_m = 25.f'_c$	$q = 0.50$
$c_1 = 0.50$	$c_2 = 1.0$	$c_3 = 5.0$	$c_{cap} = 0.70$
$P_o = 30000. \text{ lb/in}^2$	$P_{co} = 15700. \text{ lb/in}^2$		
Continuum Damage Mechanics Model			
$d_u = 0.875$	$r_o = 0.0028$	$B = 1.30$	$A_{to} = 1000.$
$\eta = 0.0008 \text{ lb/in}^2^{-1}$	$C = 8.0$	$D = 10.0$	$A_{co} = 50.$
Nonassociated Flow Rule			
$\phi = 0.10$	$\theta = 0.001$	$\Omega = 0.003$	$\omega = 2.0$

### 3.5 LOADING FUNCTIONS

The magnitude and time pulse history of the blast load were determined through interpolation of data shown by Coltharp, et al. '85. Figure 24 shows the spatial distribution of peak pressure on a 4- by 2.3-m box culvert subject to the nearby detonation of a HE device. A 20-in-wide strip was superimposed on the proposed pressure grid at the worst-case location. The pressure was then converted to a concentrated load which will act on the end of a cantilever beam. The respective areas, pressures and loads are as shown: The peak pressure of 60 MPa occurred over an elliptical region approximately 21.6 in high by 30 in wide. This region was divided into two beams spanning to opposite supports. The equivalent concentrated load from this region plus the adjacent zone of 50 MPa at 4 in wide is set at;

$$\begin{aligned} & (21.6 \text{ in}/2) * (20 \text{ in}) * (60 \text{ MPa}) * (144.5 \text{ lb/in}^2/\text{MPa}) = 1873 \text{ k} \\ & + (4.0 \text{ in}) * (20 \text{ in}) * (50 \text{ MPa}) * (144.5 \text{ lb/in}^2/\text{MPa}) = 578 \text{ k} \\ & \text{Resultant Peak Load} \quad P(t)/2 = \dots\dots\dots 2451 \text{ k} \end{aligned}$$

Adjacent lower pressure regions dissipated fairly rapidly, and therefore were not included in the calculation of the load. Ostracizing this pressure may seem unconservative; however, as stated earlier, no load reduction based on distribution to adjacent elements is considered (a conservative assumption which should more than offset the latter).

Based on the same report by Coltharp et al. '85, the time history of the load was modeled similar to that shown in Figure 25. The rise time to first peak ( $t_r$ ) was set at 0.04 ms. The duration of positive pressure ( $t_d$ ) was set at 0.53 ms (Fig. 26). Openings were tested on a load/(1 ft) basis. Therefore, the loading function described above for connections has been reduced by a factor of (12/20) for openings with a resultant peak load  $P(t)/2 = 1471 \text{ k}$  (Fig. 27).

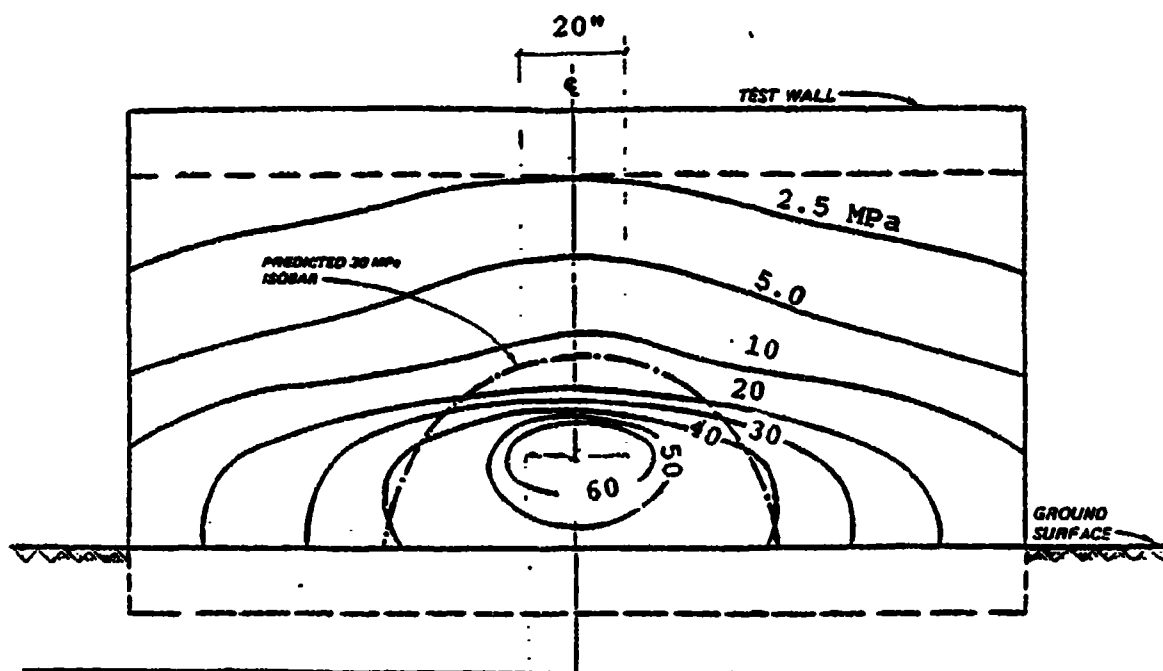


Figure 24. Distribution of peak pressure on a box culvert subjected to blast loading. (Coltharp et al.'85)

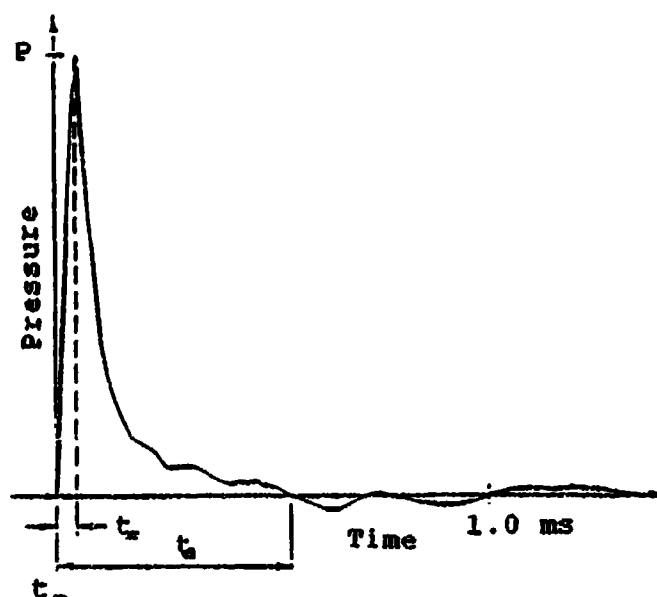


Figure 25. Typical incident pressure trace. (Coltharp et al.'85)

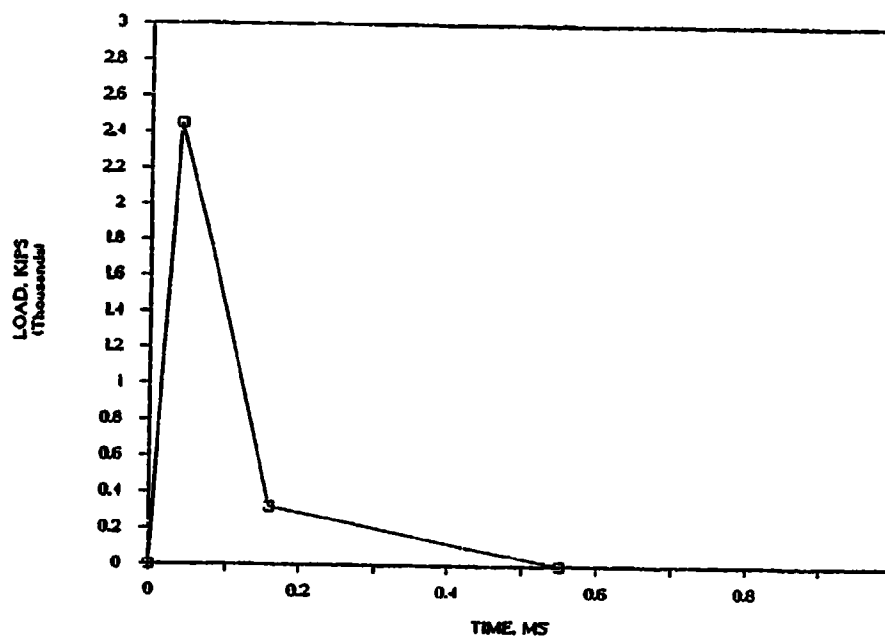


Figure 26. Applied loading function for connection details.

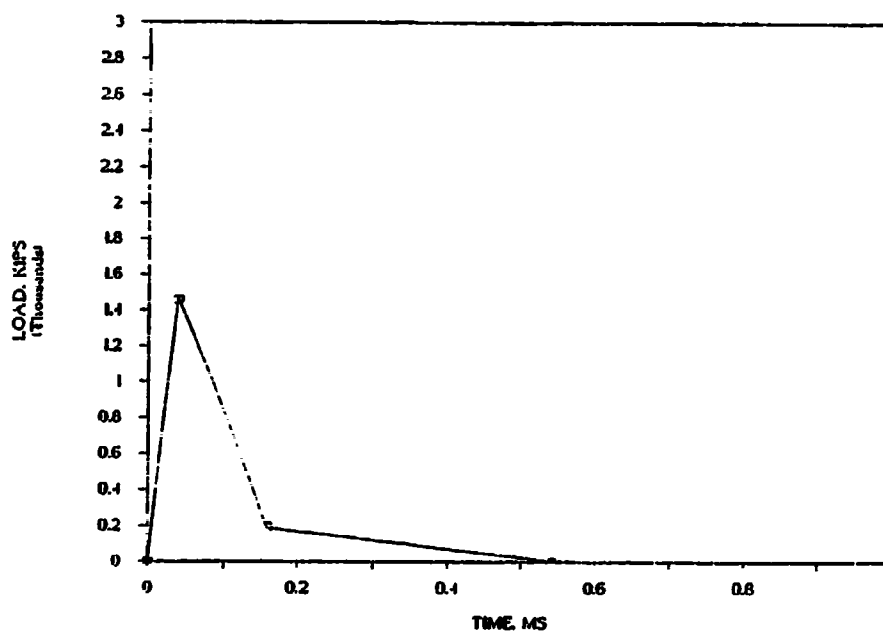


Figure 27. Applied loading function for opening details.



### 3.6 MODEL CALIBRATION

The adequacy of this procedure was checked by modeling two simply supported reinforced concrete beams subjected to an impact load at midspan. The models simulate tests completed on two beams C1 and H1 by Feldman and Siess '58. Figure 28 presents the test setup along with the respective cross sections and geometries. Figures 29 through 32 indicate the loading functions delivered by the gas-operated ram used for the experiment and the estimated piece-wise linear interpretation used in the simulations respectively. Figure 33 shows a deflected shape after loading; note that large permanent deflections were sustained by both beams (approximately 2.5 and 8 in for C1 and H1, respectively). Figure 34 shows the deflected shape of beam H1 in the simulation with contours of principal stress gradients.

The simulation was completed by using the methods described in Sections 3.2 and 3.3. The mesh (Fig. 35) consists of elements similar to those used in the coarse mesh test shown in Figure 14 and altered slightly to fit the beam geometry. One-half of the beam was modeled in order to take advantage of symmetry. The recorded compressive strengths of concrete ( $f'_c$ ) were 5830.0 lb/in<sup>2</sup> and 5960.0 lb/in<sup>2</sup> (medium strength) for beams C1 and H1, respectively. Typical values found for medium-strength concrete were used for the remaining parameters required for the concrete constitutive model (Tables 7 and 8) (Schreyer and Bean '87, and Stevens and Krauthammer '88). The hydrostatic tension cutoff ( $P_t$ ) was decreased until the recorded maximum tensile stress in the principal direction reached approximately 0.10 ( $f'_c$ ) (Fig. 36). Steel reinforcement consisted of two #6 top bars, two #7 bottom bars, and #3 vertical shear ties with a measured yield of 46.1 k/in<sup>2</sup> and 47.2 k/in<sup>2</sup> for beams C1 and H1, respectively. Tables 9 and 10 give the remaining parameters which define the stress-strain curves of a Park and Paulay '75 steel constitutive model.

TABLE 7. Beam C1 concrete parameters.  
(Stevens and Krauthammer '88)

Prager-Drucker Cap Model			
$f'_c = 5830. \text{ lb/in}^2$	$E = 4350. \text{ k/in}^2$	$\nu = 0.20$	$n = 0.50$
$\epsilon'_c = 0.0030$	$\alpha = 0.60$	$\beta = 1.25$	$h_o = 0.60$
$P_c = -230. \text{ lb/in}^2$	$m = 0.65$	$S_m = 25. f'_c$	$q = 0.35$
$c_1 = 0.40$	$c_2 = 1.0$	$c_3 = 1.0$	$c_{cap} = 0.70$
$P_o = 12000. \text{ lb/in}^2$	$P_{co} = 5830. \text{ lb/in}^2$		
Continuum Damage Mechanics Model			
$d_u = 0.875$	$r_o = 0.0035$	$B = 1.30$	$A_{co} = 700.$
$\eta = 0.0005 \text{ lb/in}^2$	$C = 8.0$	$D = 10.0$	$A_{co} = 50.$
Nonassociated Flow Rule			
$\phi = 0.10$	$\theta = 0.001$	$\Omega = 0.003$	$\omega = 2.0$

TABLE 8. Beam H1 concrete parameters.  
(Stevens and Krauthammer '88)

Prager-Drucker Cap Model			
$f'_c = 5960. \text{ lb/in}^2$	$E = 4400. \text{ k/in}^2$	$\nu = 0.20$	$n = 0.50$
$\epsilon'_c = 0.0030$	$\alpha = 0.60$	$\beta = 1.25$	$h_o = 0.60$
$P_c = -230. \text{ lb/in}^2$	$m = 0.65$	$S_m = 25. f'_c$	$q = 0.35$
$c_1 = 0.40$	$c_2 = 1.0$	$c_3 = 1.0$	$c_{cap} = 0.70$
$P_o = 12000. \text{ lb/in}^2$	$P_{co} = 5960. \text{ lb/in}^2$		
Continuum Damage Mechanics Model			
$d_u = 0.875$	$r_o = 0.0035$	$B = 1.30$	$A_{co} = 700.$
$\eta = 0.0005 \text{ lb/in}^2$	$C = 8.0$	$D = 10.0$	$A_{co} = 50.$
Nonassociated Flow Rule			
$\phi = 0.10$	$\theta = 0.001$	$\Omega = 0.003$	$\omega = 2.0$

TABLE 9. Beam C1 steel reinforcement parameters.  
(Stevens and Krauthammer '88)

Park and Paulay Steel Model				
$f_y = 46.1 \text{ k/in}^2$	$f_u = 72.0 \text{ k/in}^2$	$\epsilon_y = 0.0016$	$\epsilon_{sh} = 0.0144$	$\epsilon_u = 0.150$

TABLE 10. Beam H1 steel reinforcement parameters.  
(Stevens and Krauthammer '88)

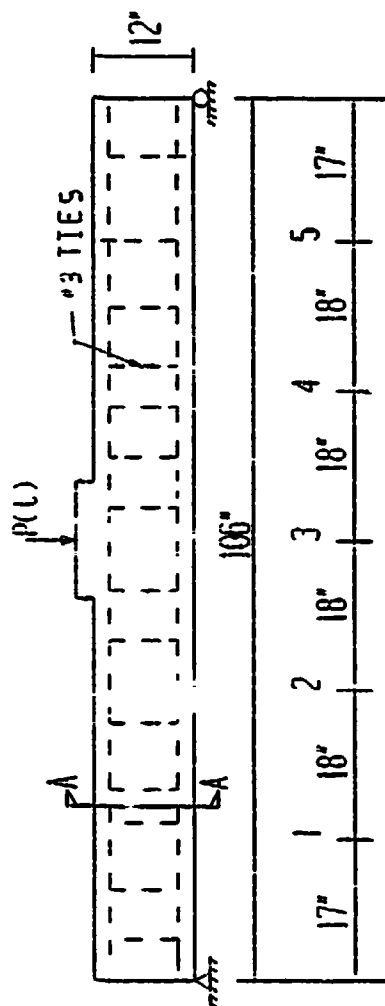
Park and Paulay Steel Model				
$f_y = 47.2 \text{ k/in}^2$	$f_u = 72.0 \text{ k/in}^2$	$\epsilon_y = 0.0016$	$\epsilon_{sh} = 0.0144$	$\epsilon_u = 0.150$

A comparison of the displacement behaviors between experimental data shown in Figures 37 and 38 (Feldman and Siess '58) and the calculated values shown in Figures 39 and 40 indicates a very good agreement between the two. The maximum displacements are shown below.

TABLE 11. Maximum displacement Beams C1 and H1

BEAM	MAX. DISPLACEMENT (inches)	
	(EXPER)	(SAMSON2)
C1	3.0	3.2
H1	8.4	7.2

Note that a large difference in displacement with a relatively small increase in load occurred between the two beams C1 and H1, which indicates a high degree of sensitivity to the loading function. Therefore the degree of accuracy in the simulation is limited to the accuracy in which the loading is interpreted. In conclusion, these results indeed show a good indication of the reliability and sensitivity of the finite element method used for this study.



Displacement Gage Locations

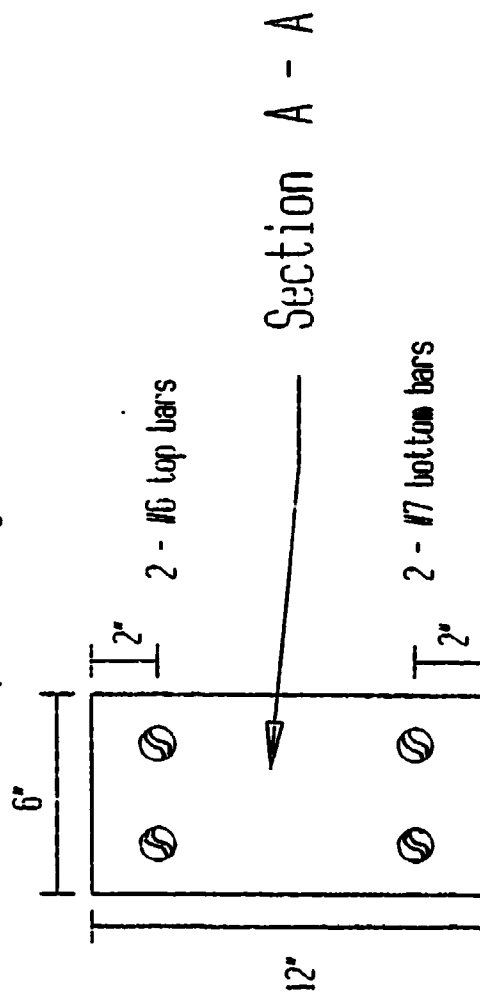


Figure 28. Geometry and instrumentation of Feldman and Siess beams.

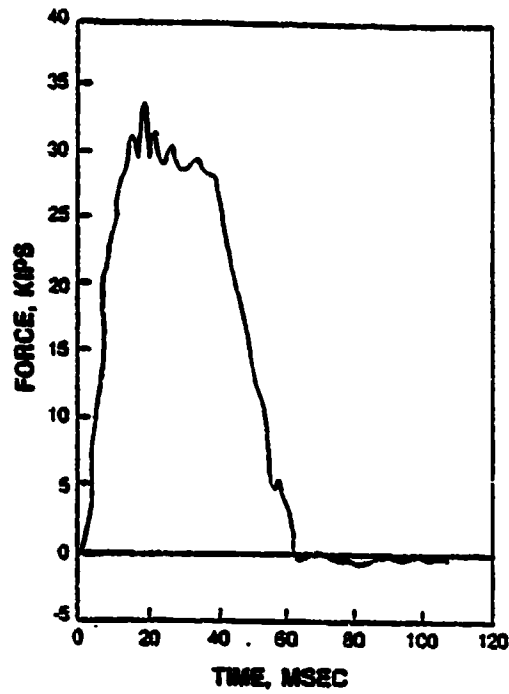


Figure 29. Applied midspan load of beam C1.  
(Feldman and Siess '58)

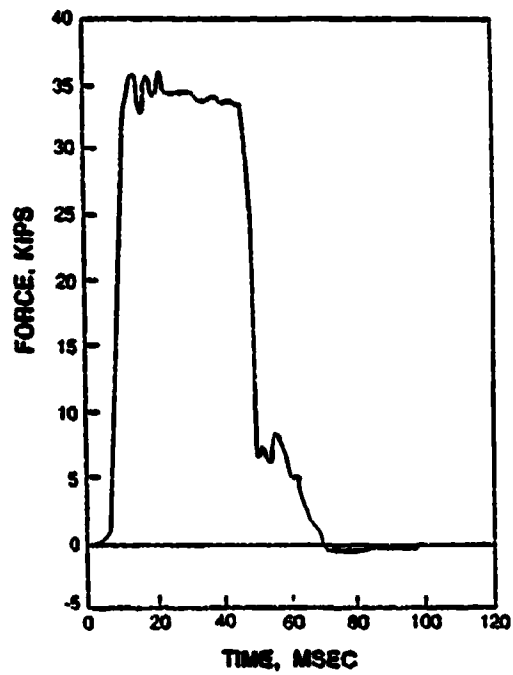


Figure 30. Applied midspan load of beam H1.  
(Feldman and Siess '58)

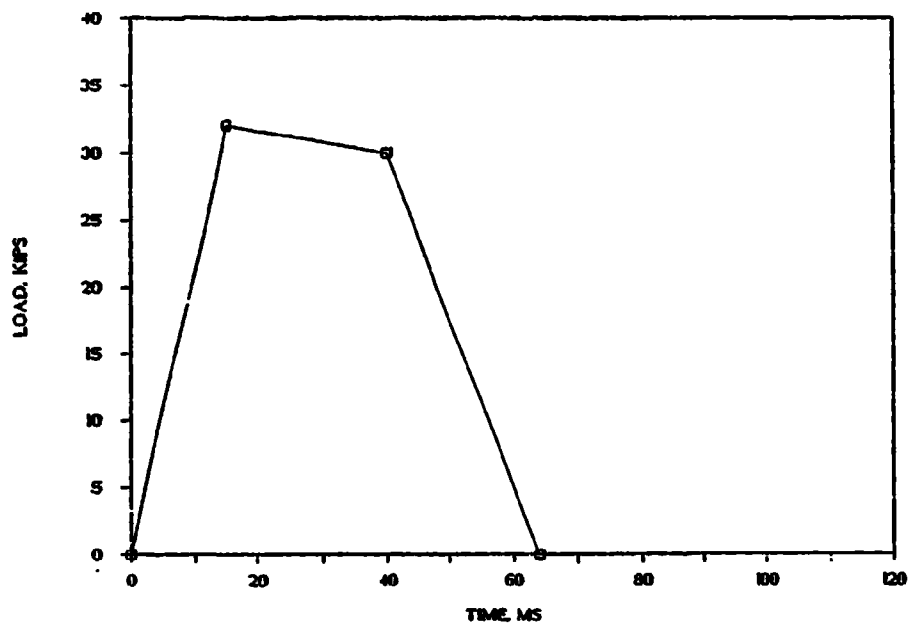


Figure 31. Applied analytical load of beam C1.

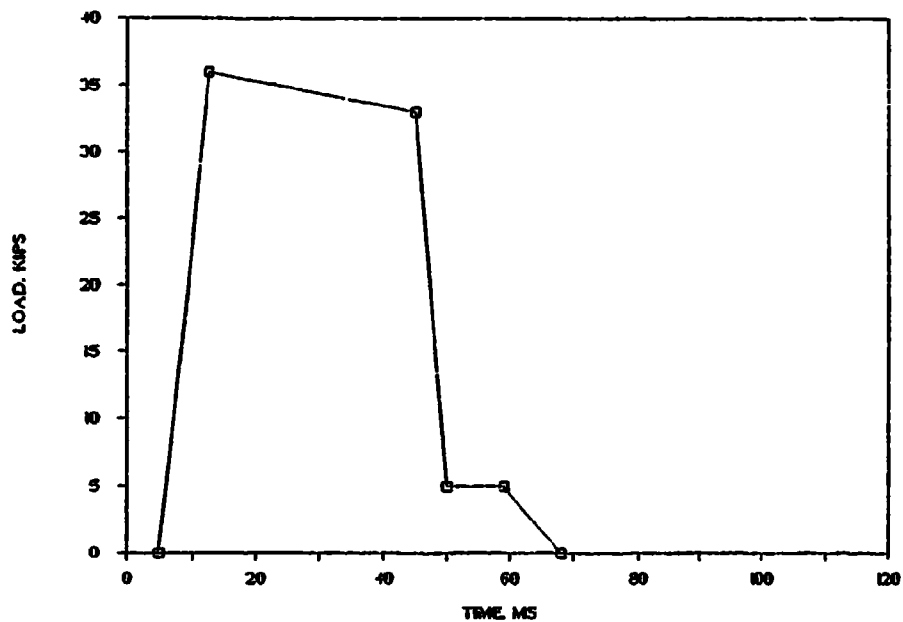


Figure 32. Applied analytical load of beam H1.

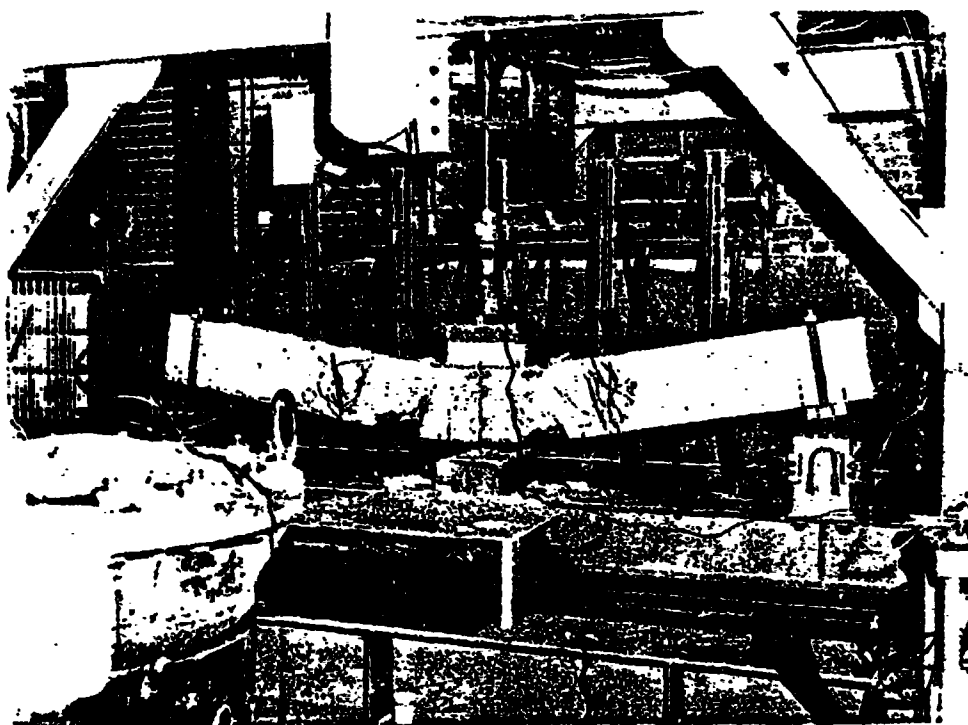
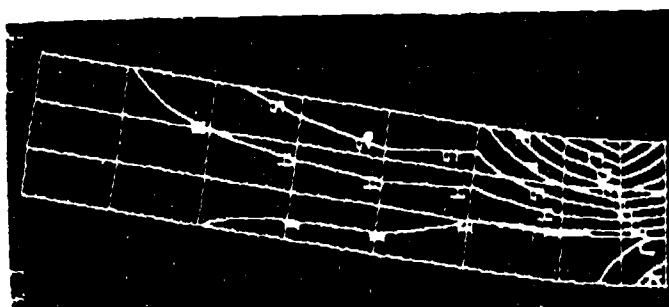


Figure 33. Impact loaded concrete beam H1.  
(Feldman and Siess '58)

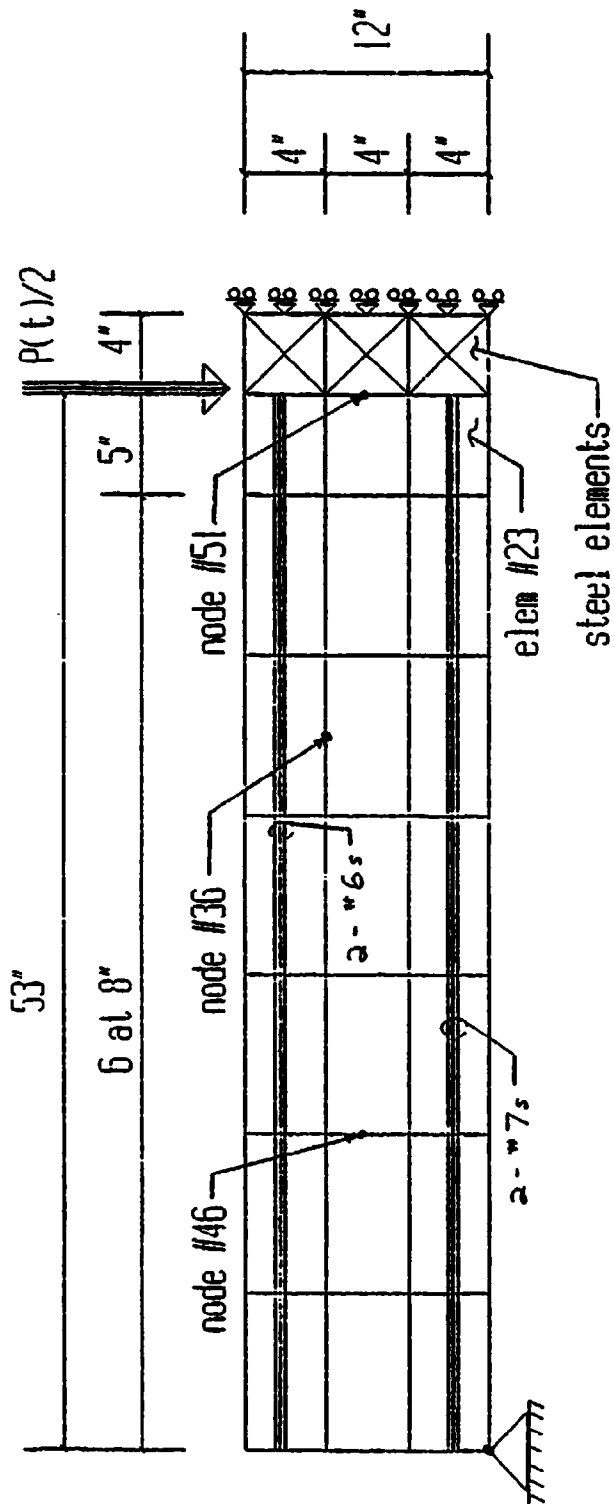


A = -7962	G = -1682
B = -6915	H = -635
C = -5868	I = 412
D = -4822	J = 1459
E = -3775	K = 2505
F = -2728	L = 3552

(values in lb/in<sup>2</sup>) 10

Figure 34. Analytically loaded model simulation of  
beam H1.





## Beams C1 and H1

Figure 35. Finite Element mesh model for beams C1 and H1 with concrete and steel elements.

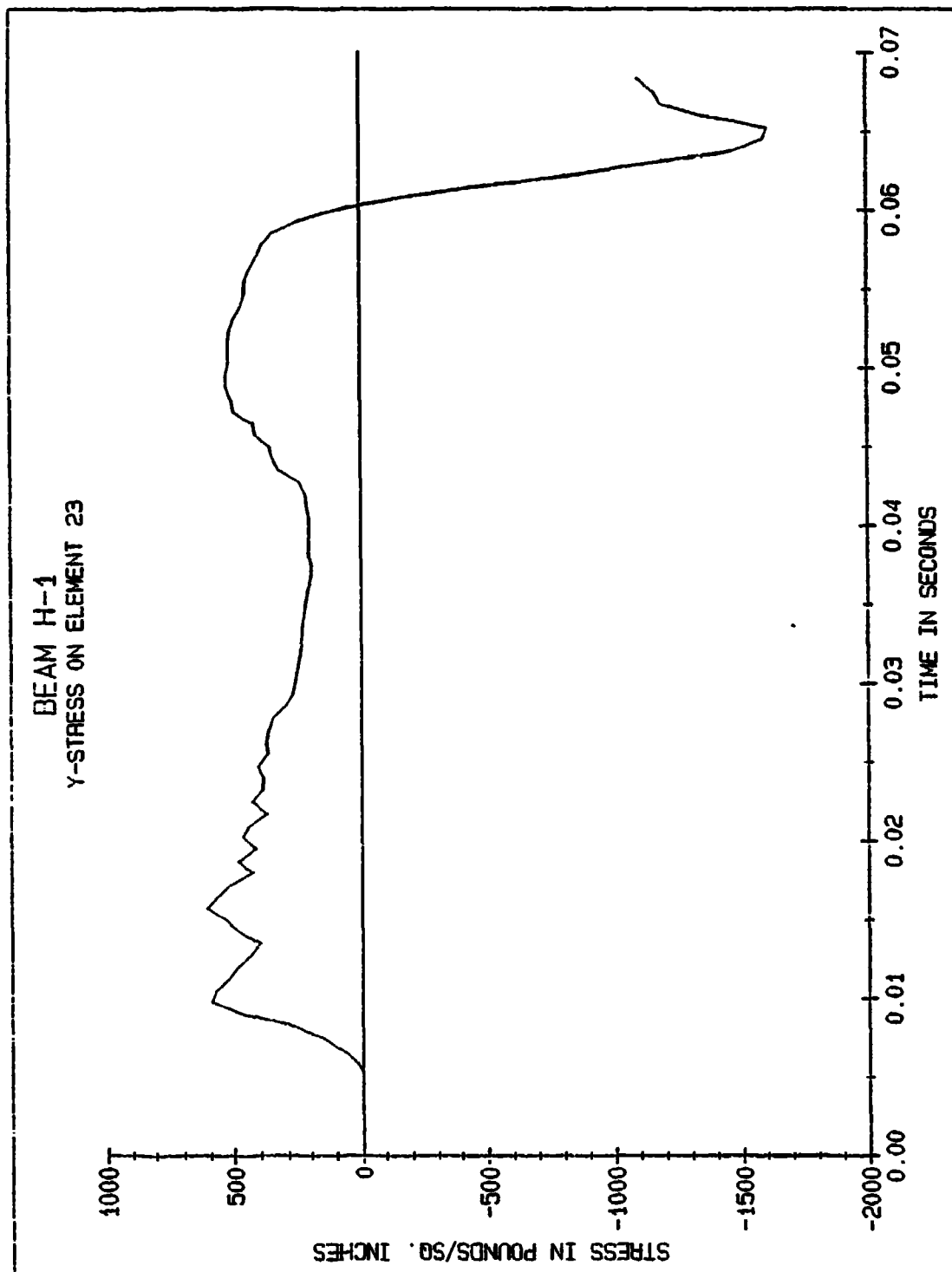


Figure 36. Time-history plot depicting the concrete tensile cutoff limit.

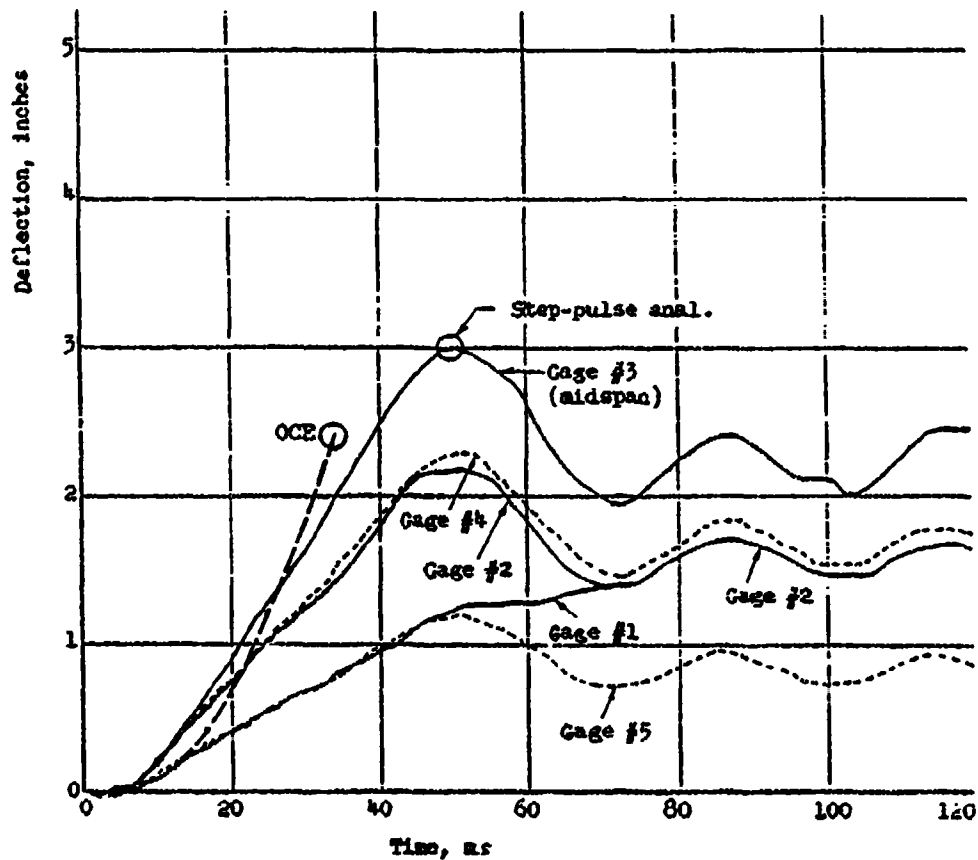


Figure 37. Deflection vs. time for beam C1.  
(Feldman and Siess '58)

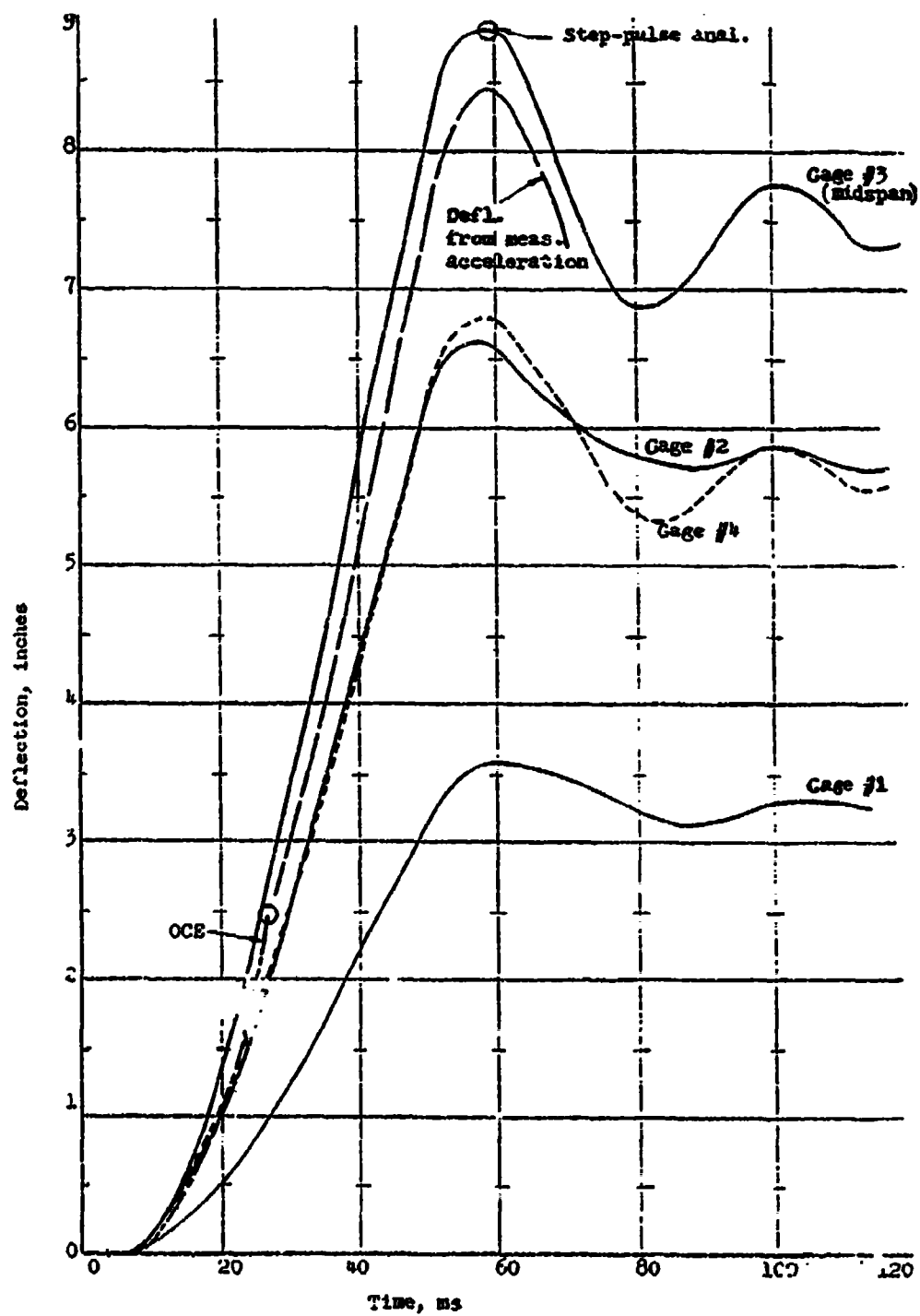


Figure 2. Deflection vs. time for beam H1.  
(Feldman and Siess '58)

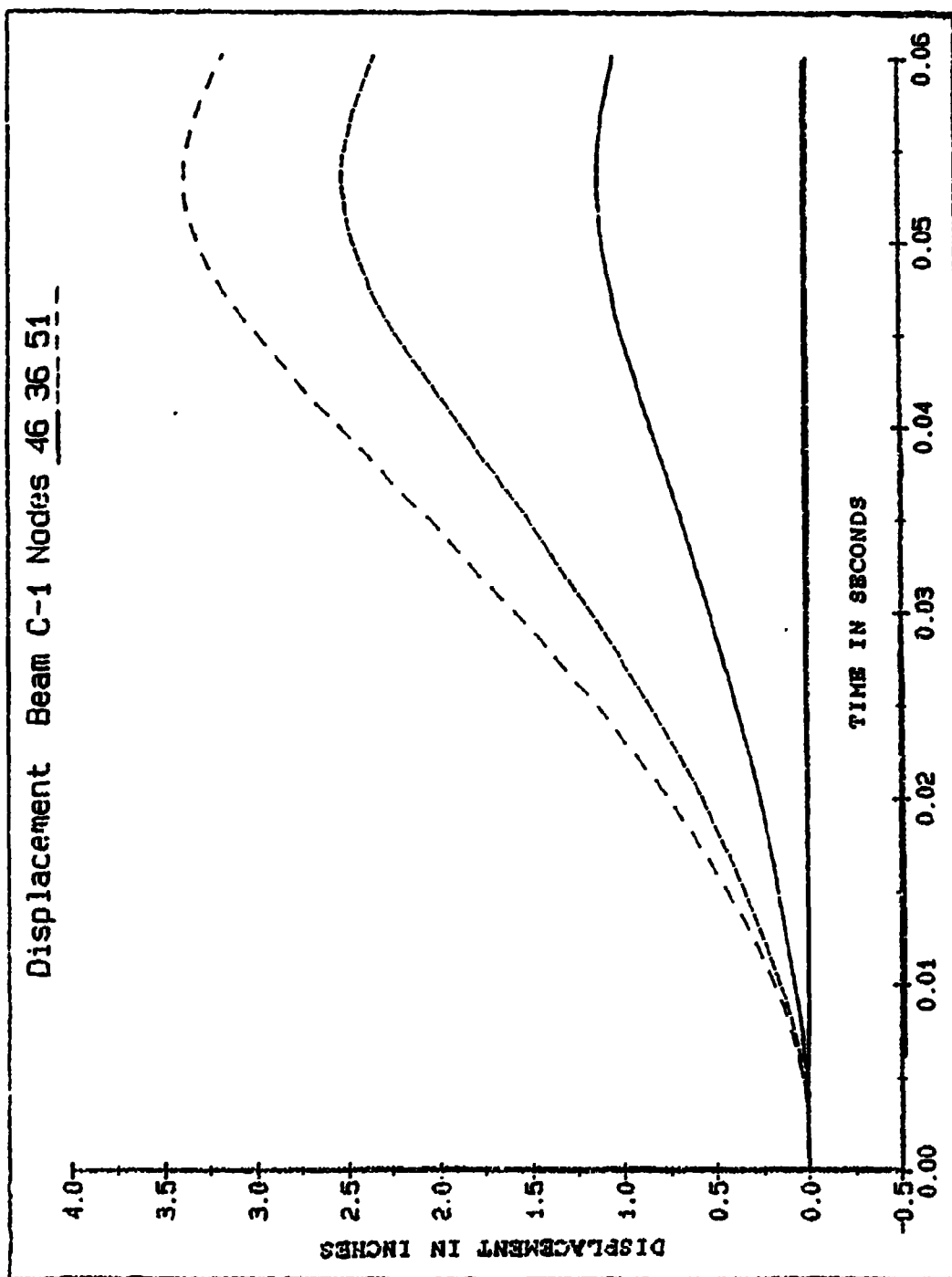


Figure 39. Model simulation of deflection vs. time  
for beam C1.

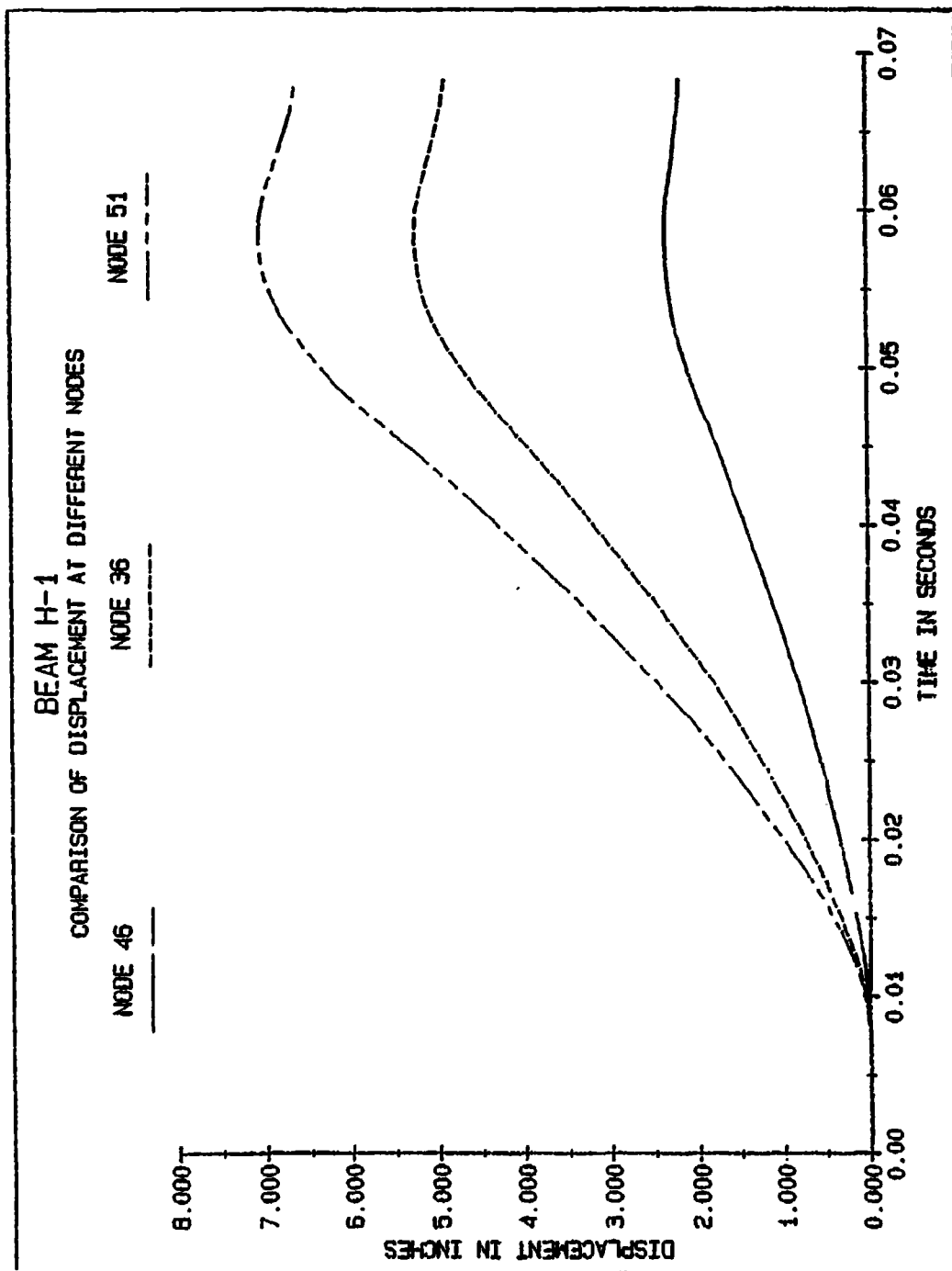


Figure 40. Model simulation of deflection vs. time for beam H1.

## 4.0 ANALYSIS

The purpose of this chapter is to select structural details of connections, openings, and attachments from the information gathered in Section 2 and subject them to simulated blast loads through the procedure outlined in Section 3. Figure 13 shows a typical protective structure with a blast load  $P(t)$  applied to the opening cover from either side. The portions of the structure (connection details, and openings) that are studied here are labeled as shown. The magnitude and time-pulse history of this blast load as outlined in Section 3.4 show a resultant Peak Load  $P(t)/2$  equal to 2451 k and 1471 k for connections and openings, respectively. The rise time to first peak ( $t_r$ ) was set at 0.04 ms with a duration of positive pressure ( $t_d$ ) set at 0.53 ms (Figs. 26 and 27).

### 4.1 DETAIL REQUIREMENTS

Several preliminary details for connections, openings and attachments were chosen based on their performance in previous research. An initial investigation was performed to determine which details would meet the design criteria as stated in Section 2. In review of Section 2 the guidelines for design and the criteria tested for (strength and serviceability) are listed below. The structural details that satisfied the design guidelines were then studied as discussed in this section for their strength and serviceability characteristics.

#### 4.1.1 Design Guidelines

- 4.1.1.1 Reinforcement ratios  $A_s/bd$  should be limited to a range of 0.5% to 0.75% for slab/wall connections. This ratio may be increased for beam/column applications; however, crossties in the joint region should be designed according to Eq. 4.

4.1.1.2 Stirrups for diagonal shear are required in all beam/column joints in accordance with:

- ACI 318-83 Type Two connections for shear and confinement (Eqs. 1 and 2)
- Park and Paulay '75, requirements for diagonal splitting (Eq. 3)

4.1.1.3 Reinforcement terminating in a knee joint should be developed in a 180-deg bend with the return leg embedded in the opposing force region.

4.1.1.4 Reinforcement terminating in a tee joint should be developed in a 90-deg hook with the legs extending through the midheight of the connection (Eq. 6).

4.1.1.5 Minimum clear cover for reinforcement should exceed  $2d_b$  and the minimum bar spacing should exceed  $3d_b$  for limiting the effects of splitting cracks as set forth in the ACI 318-89 code.

4.1.1.6 Diagonal haunches or splays should be added to all inside corners.

4.1.1.7 Diagonal reinforcement equal to half the area of the main flexural steel is required at all inside corners.

4.1.1.8 A hinge should not occur in the joint region.

4.1.1.9 Precast connections should be posttensioned to eliminate the formation of gaps which could allow the contamination of the facility.

#### 4.1.2 Strength and Serviceability Criteria

4.1.2.1 The "ductility factor" ( $\mu$ ) should not exceed 1, and deflections should not exceed approximately  $L/240$  at midspan. The value for deflections may be altered by the designer depending on the structures requirements.

4.1.2.2 Average compressive stress due to flexure in the concrete immediately above the compression reinforcement should not exceed  $0.45 * f'_c$ .



- 4.1.2.3 Tensile and compressive stress in the reinforcement located in the elements should not exceed  $2/3 f_y$ .
- 4.1.2.4 Tensile and compressive stress in the reinforcement located in the joint region should not exceed  $1/3 f_y$ .
- 4.1.2.5 Direct shear at any point in the structure should not exceed the Hawkins shear limit  $\tau_u$  (Eq. 9).
- 4.1.2.6 Diagonal shear in slab/walls should not exceed  $4 * (f'_c)^{1/2}$ . For values of shear higher than this, stirrups must be added in accordance with ACI 318-83 Type Two connections.

#### 4.2 CONNECTIONS

Two different connection types (knee and tee joints) with varying configurations (monolithic concrete, monolithic SIFCON, and precast/posttensioned) will be investigated. The selected details for each configuration were then tested for their structural integrity (Section 2) when subjected to blast loads by the procedure outlined in Section 3. Minor alterations in overall dimensions, amount of reinforcement, and location of reinforcement were made until safe and efficient behavior were observed. Material properties for steel, concrete, and SIFCON (when used) were held constant for all the details.

Based on common practice, steel reinforcement with grade 60 specification was chosen as the standard. A yield strength  $f_y$  equal to 65 k/in<sup>2</sup>, which is very common in grade 60 steel, was used for analysis purposes. (Reinforcement classification is based on meeting or exceeding the specified grade.) Parameters used for the steel model are shown in Table 12. Concrete properties will be based on medium-strength parameters, or those used for a compressive strength  $f'_c$  equal to 6000 lb/in<sup>2</sup>. The parameters used will be identical to those shown in Table 8. SIFCON will be modeled with updated medium-strength concrete parameters shown in Table 13.

TABLE 12. Steel reinforcement parameters.

Park and Paulay Steel Model				
$f_y = 65.0 \text{ k/in}^2$	$f_u = 110.0 \text{ k/in}^2$	$\epsilon_y = 0.0018$	$\epsilon_{sh} = 0.0100$	$\epsilon_u = 0.120$

TABLE 13. SIFCON parameters.

Prager-Drucker Cap Model			
$f'_c = 12000. \text{ lb/in}^2$	$E = 1200. \text{ k/in}^2$	$\nu = 0.20$	$n = 0.50$
$\epsilon'_c = 0.0030$	$\alpha = 0.60$	$\beta = 1.25$	$h_o = 0.60$
$P_c = -1000. \text{ lb/in}^2$	$m = 0.65$	$s_o = 25. f'_c$	$q = 0.35$
$c_1 = 0.40$	$c_2 = 1.0$	$c_3 = 1.0$	$c_{exp} = 0.70$
$P_o = 30000. \text{ lb/in}^2$	$P_{eo} = 18000. \text{ lb/in}^2$		
Continuum Damage Mechanics Model			
$d_o = 0.875$	$r_o = 0.0035$	$B = 1.30$	$A_{to} = 700.$
$\eta = 0.0005 \text{ lb/in}^2$	$C = 8.0$	$D = 10.0$	$A_{eo} = 50.$
Nonassociated Flow Rule			
$\phi = 0.10$	$\theta = 0.001$	$\Omega = 0.003$	$\omega = 2.0$

The geometrical approach used to model the connection behavior as outlined in Section 3.2 displays a column/wall rigidly attached at its base (mid-height between stories) with a projection of 5-ft 6-in to the top of the connection. At 90-deg from the column/wall, a beam/slab cantilevers 5-ft 6-in from the outside face of the connection. A concentrated blast load as defined earlier was then applied to the end of the cantilever. This geometry defines a structure with a story height and span length of approximately 10 and 14 ft, respectively (Fig. 13). Contained in the span is a 3-ft opening between two 5-ft 6-in cantilevers.

#### 4.2.1 Analysis Procedure

The methodology used to determine the most efficient details followed this basic outline. The monolithic concrete knee joint was picked as the first detail to investigate. Initializing the analysis with this detail stems from three primary observations.

- 4.2.1.1 To date most structures built to withstand blast loads consist primarily of walls and slabs connected at the exterior in a knee joint.
- 4.2.1.2 Structural response of knee joints is subjected to extreme behavior in terms of stress gradients.
- 4.2.1.3 Details sufficient for the knee joint should translate very well to other types of joints.

Box structures tested in the report by Coltharp et al. '85 consisted of walls with thicknesses of 13, 16, 19 and 22 in (Fig. 41). In the first test run, the thickness of the connected elements was set at 12 in. After completion of the tests, it was determined that 12 in would be insufficient to provide adequate strength and serviceability as noted above. Consequently, thicknesses for the following tests were increased to 18 in. Subsequent details were shown to give reliable results.

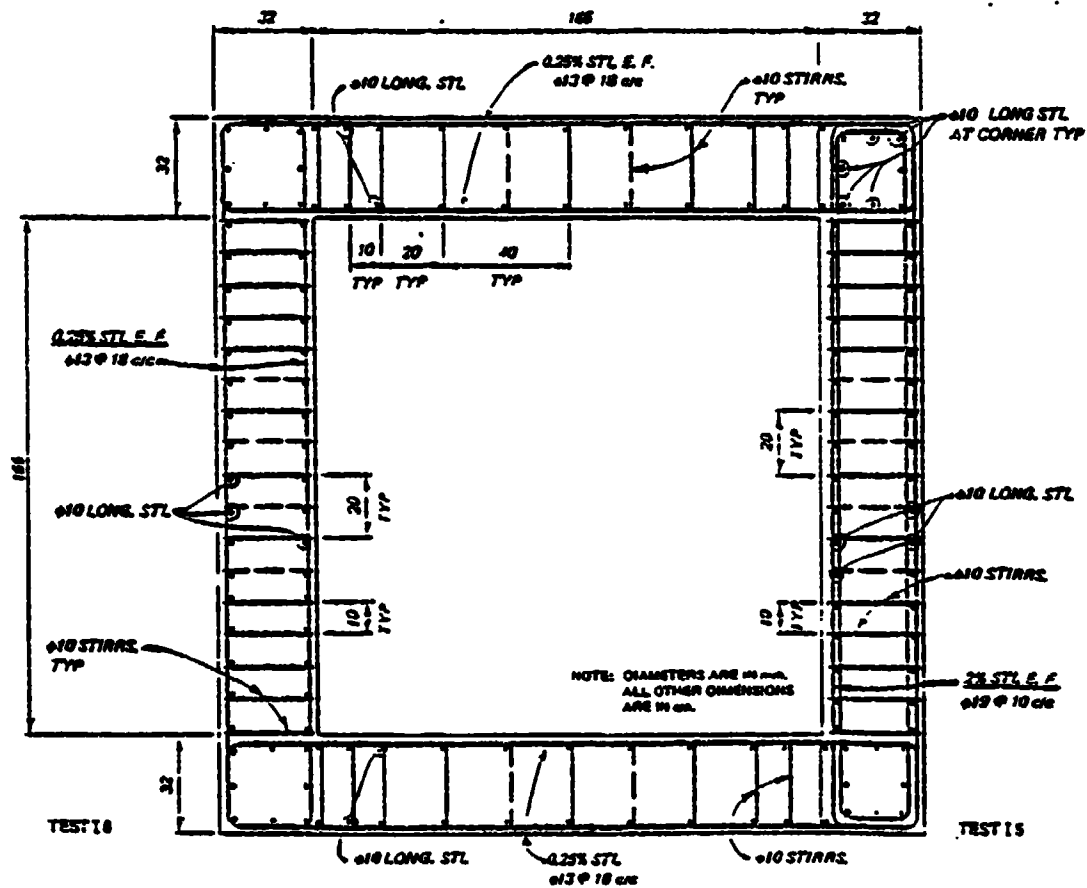


Figure 41. Reinforcement detail for a blast resistant box culvert. (Coltharp et al.'85)

Details for the monolithic knee joint which contained the best characteristics and performance record will be extended to monolithic SIFCON knee joints, monolithic tee joints, and precast knee and tee joints. Details for these connection types will then be tested, analyzed, and compared in a similar fashion.

#### 4.2.2 Monolithic Knee Joint

The first connection tested (BSL2A, Fig. 42) incorporates a 20-in-wide by 12-in-thick column/wall and a 20-in-wide by 12-in-thick beam/slab detail. The mesh shown in Fig. 42 utilizes quadratic 8-node rectangular elements to model the concrete as stated in Section 3, with element sizes in the connection region similar to that shown for the coarse mesh in Fig. 14. The maximum element size is 16-in-long by 4-in-wide located at the base of the column/wall, with three elements stacked across the thickness. Each of the seven nodes along the base of the column/wall are restrained from vertical and horizontal translation to simulate base fixity. At 32 in from the base the elements are decreased in size to 8-in-long by 4-in-wide elements. The joint area is defined by twelve 4-in-long by 3-in-wide elements. The diagonal concrete strut at the connection interface is described by a 6-node triangular element with two 8-in sides. The beam/slab portion consists of a mesh pattern similar to that of the column/wall, with four 3-in-wide elements stacked across the thickness. The concentrated blast load is applied to the end of the beam/slab through 6-in-long steel elements. These elements are incorporated to distribute the load to the end of the beam/slab while minimizing the effects of local failure in the concrete, and are not indented for actual use in design. For the effects of local failure, see the analysis on openings in Section 4.3.

The overlaid reinforcement mesh consisting of steel 2-node bar elements are connected to the midline nodes of the concrete

elements. Note that diagonal reinforcement will also be attached to corner nodes to ensure proper geometry. The reinforcement sizes are shown as follows. The beam/slab and column/wall are reinforced with 1.5% steel (three #9 bars) on each face, with 0.95 and 1.45 in of cover, respectively. Diagonal steel (three #8 bars) is placed 2 in from the exterior face of an 8-in diagonal concrete strut located on the inside corner of the connection interface. The #9 main flexural bars are anchored in the joint with 180-deg hooks returning into the opposing stress region. Due to the high reinforcement ratio (1.5%), transverse stirrups are tied around the #8 diagonal bars and the outer face flexural bars in both the beam/column and slab/wall connections. Note that the initial test connection contained a steel ratio of 0.5% and was subsequently increased in an attempt to improve the results.

The second connection detail (BL-17, and BL-1A; Fig. 43) incorporates a 20-in-wide by 18-in-thick column/wall and a 20-in-wide by 18-in-thick beam/slab detail. The mesh scheme used for this test is identical to that used for connection BSL2A, with two exceptions. Width of the elements has been increased to 6 and 4.5 in for the column/wall and beam/slab members, respectively. And, the diagonal concrete strut located at the connection interface was deleted from the detail. Two different flexural reinforcement ratios were tested; 0.6% for BL-17 (three #7 bars), and 1.0% for BL-1A (three #9 bars), on each face. The clear cover at the beam/slab is 1.83 and 1.7 in for the #7 and the #9 bars, respectively. The clear cover at the column/wall is 2.58 and 2.45 in for the #7 and the #9 bars, respectively. The steel ratio was increased for BL-1A in order to reduce high deflections and bar stresses encountered in BL-17. Diagonal steel (two #6 bars for BL-17) and (two #8 bars for BL-1A) is placed on the inside corner of the beam-column interface at a 45-deg angle with 2 in of cover. The main flexural bars are anchored in the joint with 180-deg hooks returning into the







opposing stress region. Due to the high percentage of steel reinforcement in BL-1A, transverse stirrups are required in both the beam/column and slab/wall connections. The stirrups should be tied around the #8 diagonal bars and the outer face flexural bars.

The third connection (BL-6A, Fig. 44) incorporates a 20-in-wide by 18-in-thick column/wall and a 20-in-wide by 18-in-thick beam/slab detail. The mesh layout is identical to BL-1A with an 8-in diagonal concrete strut added to the interior corner of the connection interface. The beam/slab and column/wall are reinforced with 0.6% steel (three #7 bars) on each face with 1.8 and 2.5 in of cover, respectively. Diagonal steel (two #6 bars) equal to  $0.5(A_s/bd)$  is placed 2 in from the exterior face of the 8-in diagonal concrete strut. The #7 main flexural bars are anchored in the joint with 180-deg hooks returning into the opposing stress region. Transverse stirrups tied around the #6 diagonal bars and the outer face flexural bars are required only for beam/column connections. These stirrups are not required for wall-slab connections if the joint shear is within the ACI 318-83 specified limits as outlined in the strength and serviceability criteria above.

The fourth connection (BL-6C) is identical to BL-6A (Fig. 44) with one exception. The diagonal bar steel is increased to three #7s, which is equal to the amount of steel used for the main flexural bars or  $0.60(A_s/bd)$ .

The fifth connection (BLS6A) incorporates a 20-in-wide by 18-in-thick column/wall and beam/slab detail with SIFCON material used in the connection region as shown in Fig. 45. The geometry and reinforcement used in this detail are identical to that used for the BL-6A connection.

Diagonal crossties located in the joint region (Fig. 46) were added to three of the connections described above and run separately for comparison reasons. Two of the connection details (BSL2A, and BL-1A) require ties as set forth in Section 4.1.1, and the third detail (BL-6A) does not. Four closed #3 ties will be considered with an area/tie-leg ( $a_{s,j}$ ) calculated from Eq. 4 for wall/slab connections using the detail BL-1A. Stress measured in these ties and their effect on the overall behavior of the connection should indicate which details benefit from their use. Details with the ties are designated with an "S" in place of the "A" at the end of the detail title (i.e., BL-1S).

#### 4.2.3 Monolithic Tee Joint

The geometry used to study tee joints consists of a 48-in-long, 20-in-wide by 18-in-thick cantilevered beam/slab framing at 90 deg into the center of a 108-in-long, 20-in-wide by 18-in-thick column/wall. A blast load as defined in Section 3.4 is applied to the end of the cantilever through a 6-in-long, 20-in-wide by 18-in-thick steel plate similar to that described in Section 4.22. Two types of details based on the detail BL-6A were tested. This detail type was chosen for its overall performance in the tests on knee joints outlined above. The characteristics that varied between the three details were the size of haunches used at the connection interface and the amount of diagonal steel located in the haunch.

The first detail (BT-6A, Fig. 47) incorporates the geometry shown above with a 4.5-in-haunch located at the connection interface. The mesh layout and element size is similar to that used for the knee joint. Three 6-in-wide elements are stacked across the thickness of the column/wall and broken into three sets along its length. The first and third sets near the supports consist of three 12-in-long elements. The interior set consists of eight 4.5-in-long elements. The



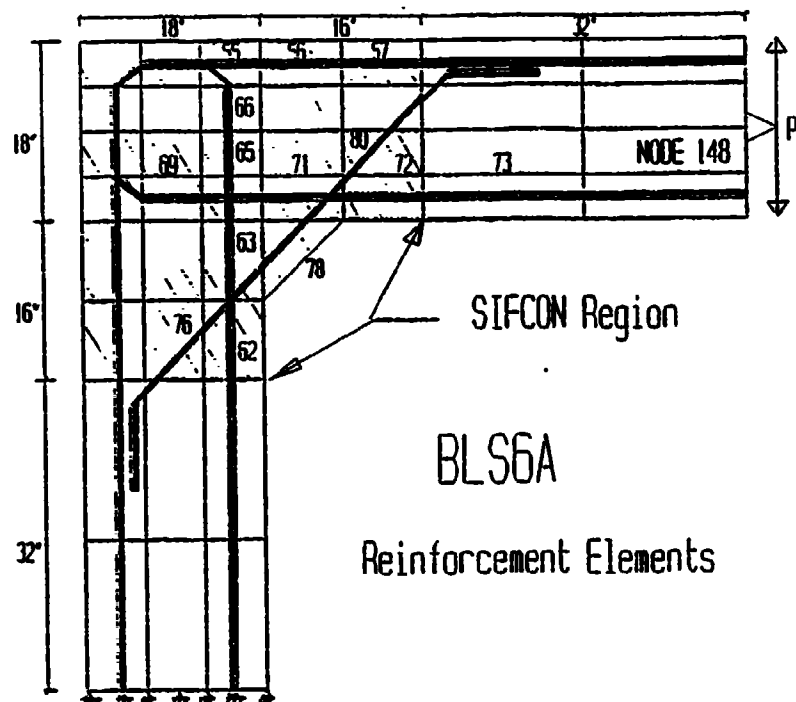


Figure 45. Connection detail BLS6A with SIFCON material and labeled steel reinforcement elements.

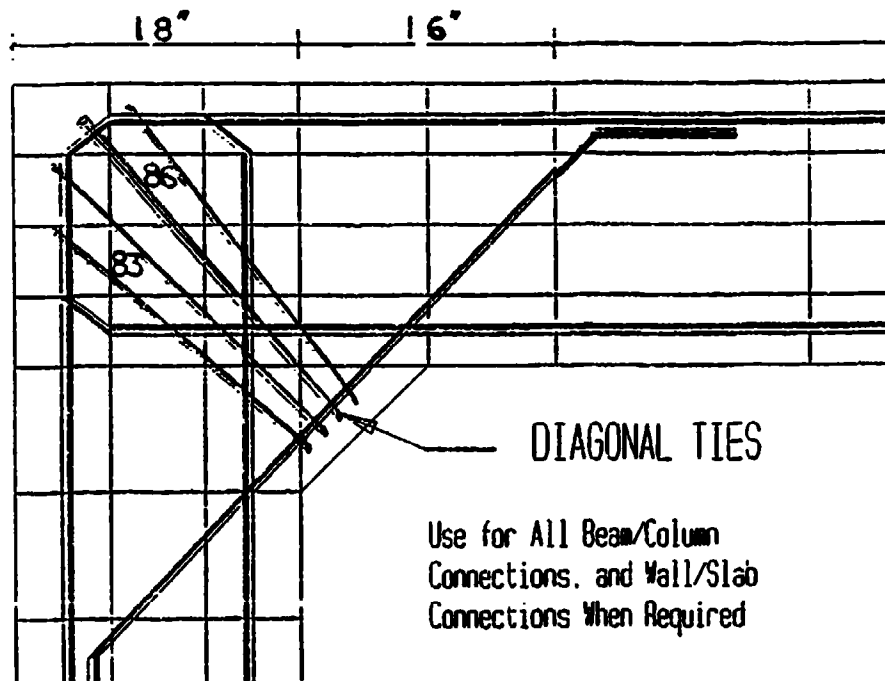


Figure 46. Connection detail with diagonal steel reinforcement crossties.

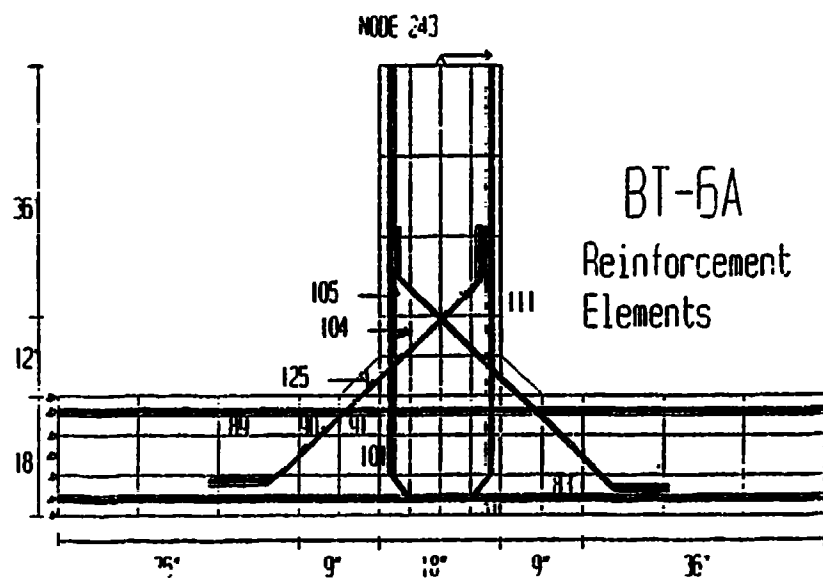
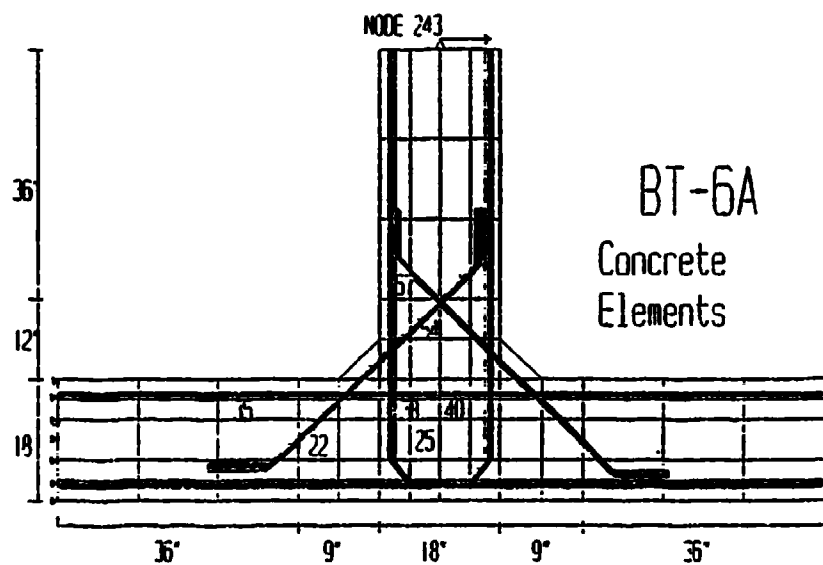


Figure 47. Connection detail BT-6A with labeled concrete and steel reinforcement elements.

beam/slab is made up of four sets of elements 4.5 in wide across the thickness, with three elements 12 in long at the end, and two elements 6 in long near the joint. The steel plate elements at the end of the beam/slab are similar to those described in Section 4.2. The haunch is described by a 6-node triangular element. Pinned restraints are located at seven nodes across the thickness on the top and bottom of the column/wall.

Reinforcement mesh is overlaid in a manner similar to that described in the knee joints above. The beam/slab and column/wall are reinforced with 0.6% steel (three #7 bars) on each face with 1.8 and 2.5 in of clear cover respectively. Diagonal steel (two #6 bars) is placed 2 in from the exterior face of a 4.5-in diagonal concrete strut located on the inside corner of the connection interface. The #7 flexural bars extending from the beam/slab are anchored in the joint with standard 90-deg hooks with the legs crossing the midheight of the connection. The column/wall reinforcement is continuous through the joint.

The second detail (BT-9A, Fig. 48) incorporates the same beam/slab and column/wall dimensions with the same steel reinforcement as that for BT-6A. However, the diagonal haunches are increased to 9 in and the diagonal steel is increased to three #7 bars. The haunches are described with a 6-node triangular element and an 8-node quadrilateral element.

#### 4.2.4 Precast Knee Joint

The overall geometry of the precast structure is identical to the monolithic structure described in Section 4.1. For this case, a precast beam/slab is posttensioned to a precast column/wall. Two types of precast details with this configuration were then subjected to a blast load applied to the end of the beam/slab through steel plates as outlined earlier.

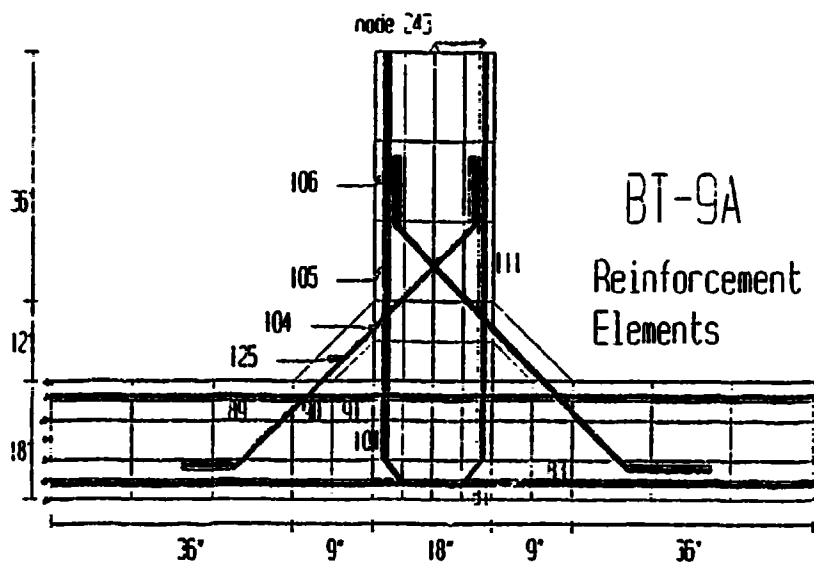
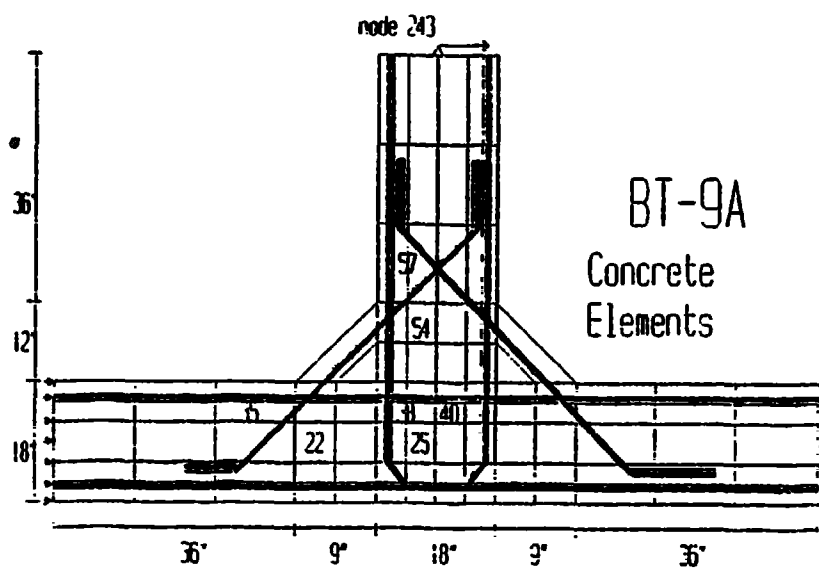


Figure 48. Connection detail BT-9A with labeled concrete and steel reinforcement elements.

The first detail (PL-1D, Fig. 49) incorporates a 20-in wide by 18-in-thick beam/slab with a 20-in-wide by 18-in-thick column/wall. The beam is placed on a corbel which protrudes 6 in from the face of the column. A 0.5-in cotton duck pad is placed between the bottom of the beam and the top of the corbel. A second pad is placed between the end of the beam and the face of the column. The beam is then post-tensioned to the column with four #9 threaded bars as shown in Fig. 11. The #9 bars are placed in 3-ft-long sleeves cast in the beam and threaded into lenton couplers located in the column. These bars are then stressed to  $33 \text{ k/in}^2$  which will compress the pad and ensure a uniform seal. In addition, a continuous steel angle with a  $3/8$ -in diagonal strut located at 20 in on center is welded to the face of the corbel and the bottom of the beam. The only steel modeled in the corbel is a continuation of the diagonal steel with an area of  $1.0 \text{ in}^2$ . For a complete corbel design, see the precast information in Section 2.

The second detail (PL-2S, Fig. 50) is identical to PL-1D with one exception. The end of the beam/slab is placed 4 in from the face of the column/wall. This gap will then be grouted solid with concrete. The beam is then posttensioned to the column with four #9 threaded bars in a procedure similar to detail PL-1D. The third detail (PL-4S) is identical to PL-2S; however, the posttensioning stress in the #9 threaded bars is limited to  $10 \text{ k/in}^2$ . The fourth detail (PL-7S), constructed in a manner similar to PL-4S, incorporates four 1.25-in-diameter high strength ( $88 \text{ k/in}^2$ ) coil rods for the flexural reinforcement ( $A_s/bd = 0.66\%$ ) and diagonal struts welded to the continuous angle at 10 in on center.

#### 4.2.5 Precast Tee Joint

One precast tee joint was tested (PL-8S). The overall geometry of the connection is similar to the monolithic tee joint



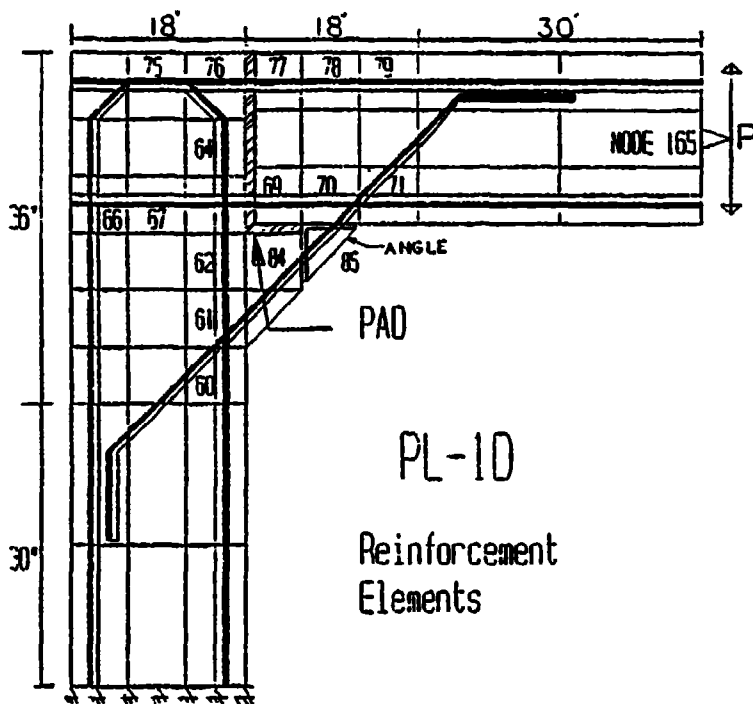
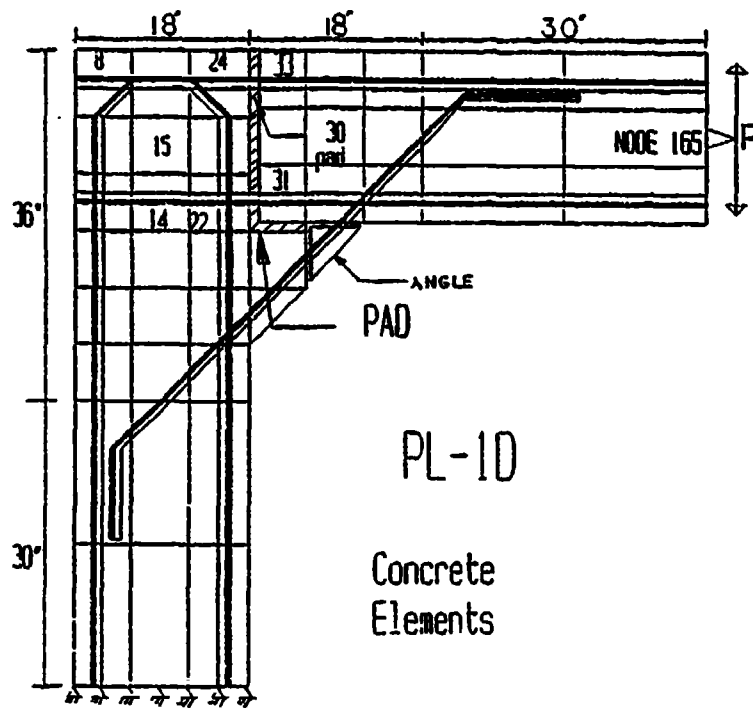


Figure 49. Connection detail PL-1D with labeled concrete and steel reinforcement elements.

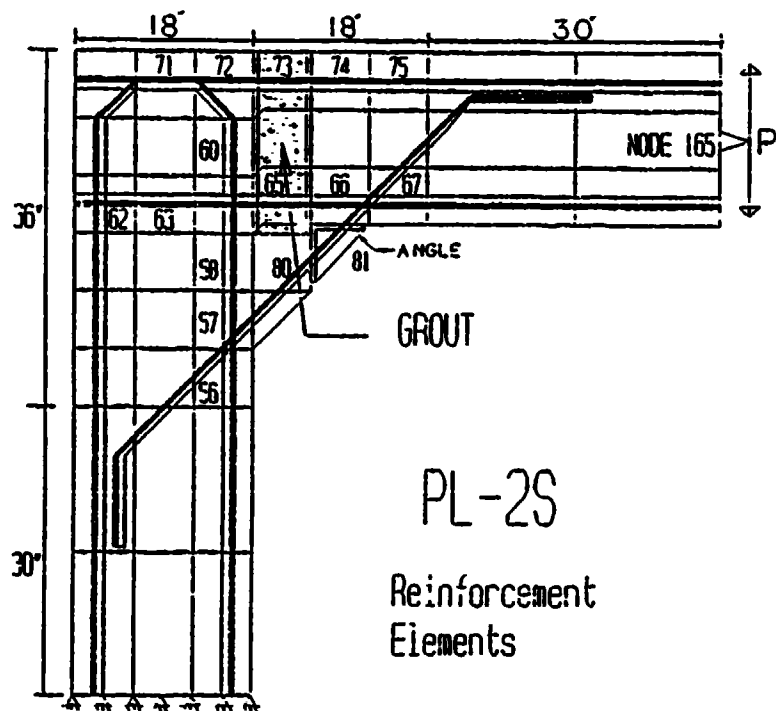
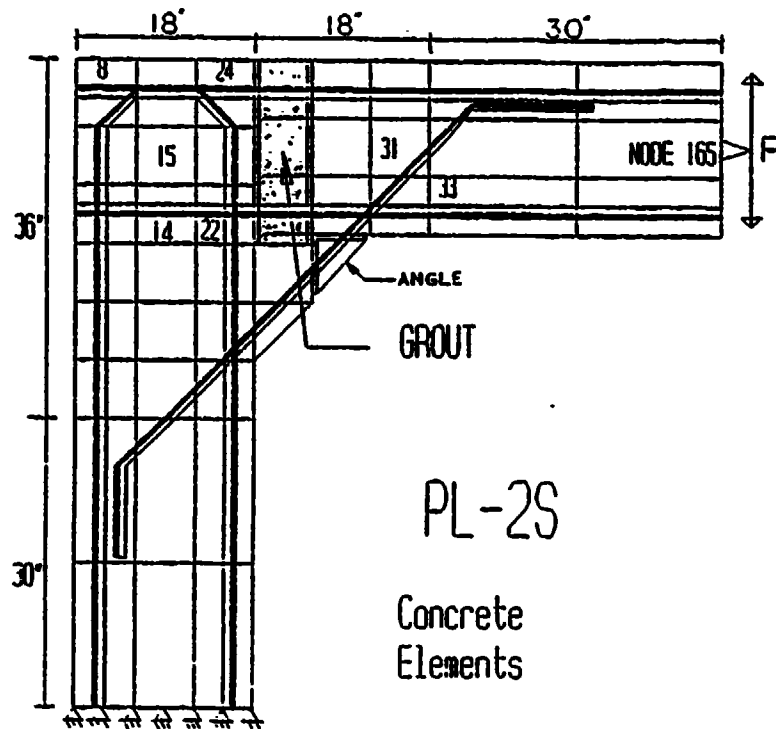


Figure 50. Connection detail PL-2S with labeled concrete and steel reinforcement elements.

(BT-6A, Fig. 47), with details similar to PL-4S. Two beam/slabs are cantilevered from opposite faces of the column/wall with restraints applied to the end of one and the load applied to the end of the other.

#### 4.3 OPENINGS

As stated in Section 2, the object of this report was to determine adequate edge reinforcement at the opening along with the means of transferring blast loads from the edge to the interior of the slab and ultimately the support via the connections. The critical factor for determining successful opening behavior is the amount of local material failure. To accomplish this, the load transferred from the opening cover to the slab must be distributed to a large enough area to keep stresses within a tolerable range. The material (concrete or SIFCON) at the edge of all openings will be confined by steel plates and the opening covers will transfer load only at these plate locations. Therefore, the width of these plates and their anchorage to the slab is critical to the behavior of the slab edge and will be determined by analyzing the stresses in the material directly under the plates.

Two different material types, one using reinforced concrete and the other using reinforced SIFCON, will be investigated. A two-dimensional analysis will be completed on a strip of slab 12 in wide. The applied blast load magnitude is a ratio of 12/20 times the value determined in Section 3.4 with an identical time history.

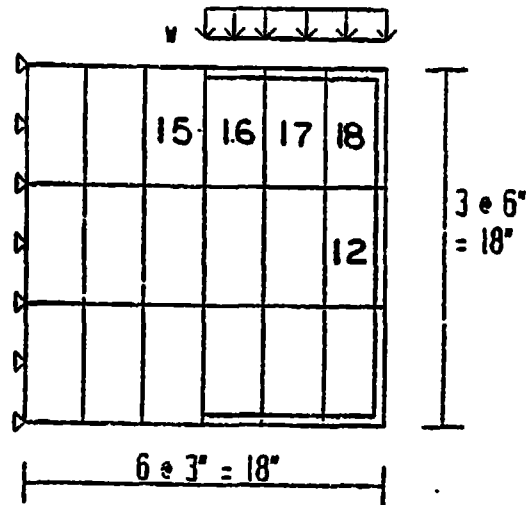
##### 4.3.1 Openings in Reinforced Concrete Structures

The analysis considers the last 18 in of the slab preceding the edge of the opening. The overall geometry of the slab edge consists of a 12-in-wide strip 18 in thick (STAND, Figs. 51 and

52). The concrete is modeled with eighteen 3-in by 6-in quadratic rectangular elements. In addition, steel plates represented by beam elements are attached to the exterior nodes of concrete elements along the free edge and return back 12 in at the top and bottom to form a continuous channel. Note, the 12-in dimension was determined through preliminary test runs and found to be the minimum required for the concrete opening. Steel bar elements are attached to the plates to simulate reinforcement anchorage. The edge opposite the opening is pinned at seven nodes to simulate continuity with the supporting leg of the slab.

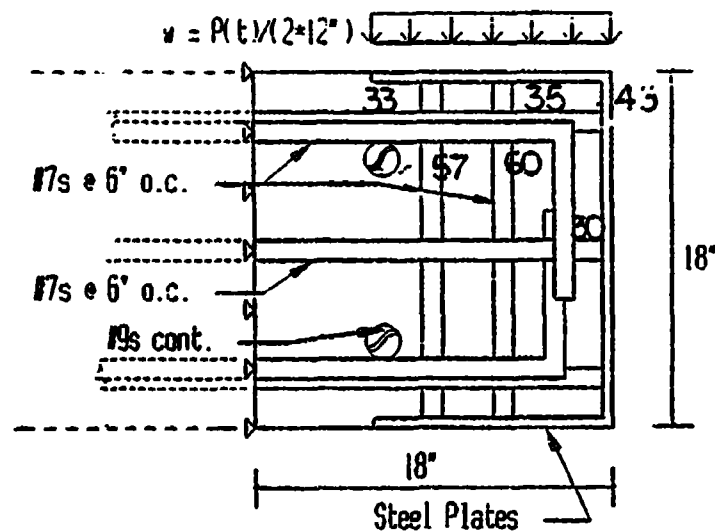
The reinforcement mesh will be overlaid and connected to the midline nodes of the concrete elements similar to the procedure outlined in Section 4.2.2. Slab reinforcement consisting of #7 bars at 6 in on center top and bottom (see BL-6A) are extended into the edge region and terminate in a standard 90-deg hook turned toward the midheight of the slab with 2.5 in of cover. Plate anchorage parallel with the slab reinforcement also consists of #7 bars at 6 in on center located at the top, center, and bottom of the slab. The length of these bars should extend a minimum of  $1.7(l_d)$  into the slab. Vertical plate anchorage attached to the top and bottom plates consists of two #7 bars located at 5 and 10 in from the opening edge and spaced at 6 in on center along the length of the opening.

After the initial blast load, a region of high stress directly below the top 12-in load transferring plate will crush approximately the top 1 in of concrete. To simulate the damaged concrete, soft elements (with a modulus of elasticity equal to  $1/4$  that of concrete) are inserted between the top plate and the undamaged concrete elements. A second blast load is applied to this configuration (CRUSH, Fig. 53) to monitor the effects of repeated loading on the plate anchorage and undamaged concrete.



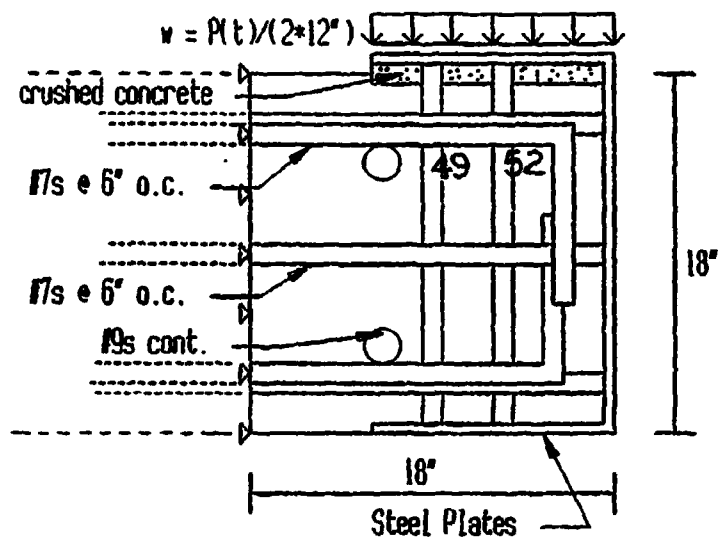
### OPENING (mesh)

Figure 51. Mesh for opening details with labeled concrete elements.



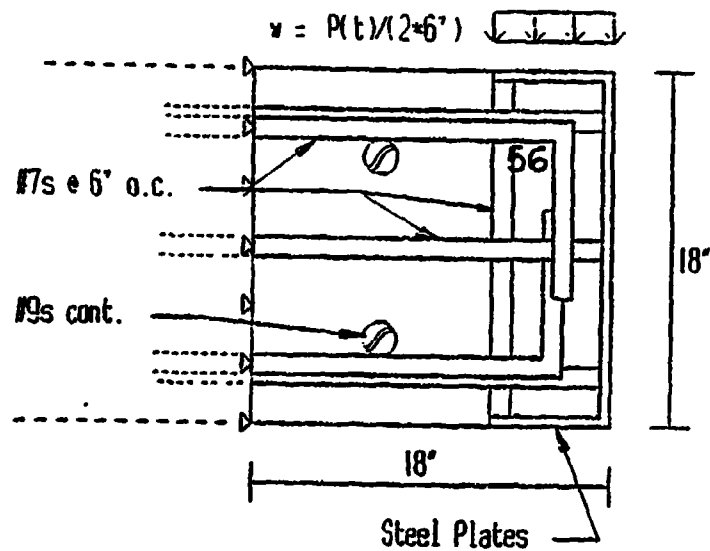
### OPENING (plain concrete)

Figure 52. Opening detail STAND with labeled steel reinforcement elements.



### OPENING (crush)

Figure 53. Opening detail CRUSH with labeled steel reinforcement elements.



### OPENING (sifcon)

Figure 54. Opening detail SIFCO with labeled steel reinforcement elements.

#### 4.3.2 Openings in Reinforced SIFCON structures

The SIFCON opening detail (SIFCO, Fig. 54) is identical to the concrete opening detail shown previously, with three exceptions. As expected the concrete elements are replaced with SIFCON elements. Preliminary test runs indicate that a 6-in return plate at the top and bottom is sufficient for distributing the load. And, only one vertical #7 bar anchor at 6 in on center is required between the top and bottom plates. Due to the high compressive strength of SIFCON, crushing under the top transfer plate did not occur; therefore, it was not necessary to run a repeated loading condition.

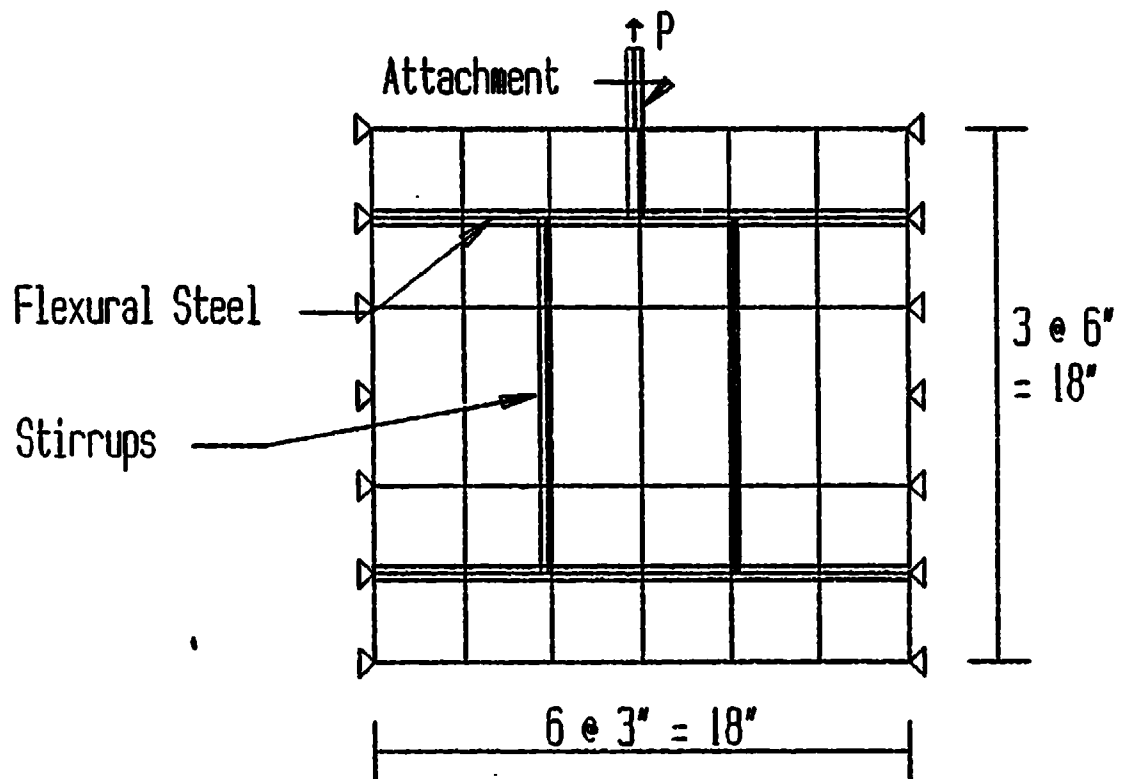
#### 4.4 ATTACHMENTS

The test for attachments simulates the effects of a 1000-lb object subjected to an acceleration of 20 g on an insert embedded in a concrete slab. The resultant horizontal peak load is equivalent to 20 k with a load-time history similar to that described in Section 3.4. The insert is attached to the main slab flexural reinforcement with a minimum of one stirrup wrapped around the bars on each side of the insert (Fig. 55). The area of the steel insert is set at 0.31 in, with a yield strength ( $f_y$ ) equal to 60 k/in<sup>2</sup>.

#### 4.5 GENERAL TEST RUN INFORMATION

SAMSON2 relies on a central difference method for the explicit integration solution scheme. To assure solution stability the maximum time step for each particular model is limited to the following:

$$\Delta t \leq 2/w_{\max} ((1 + \mu^2)^{1/2} - \mu) \quad (14)$$



## Attachment detail

**Figure 55.** Attachment detail with labeled concrete and steel reinforcement elements.



where  $w_{\max}$  is the maximum eigenvalue (highest frequency) of the system and  $\mu$  is the fraction of critical damping in the highest frequency. For constant strain elements the highest frequency may be estimated by

$$w_{\max} = 2c/l \quad (15)$$

where  $c$  is the maximum elastic wave speed of the material and  $l$  the minimum element dimension (Schreyer et al. '84). One can see that the time step between stiffness calculations is directly dependent on the size of the smallest element in the model. For this reason, use the largest elements possible which will not create stress discontinuities in the mesh scheme.

The total time required to see the full reaction picture is related to the fundamental period ( $T$ ) of the structure. Determination of  $T$  for the structures tested above is difficult, based on the particular geometries in question; however, the time required for a cantilevered beam of length equal to the total length of the structure is a reasonable upper bound for  $T$ . An approximate solution for  $T$  based on a cantilevered beam is as follows

$$T = [2\pi/(1.875)^2] * (ml^4/EI)^{1/2} \quad (16)$$

where  $m$  is the mass/unit length of beam,  $l$  is the total length,  $E$  is the modulus of elasticity, and  $I$  the moment of inertia.

#### 4.6 OUTPUT INFORMATION

Two main types of output data were used to interpret the results of the tests. Time-history plots of stress and strain were taken at various elements in order to determine their response throughout the history of the loading and its effects on the structure. Critical elements for which data will be shown in

this report are called out on each particular figure. The critical elements were chosen from the field of elements by the amount of stress imposed on them. The stress on these elements is then checked against the design criteria for strength and serviceability.

The second type of output data depicts the stress or strain contours over the entire structure at a particular time instant. This was accomplished through the use of the graphics code MOVIE.BYU. These pictures are extremely helpful in determining areas of high stress concentrations. The SAMSON2 code is run on an IBM 4341 main frame computer, and MOVIE.BYU is illustrated on an IRIS graphics workstation. The two computers were interfaced for creating these pictures.

## 5.0 RESULTS AND DISCUSSION

Presented in this chapter is a summary of the results obtained from the completed tests outlined in Section 4. The data collected from time-history plots are displayed in tabular form by listing the observed maximum values. Peak deflections and stresses are shown for concrete and steel elements at critical locations in each detail. Comparisons are made between details, and ultimately with the allowable values as determined in the section on strength and serviceability.

Several time-history plots of displacements, stresses, and strains were recorded for each detail during the simulation runs. A typical plot displays the quantity in question along the y-ordinate of the graph, with the time in seconds increasing along the positive x-ordinate. The elements and nodes chosen for analysis were assumed to be critical to the survival of the structure and representative of the aggregate behavior of the structure. Numbers and locations of nodes and elements for each detail are shown in the figures described in Section 4. An example of each type of time-history plot for the connection detail BL-6A is shown in the following figures: where displacement is shown in Fig. 56, shear in Fig. 57, y-strain and x-stress in Fig. 58, and bar stresses in Figs. 59 through 61.

In addition to the individual element time-history plots, pictures were taken at specified times of stress and strain gradients over the entire structure. Due to the large amount of data required for each picture, the maximum values for each type of stress and strain could not be pinpointed. However, data from the values given for each gradient can be interpolated with the maximum values given in the tables. Pictures of various details are shown in Figures 62 through 78.

**BL-6A KNEE JOINT W/.6Z STL& DIAG.**

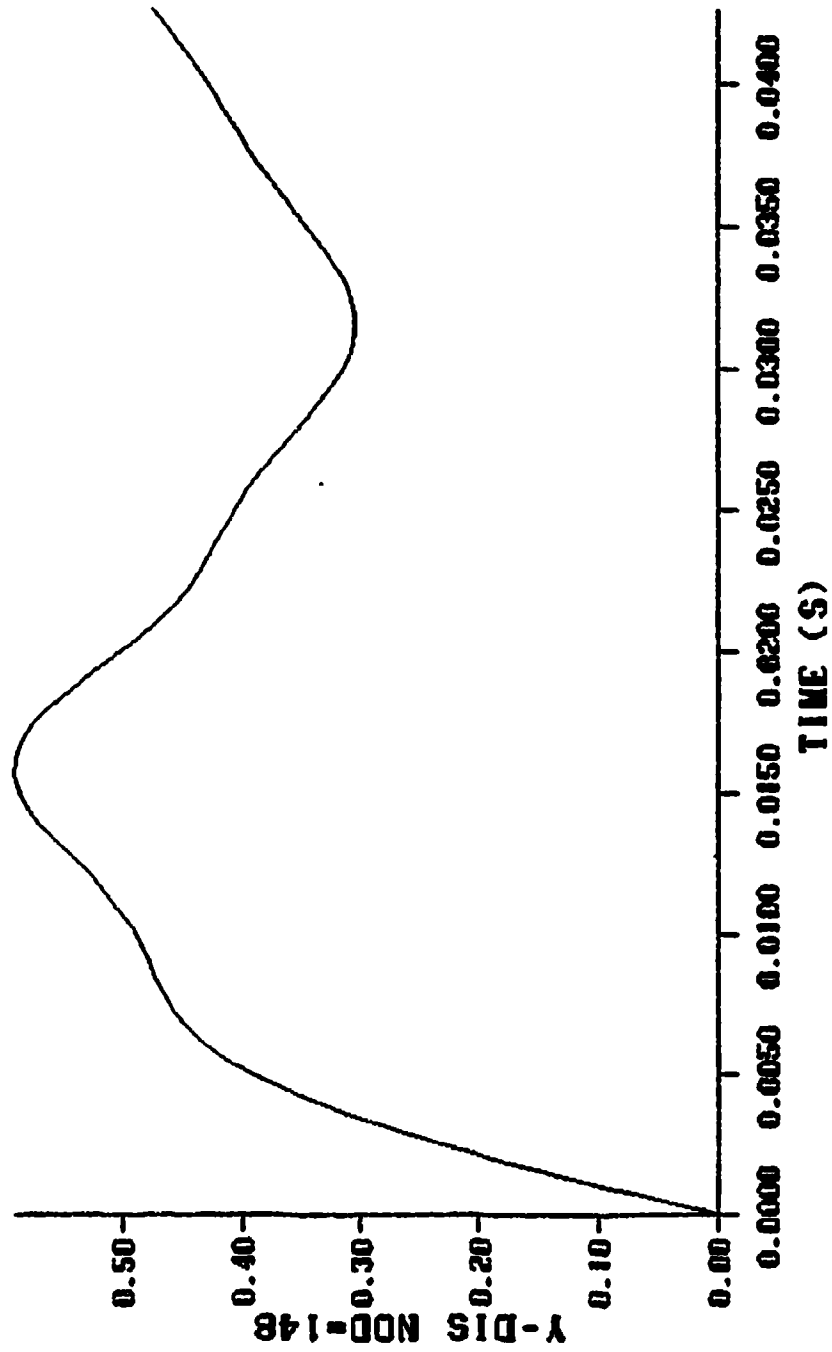
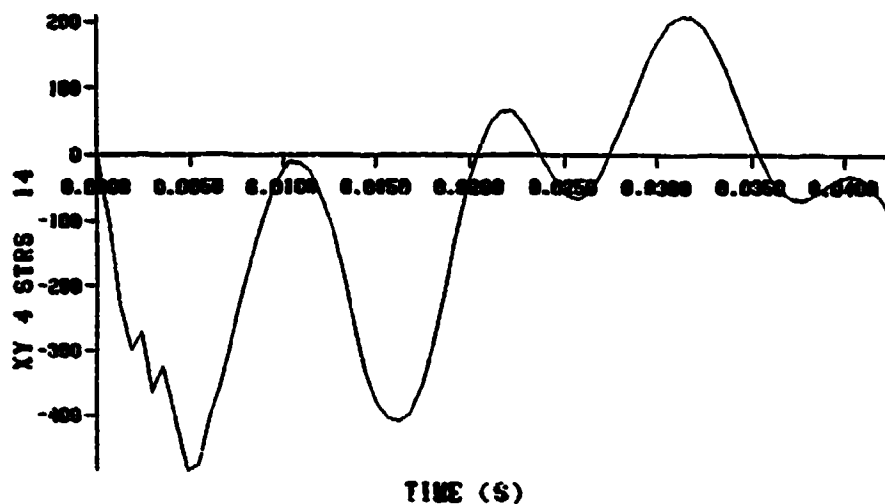


Figure 56. Time-history plot of displacement for connection detail BL-6A.

**BL-6A KNEE JOINT W/.6Z STL8 DIAG.**



**BL-6A KNEE JOINT W/.6Z STL8 DIAG.**

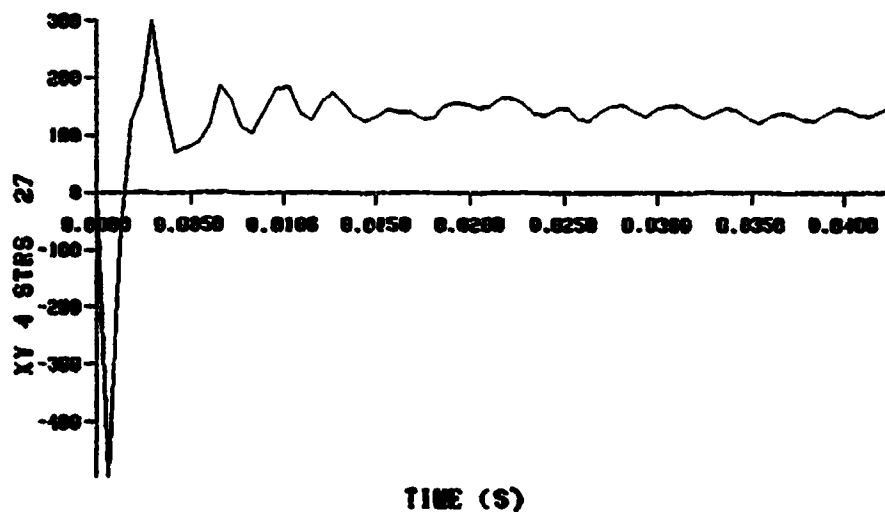
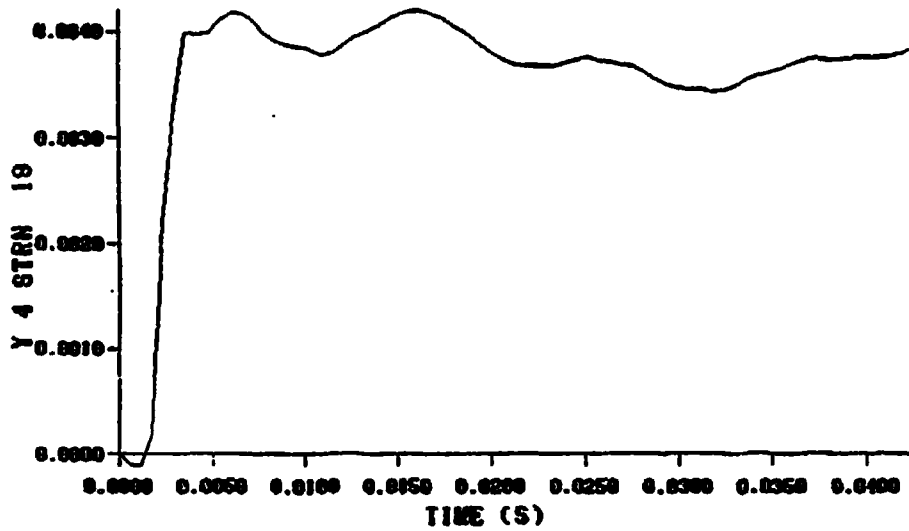


Figure 57. Time-history plots of shear for connection detail BL-6A.

**BL-6A KNEE JOINT W/.6Z STL8 DIAG.**



**BL-6A KNEE JOINT W/.6Z STL8 DIAG.**

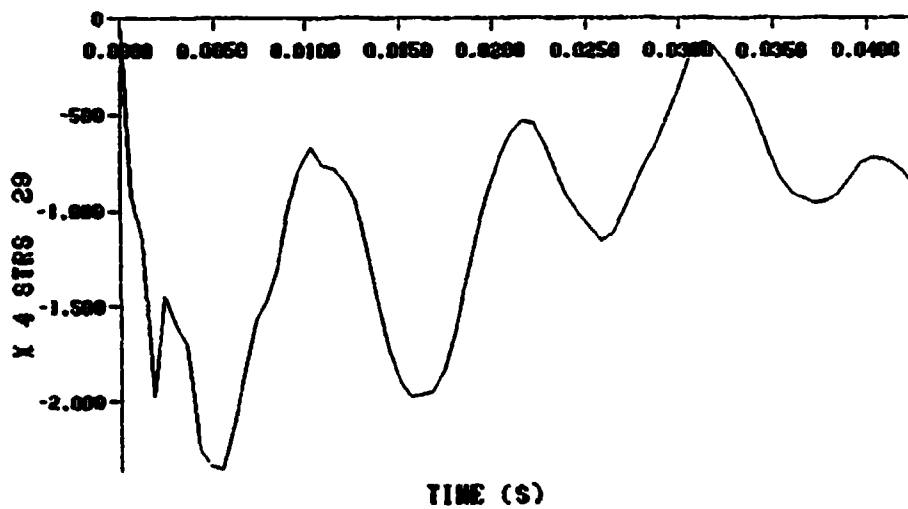
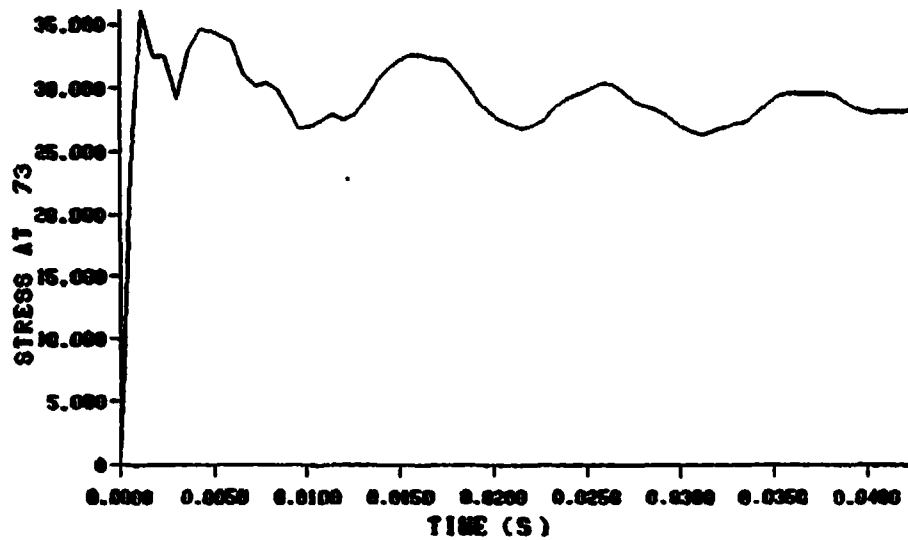


Figure 58. Time-history plots of y-strain and x-stress for connection detail BL-6A.

**BL-6A KNEE JOINT W/.6Z STL8 DIAG.**



**BL-6A KNEE JOINT W/.6Z STL8 DIAG.**

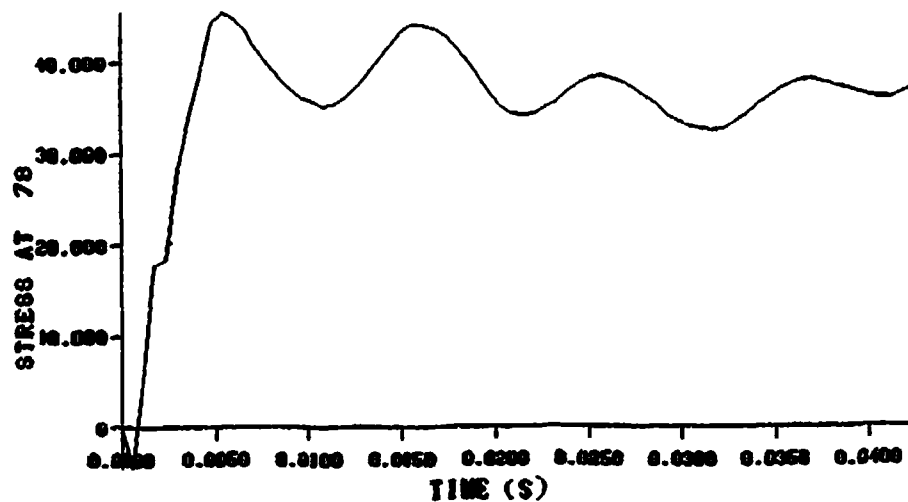
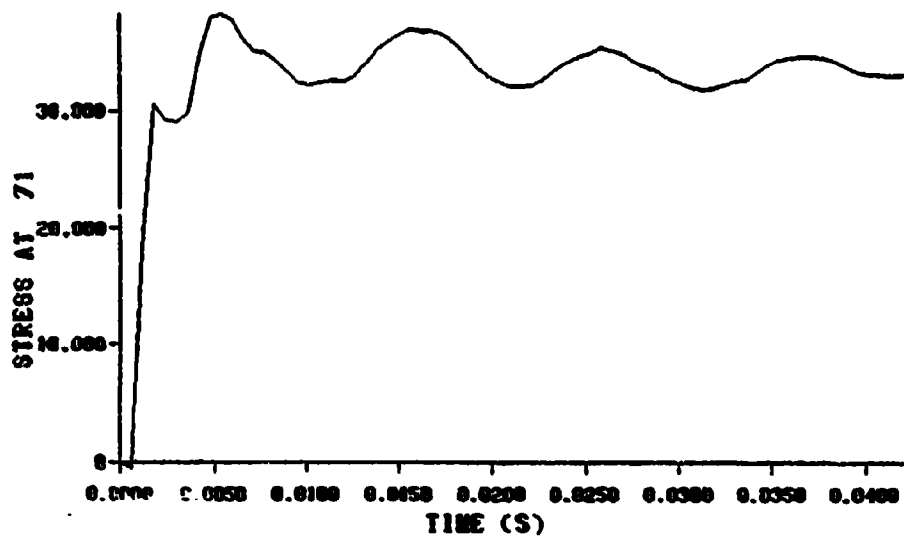


Figure 59. Time-history plots of uniaxial bar stress for connection detail BL-6A.

**BL-6A KNEE JOINT W/.6Z STL8 DIAG.**



**BL-6A KNEE JOINT W/.6Z STL8 DIAG.**

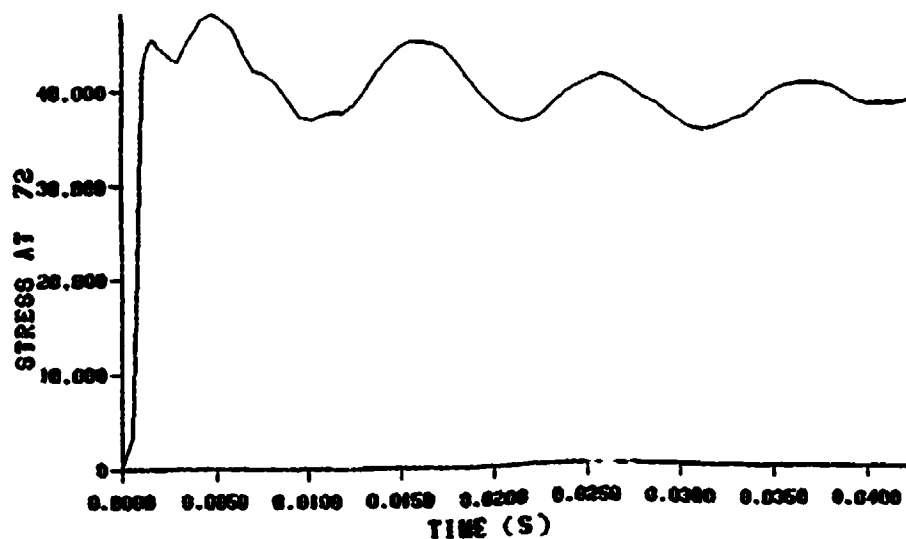
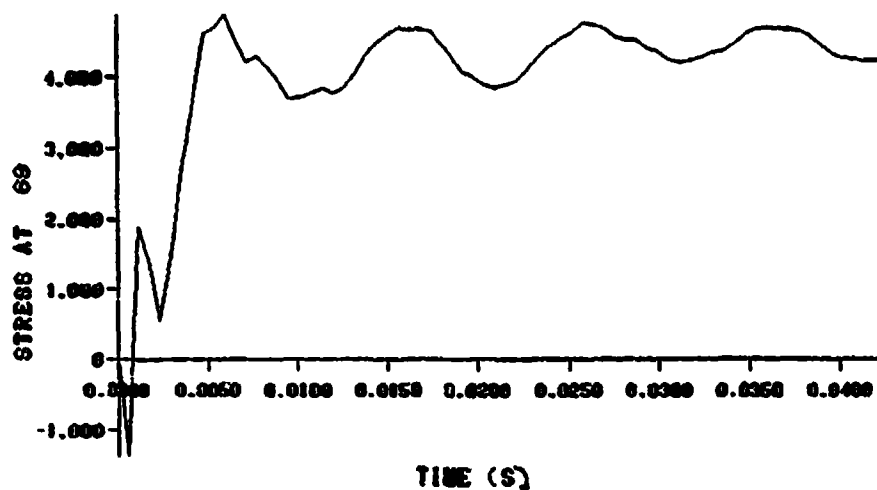


Figure 60. Time-history plots of uniaxial bar stress for connection detail BL-6A.



**BL-6A KNEE JOINT W/.6Z STL8 DIAG.**



**BL-6A KNEE JOINT W/.6Z STL8 DIAG.**

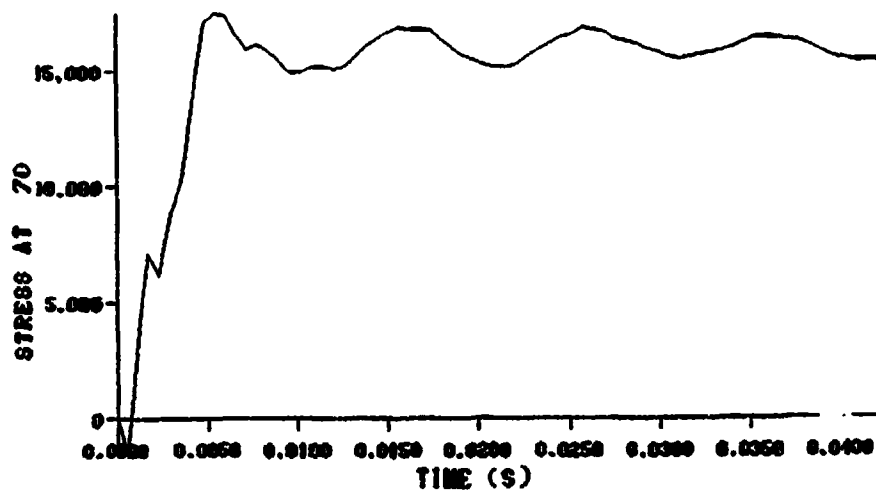
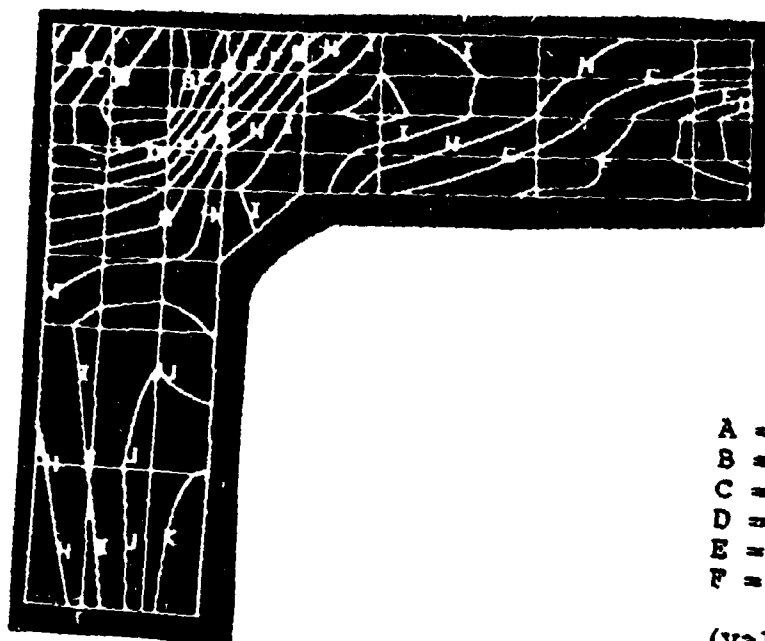


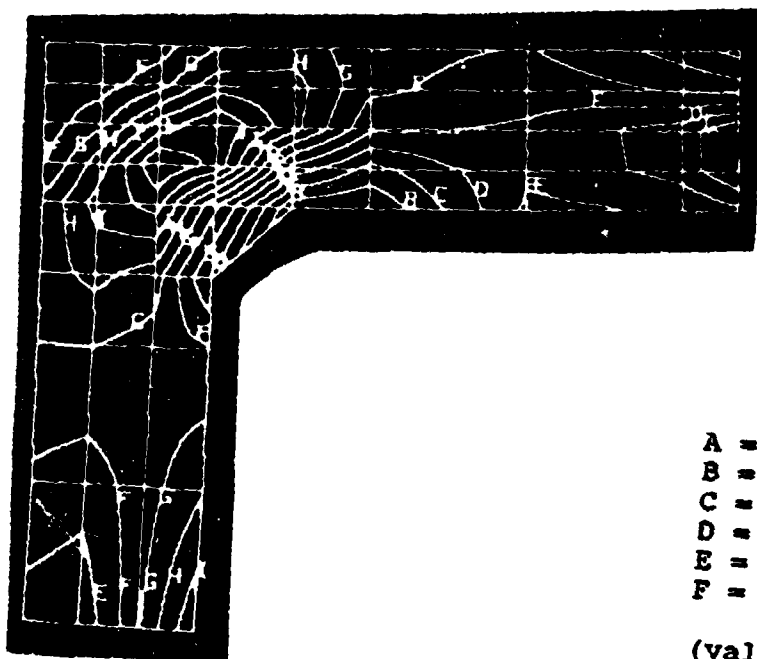
Figure 61. Time-history plots of uniaxial bar stress for connection detail BL-6A.



A = -388	G = 49
B = -274	H = 113
C = -209	I = 178
D = -144	J = 242
E = -80	K = 307
F = -16	L = 371

(values in lb/in<sup>2</sup>) 1

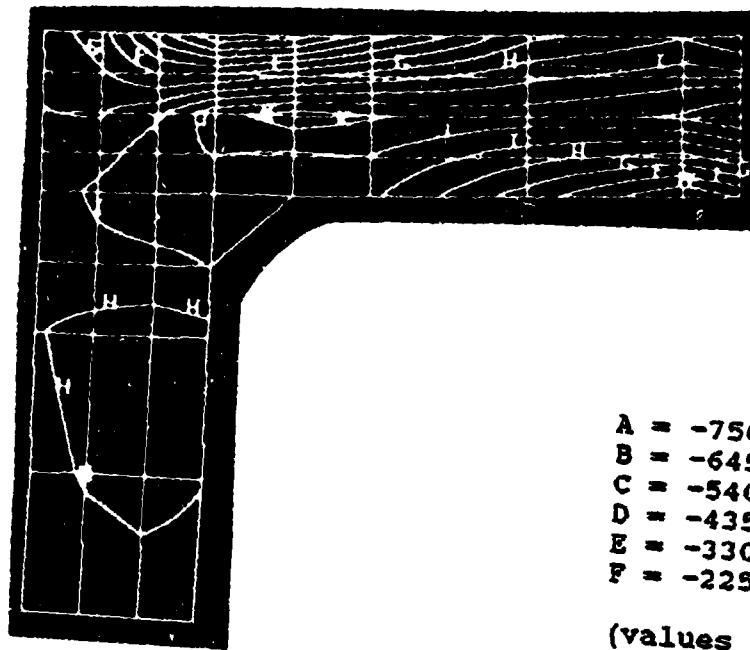
Figure 62. Picture of shear stress at an early time for connection detail BL-6A.



A = -267	G = 35
B = -217	H = 86
C = -166	I = 136
D = -116	J = 187
E = -65	K = 237
F = -14	L = 288

(values in lb/in<sup>2</sup>) 2

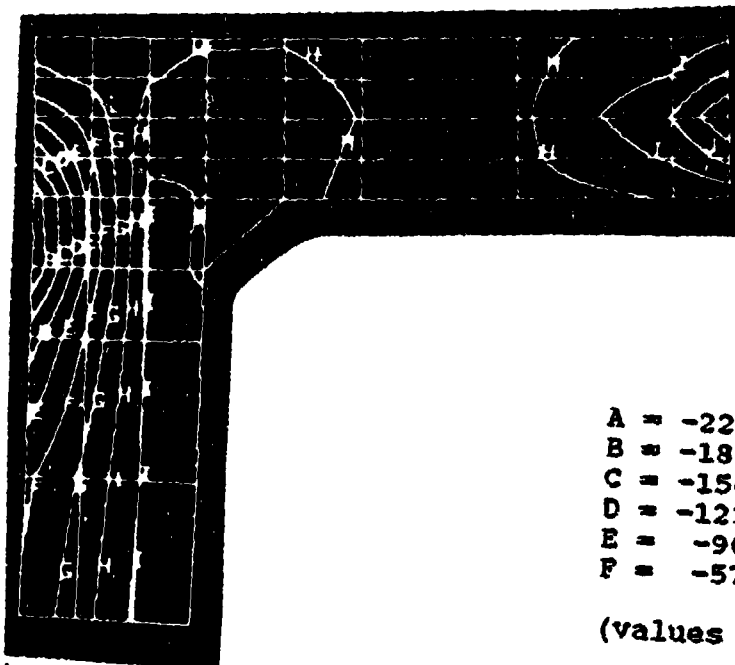
Figure 63. Picture of shear stress at a late time for connection detail BL-6A.



A = -750	G = -120
B = -645	H = 14
C = -540	I = 91
D = -435	J = 196
E = -330	K = 301
F = -225	L = 406

(values in lb/in<sup>2</sup>) 3

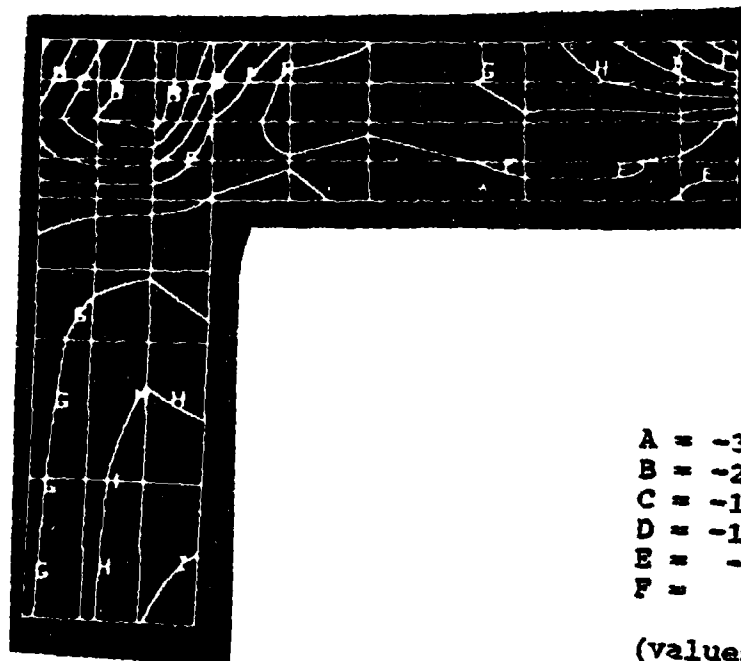
Figure 64. Picture of x-direction stress for connection detail BL-6A.



A = -2219	G = -243
B = -1890	H = 87
C = -1560	I = 416
D = -1231	J = 745
E = -902	K = 1075
F = -572	L = 1404

(values in lb/in<sup>2</sup>) 4

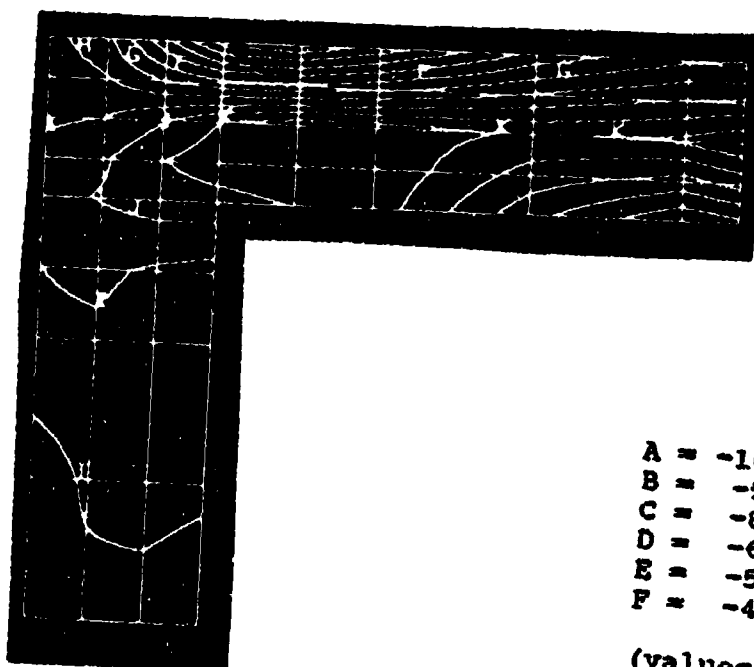
Figure 65. Picture of y-direction stress for connection detail BL-6A.



A = -318	G = 79
B = -252	H = 146
C = -186	I = 212
D = -120	J = 278
E = -53	K = 344
F = 13	L = 410

(values in lb/in<sup>2</sup>) 5

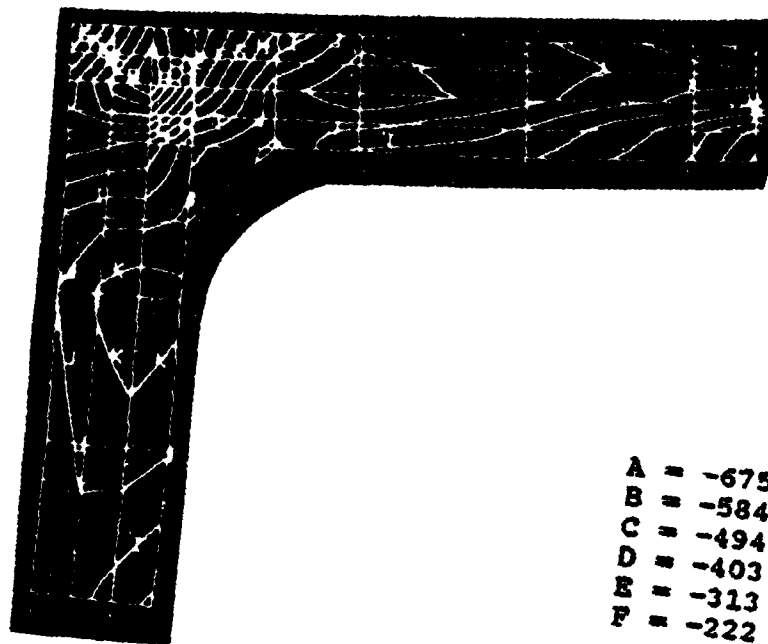
Figure 66. Picture of shear stress at an early time for connection detail BL-1A.



A = -1067	G = -272
B = -935	H = -139
C = -802	I = -7
D = -669	J = 126
E = -537	K = 259
F = -404	L = 391

(values in lb/in<sup>2</sup>) 6

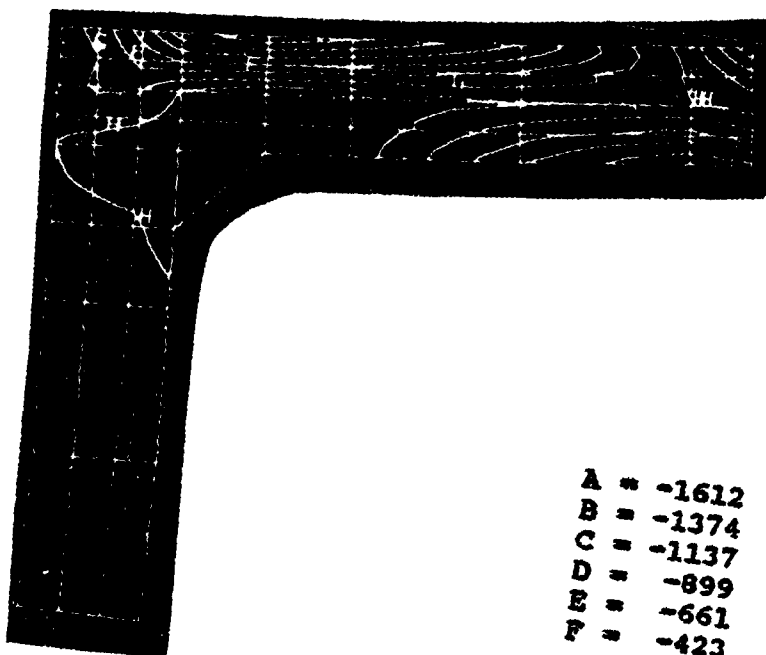
Figure 67. Picture of x-direction stress for connection detail BL-1A.



A = -675	G = -131
B = -584	H = -41
C = -494	I = 50
D = -403	J = 141
E = -313	K = 231
F = -222	L = 322

(values in lb/in<sup>2</sup>) 7

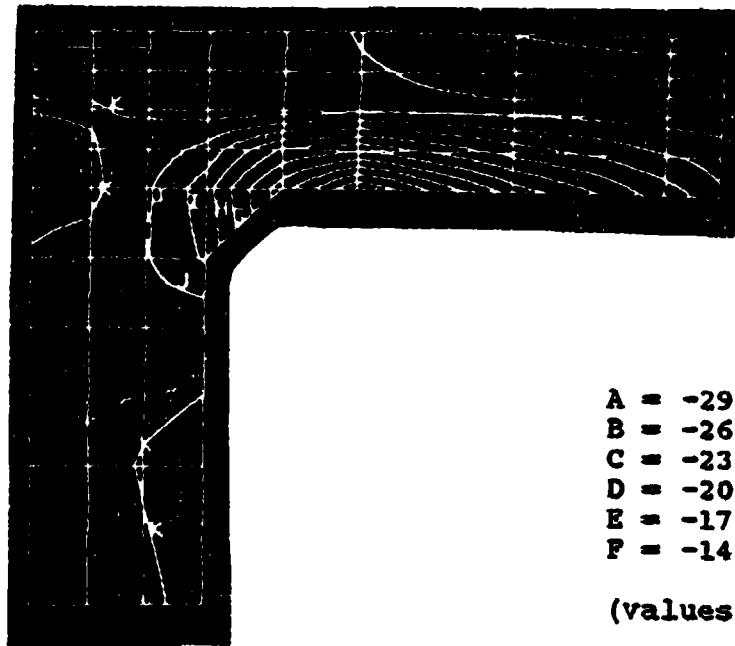
Figure 68. Picture of shear stress at an early time for connection detail BSL2A.



A = -1612	G = -186
B = -1374	H = 52
C = -1137	I = 290
D = -899	J = 528
E = -661	K = 765
F = -423	L = 1003

(values in lb/in<sup>2</sup>) 8

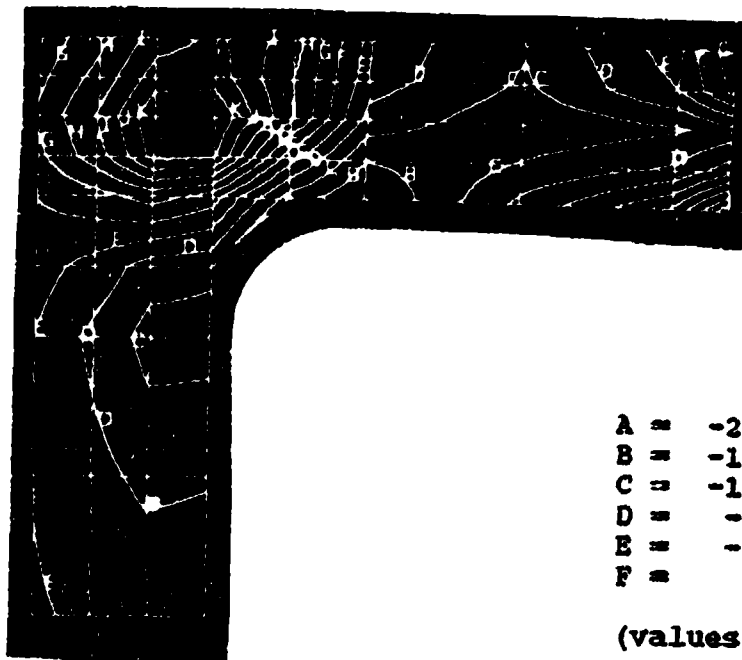
Figure 69. Picture of x-direction stress for connection detail BSL2A.



A = -2959	G = -1193
B = -2665	H = -898
C = -2370	I = -604
D = -2076	J = -309
E = -1782	K = -15
F = -1487	L = 279

(values in lb/in<sup>2</sup>) 11

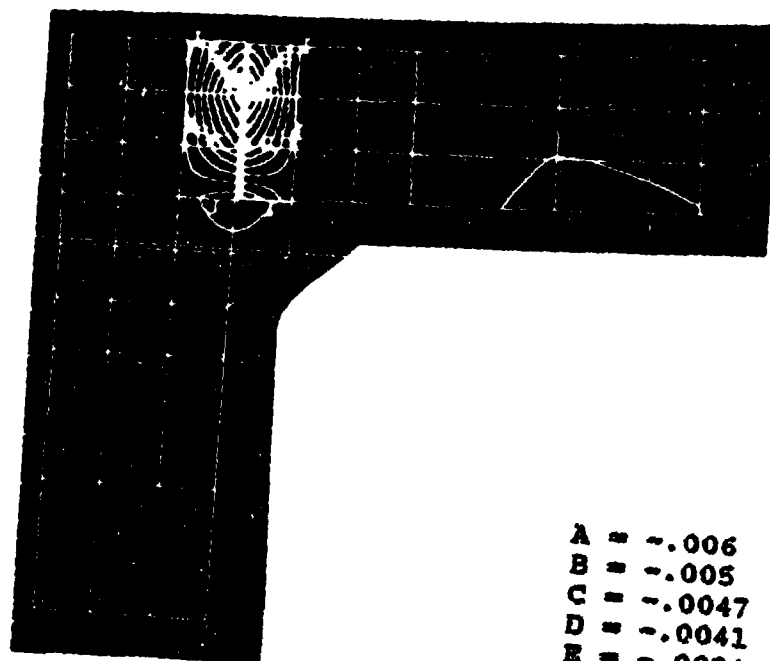
Figure 71. Picture of x-direction stress for connection detail BL-6B.



A = -243	G = 62
B = -192	H = 113
C = -141	I = 164
D = -91	J = 214
E = -40	K = 265
F = 11	L = 316

(values in lb/in<sup>2</sup>) 12

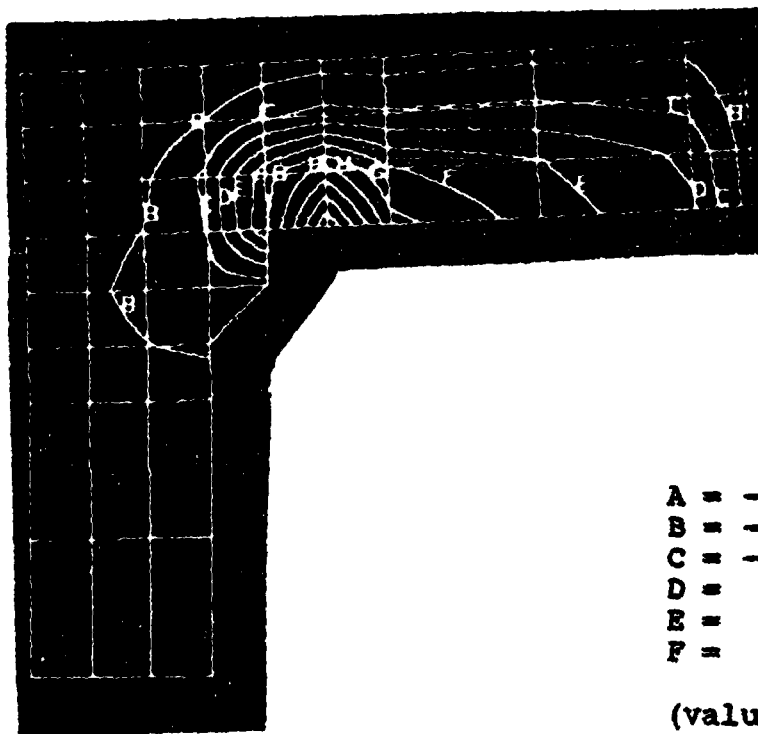
Figure 70. Picture of shear stress at an early time for connection detail BL-6B.



A = -.006	G = -.0021
B = -.005	H = -.0015
C = -.0047	I = -.0008
D = -.0041	J = .0001
E = -.0034	K = .0011
F = -.0028	L = .0020

(values in inch/inch) 9

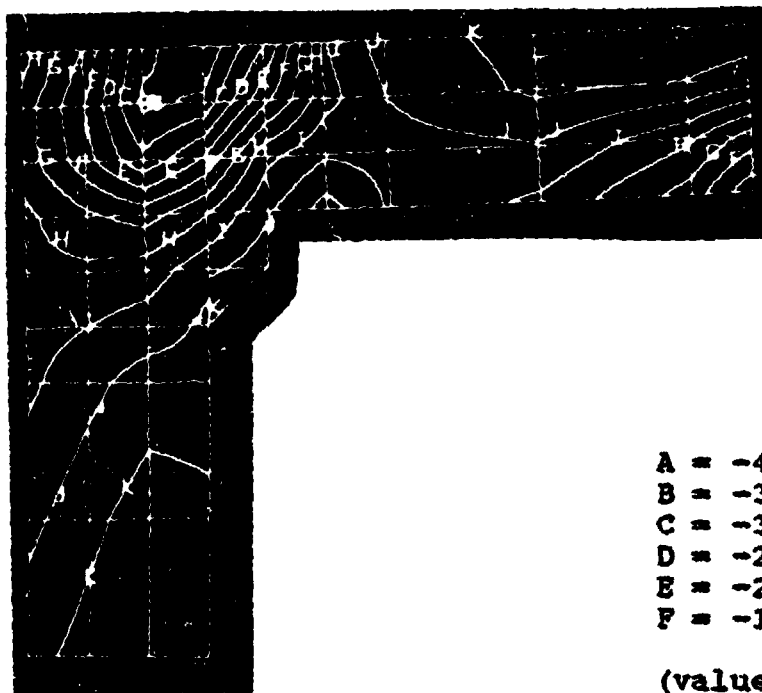
Figure 72. Picture of x-direction strain for connection detail PL-1D.



A = -.0001	G = .001
B = -.000	H = .001
C = -.000	I = .001
D = .000	J = .002
E = .000	K = .007
F = .001	L = .020

(values in inch/inch) 15

Figure 73. Picture of x-direction strain for connection detail PL-2S.

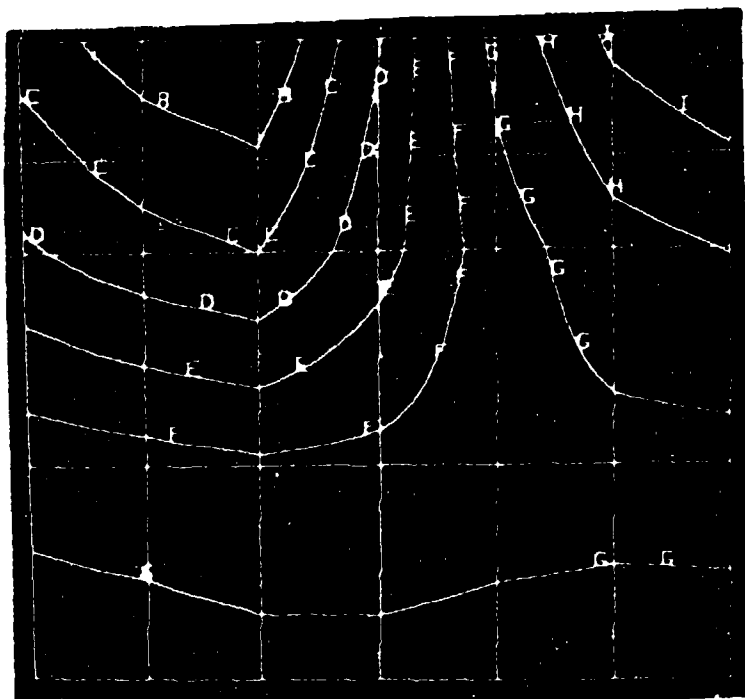


A = -460	G = -83
B = -397	H = -20
C = -334	I = 42
D = -271	J = 105
E = -208	K = 160
F = -145	L = 231

(values in lb/in²) 16

Figure 74. Picture of shear stress at an early time for connection detail PL-2S.

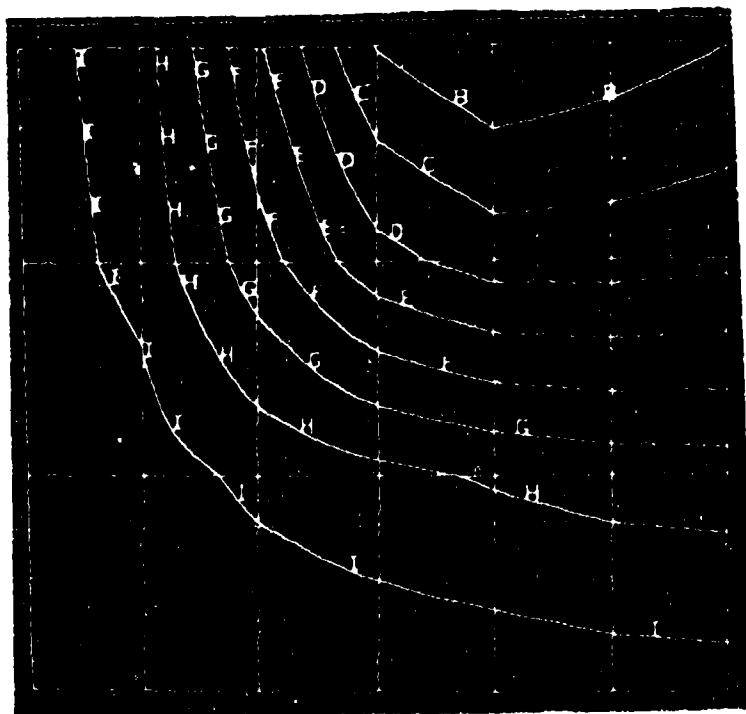




A = -1510	G = -172
B = -1282	H = 51
C = -1064	I = 274
D = -841	J = 497
E = -618	
F = -395	

(values in lb/in<sup>2</sup>) 13

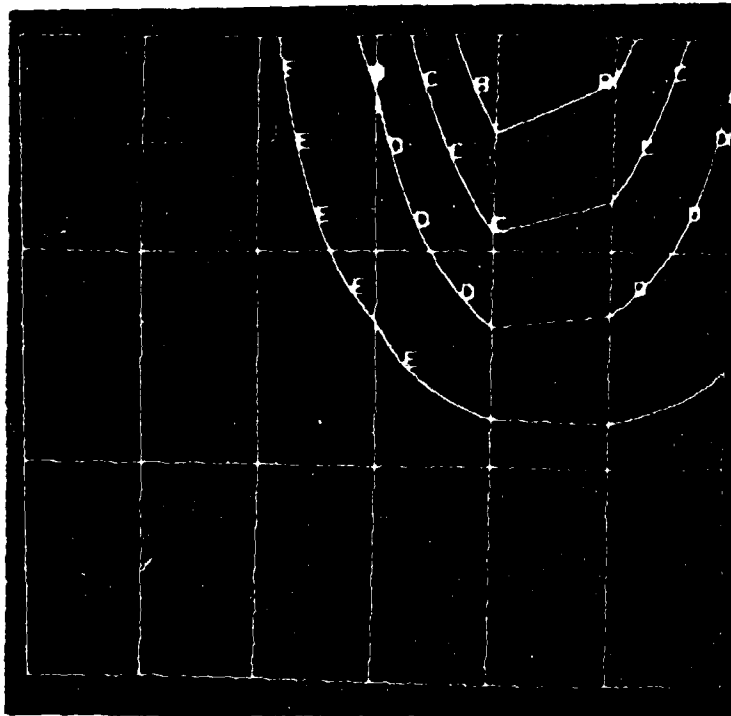
Figure 75. Picture of shear stress for opening detail STAND.



A = -6243	G = -2115
B = -5555	H = -1427
C = -4867	I = -739
D = -4179	J = -51
E = -3491	
F = -2803	

(values in lb/in<sup>2</sup>) 14

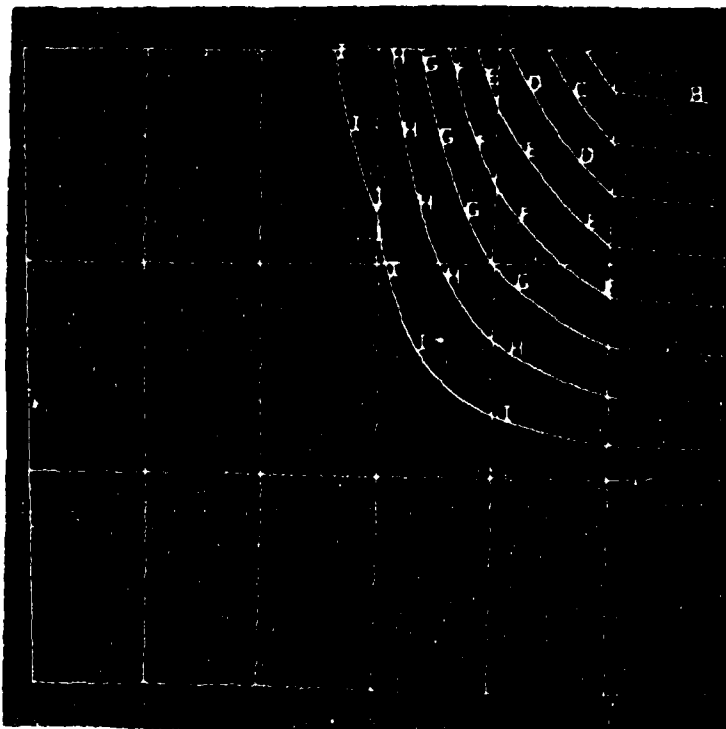
Figure 76. Picture of y-direction stress for opening detail STAND.



A = -2057	G = 548
B = -1623	H = 983
C = -1189	I = 1417
D = -754	J = 1851
E = -320	
F = 114	

(values in lb/in<sup>2</sup>) 17

Figure 77. Picture of shear stress for opening detail SIFCO.



A = -6597	G = -2198
B = -5864	H = -1465
C = -5131	I = -731
D = -4397	J = 2
E = -3664	
F = -2931	

(values in lb/in<sup>2</sup>) 18

Figure 78. Picture of y-direction stress for opening detail SIFCO.

## 5.1 CONNECTIONS

Connections are discussed in the same order for which they were investigated, beginning with the monolithic knee joint. As stated in Section 3, results were monitored during the course of the investigation, allowing an evolution of improvements to each successive detail. The intent is not to exhibit all of the trials; however, descriptive details along the path of improvement have been singled out for comparison reasons. As stated earlier, these comparisons are described in a table of maximum values for critical elements for each type of connection detail studied. These values will then be compared to limits set forth in Section 2.8.2, the strength and serviceability criteria.

### 5.1.1 Calculated Maximum Allowable Values

In reference to Section 2.8.2, the specific maximum allowable values pertaining to each parameter at critical points in the structure are calculated as follows:

5.1.1.1 Maximum deflection at midspan (or the end of a cantilever)  $d_{max} = L/240 = 0.5$  in  
( $L = 120$ -in clear span)

5.1.1.2 Compressive stress  $< 0.45 * f'_c = 2700$  lb/in<sup>2</sup>  
( $f'_c = 6000$  lb/in<sup>2</sup>)

5.1.1.3 Element bar stress  $< 2/3 * f_y = 43,300$  lb/in<sup>2</sup>  
( $f_y = 65,000$  lb/in<sup>2</sup>)

5.1.1.4 Joint bar stress  $< 1/3 * f_y = 21,600$  lb/in<sup>2</sup>

5.1.1.5 Direct shear  $< 0.8 \tau_u = 908$  lb/in<sup>2</sup>  
 $0.8 \tau_u = 0.8 [8(f'_c)^{1/2} + 0.8 \tau_y] < 0.35 f'_c$   
(The limiting detail for this case is BL-17.)

5.1.1.6 Flexural shear  $< (0.85) * 4 * (f'_c)^{1/2} = 263$  lb/in<sup>2</sup>  
when ties are not present in the joint.  
 $< [(0.85) * 12 * (f'_c)^{1/2/1.25} = 610$  lb/in<sup>2</sup>  
when ties are present in the joint.

### 5.1.2 Monolithic Knee Joints

The results of the monolithic knee joint tests are summarized in Tables 14 through 18. Tables 14 and 15 give values for joints without diagonal crossties subjected to loads accompanied with opening moments. Table 16 shows values of stress on crossties added to the joint. Tables 17 and 18 represent connections subjected to loads accompanied with closing moments.

The detail with a 12-in beam and column (BSL2A, Fig. 42) shows values of deflections and stresses which exceed the allowable in all respects. The reinforcement ratio (1.5%) is already quite high, which indicates that the overall size of the joint in this detail is not sufficient to resist the applied load.

The second detail (BL-17, Fig. 43) connects 18-in-thick members with a reinforcement ratio of 0.6%. The concrete elements remained within allowable values; however, the deflection at the cantilevered end was over by 24%. Also, very high bar stresses were recorded at the interior of the joint and along the diagonal bar. To strengthen the detail, the reinforcement ratio was increased to 1.0% (BL-1A). The performance of this connection was very good, with only two bars exceeding the allowable in the joint region. Bond loss and slippage may be a problem with these bars. Note that crossties are required for all applications of this detail.

The third connection (BL-6A, Fig. 44) is very similar to BL-17 with an 8-in haunch located at the interior of the joint interface and a steel ratio of 0.6%. This detail satisfied all the criteria required, with one exception - the deflection was over by 14%. The bar stresses at the interior of the joint were

very low, which indicates a high survivability rate under repeated loading conditions. Increasing the size of the diagonal steel (BL-6C) was of little benefit to the connection, which indicates that the area of diagonal steel should be held to  $0.5 A_{s1}$ . Both connections BL-1A and BL-6A performed very well when subjected to loads accompanied with a closing moment. Tables 17 and 18 show all parameters within the allowable range, with only a slight overstress noted in the tensile reinforcement in elements 55 and 56.

The connection which performed the best out of the five, incorporated SIFCON material (BLS6A, Fig. 45) in the joint region. Both deflections and bar stresses in the joint region decreased dramatically. The use of SIFCON in the connection should virtually eliminate the need for shear and confinement ties. Reinforcement bond loss will be almost nonexistent due to the high crack-control qualities inherent in SIFCON.

Diagonal crossties have been added to the interior of the joint (Fig. 46) in details BSL2A, BL-1A, and BL-6A in accordance with the proposed Eq. 4. The titles of the new details are BSL2S, BL-1S, and BL-6S, respectively. The first two connections required the use of these ties due to their high ratio of steel (1.5% and 1.0%), while the third with a ratio of 0.6% did not. The results of this test are shown in Table 16. Note that only the stresses in the crossties have been shown since their effect on the rest of the parameters was minimal. The stresses developed in the bar element 83 correlate well with the expected behavior. The values shown for BSL2S ( $20000 \text{ lb/in}^2$ ) and BL-1S ( $18200 \text{ lb/in}^2$ ) are approximately four times that recorded for BL-6S ( $5500 \text{ lb/in}^2$ ). The corresponding tensile strains developed in the concrete definitely indicate that diagonal cracking has occurred in the first two connections, while strains were still in the uncracked range for the third - good indication that proposed Eq. 4 is appropriate for wall/slab connections.

TABLE 14. Results for monolithic knee joints subjected to opening moments (concrete elements).

ELEMENT no.	PARAMETER	ALLOW.	BSL2A	BL-17	BL-1A	BL-6A	BL36A
node 148	disp. in	0.5	1.03	0.62	0.53	0.57	0.46
19	Y-strain	%	0.51	0.27	0.26	0.42	0.16
29	X-stress	-2700	-3600	-2400	-2400	-2400	-1400
	shear						
14	flexure	610	-1100	-490	-470	-480	-480
22	direct flexure	-908 610	-900 430	-340 310	-340 280	-260 250	-390 120
27	direct flexure	-908 610	-590 350	-525 435	-550 410	-480 302	-280 210
31	direct flexure	-908 610	-550 420	-570 250	-540 260	-610 250	-480 330

TABLE 15. Results for monolithic knee joints subjected to opening moments (bar elements).

ELEMENT no.	STRESS lb/in <sup>2</sup>	ALLOW.	BSL2A	BL-17	BL-1A	BL-6A	BL36A
55	bar	21660	-9500	-10000	-9300	-7800	-15000
56	bar	43330	-14400	-11000	-12000	-10000	-23000
57	bar	43330	-19600	-9000	-10000	-9600	-26000
62	bar	43330	52000	36000	32000	43000	24000
63	bar	43330	45000	46000	36000	32000	17000
64	bar	21660	25000	40000	31000	18000	10000
65	bar	21660	19000	25000	21000	7500	6100
66	bar	21660	8100	9000	8000	1700	4000
69	bar	21660	17000	19000	16000	4800	7200
70	bar	21660	26000	34000	27000	17000	15000
71	bar	43330	44000	49000	41000	36000	18000
72	bar	43330	57000	38000	34000	45000	26000
73	bar	43330	56000	35000	31000	36000	41000
76	bar	43330	33000	15000	15000	18000	9400
78	bar	43330	46000	63000	46000	43000	26000
80	bar	43330	17000	23000	28000	13000	14000

TABLE 16. Results for diagonal crossties.

ELEMENT no.	STRESS lb/in <sup>2</sup>	ALLOW.	BSL2S	BL-1S	BL-6S
83	bar	21660	20000	18200	5500
86	bar	21660	7500	5200	3500

TABLE 17. Results for monolithic knee joints subjected to closing moments (concrete elements).

ELEMENT no.	PARAMETER	ALLOW.	BL-1A	BL-6A
node 148	displ. in.	0.5	-0.43	-0.45
19	Y-strain	‡	0.07	0.07
29	X-stress	-2700	500	500
	shear			
14	direct flexure	-908 610	810 810	430 -220
22	direct flexure	-908 610	440 480	560 400
27	direct flexure	-908 610	440 -680	440 -230
31	direct flexure	-908 610	370 -370	350 -350

TABLE 18. Results for monolithic knee joints subjected to closing moments (bar elements).

ELEMENT no.	STRESS lb/in <sup>2</sup>	ALLOW.	BL-1A	BL-6A
55	bar	21660	33000	27000
56	bar	43330	41000	46000
57	bar	43330	38000	37000
72	bar	43330	-17000	-17000
73	bar	43330	-13000	-13000
78	bar	43330	-8000	-17000

### 5.1.3 Monolithic Tee Joints

The results for the monolithic tee joint are shown in Tables 19 and 20. The connection BT-6A (Fig. 47) utilizes a detail similar to the knee joint BL-6A modeled with a 4.5-in diagonal strut. The tensile reinforcement in the beam extending into the core of the joint (elements 102 through 105) are stressed well into the yield range. Therefore, we increased the strut size to 9 in and the area of the diagonal steel to 0.6% in detail BT-9A (Fig. 48). This reduced the tensile stresses in the joint region to within acceptable values; however, stresses in elements 104 and 105 are still beyond the designated two-thirds yield limit. These bars are expected to yield and create a hinge at the tip of the diagonal haunch. The core of the joint in this detail is relatively unaffected by the hinge, and therefore anchorage failure in the connection is not anticipated. Both details have shown high flexural shear stresses at the interface and interior of the joint. This is due to a stiff column and flexible beam configuration. Correct design of shear stirrups at these regions of concentrated moment and shear is a necessity. As stated earlier, beam/slab ties should be continued to the face of the joint, while column/wall ties should be continued through the joint. The reinforcement in the column was subject to very light stress (a maximum of 23000 lb/in<sup>2</sup> located in element 90).

### 5.1.4 Precast Knee Joints

The results of the precast knee joint connection tests are summarized in Tables 21 and 22. Detail PL-1D (Fig. 49) transfers all compressive loads through a flexible, reinforced fiber pad. Deflections are maintained at an acceptable value; however, compressive stress in the top reinforcement (element 76) is well into the yield range, which may cause local buckling of the bar. The stress in the tensile reinforcement (element 68) does not reach yield; however, the stress is 20% higher than allowable.



TABLE 19. Results for monolithic tee joints  
(concrete elements).

ELEMENT no.	PARAMETER	ALLOW.	BT-6A	BT-9A
node 243	disp. in.	0.5	0.33	0.27
57	Y-strain	$\frac{1}{3}$	0.28	0.24
35	X-strain	$\frac{1}{3}$	0.06	0.14
	shear			
22	direct flexure	-908 610	-220 240	-180 220
25	direct flexure	-908 610	-660 310	-600 410
38	direct flexure	-908 610	-280 170	-240 430
40	direct flexure	-908 610	-520 210	-580 210
54	direct flexure	-908 610	-530 320	-580 160

TABLE 20. Results for monolithic tee joints  
(bar elements).

ELEMENT no.	STRESS lb/in <sup>2</sup>	ALLOW.	BT-6A	BT-9A
81	bar	21660	8000	4000
83	bar	21660	12000	12000
89	bar	43330	9000	16000
90	bar	43330	23000	14000
91	bar	21660	16000	7300
101	bar	21660	1000	2000
102	bar	21660	38000	14000
103	bar	21660	56000	40000
104	bar	43330	65000	57000
105	bar	43330	64000	63000
106	bar	43330	36000	44000
111	bar	43330	-22000	-15000
124	bar	21660	54000	43000
125	bar	43330	63000	56000
127	bar	43330	41000	33000

Table 21. Results for precast knee joints subjected to opening and closing moments (concrete elements).

ELEMENT no.	PARAMETER	ALLOW. lb/in <sup>2</sup>	PL-1D	PL-2S	PL-4S	PL-7S	PL-4B
node 165	disp. in	0.5	0.53	0.45	0.47	0.43	-0.37
8	X-stres	-2700		-600	-300	-380	-130
24	X-stres	-2700		-2050	-1450	-1700	500
33	X-stres	-2700	-1550	550	560	560	-1200
	shear						
14	flexure	-620	-505	-424	-365	-480	500
15	flexure	-620		-580	-465	550	540
22	flexure	-620		-300	-400	-450	510
31	direct flexure	-620		-550 210	-460 190	-480 175	380 -300

Table 22. Results for precast knee joints subjected to opening and closing moments (bar elements).

ELEMENT PL-1D	ELEMENT PL-#S	ALLOW. lb/in <sup>2</sup>	PL-1D	PL-2S	PL-4S	PL-7S	PL-4B
60	56	43000	41000	42500	44100	43000	-15000
61	57	43000			42000	41000	-13000
62	58	43330			25000	22000	-6500
63	59	43000			16000	11000	-3000
64	60	43330			4500	3000	-2000
66	62	43000		30000	10000	1900	7000
67	63	43330		33000	12000	20000	8000
68	64	43000	56000	38000	23000	24000	8000
69	65	43000		58000	43000	42000	7000
70	66	43330	53000	65000	55000	58000	7000
71	67	43000	59000	62000	48000	50000	4000
75	71	-43330		30000	7000	17000	11000
76	72	-43000	65000	27000	6000	16000	28000
77	73	-43330		27000	8000	14000	65000
78	74	-43000		27000	6500	14000	54000
79	75	-43000		27000	7000	15000	45000
84	80	43330	25000	32000	35000	34000	-10000
85	81	43330	25000	65000	65000	53000	-65000

The stress developed in the strut of the angle (element 85) reaches a maximum of  $25000 \text{ lb/in}^2$  which is lower than expected. Shear in both the column/wall and beam portion of the connection requires the use of ties which should be extended into the joint region.

Details PL-2S and PL-4S (Fig. 50) are grouted in place with a  $6000\text{-lb/in}^2$  concrete. stress in the compressive reinforcement is well within allowable limits; however, tensile stress in the bottom bars of detail PL-2S (elements 65 and 66) is very near yield. Reducing the amount of prestress in details PL-4S to  $10 \text{ k/in}^2$  has lowered the stress to near acceptable values. Stiffening the compressive region of this connection with grout has increased the tensile stress into the yield range on the continuous angle assembly, located at the corbel. The spacing of the stiffeners on this assembly should be decreased to 10 in on center. Detail PL-4B, similar in configuration to PL-4S, has been subjected to a loading associated with a closing moment. Stress in the tensile reinforcement (element 73) extends into the yield range which is expected at the grout region or cold joint locations. Compressive stress in the angle strut also extends into the yield range and may cause local buckling. Again it is recommended that the spacing of these stiffeners be decreased to 10 in on center to help alleviate this problem. Furthermore, it is advisable to increase the reinforcement yield stress to  $88 \text{ k/in}^2$  for steel crossing the discontinuous gap between elements, due to the buildup of stress at that point. Connection detail PL-7S, which follows this recommendation, exhibits a behavior with stress values very near the acceptable range. Maximum tensile stress in the bar elements reaches  $58000 \text{ lb/in}^2$  in element 66, which is slightly less than two-thirds  $f_y$ . In addition, stress in the diagonal strut (element 81) is reduced to  $53000 \text{ lb/in}^2$ . Mechanical bond plates in the column/wall should eliminate bond slippage and loss; however, confinement ties designed according to Eqs. 1 and 2 are a necessity.

#### 5.1.5 Precast Tee Joints

One precast tee joint detail (PL-8S) was examined in a manner similar to PL-4S, with an additional beam attached to the opposite face of the column. The additional beams restraint at midspan is similar to the restraint located at the base of the column. The maximum tensile stress developed in the reinforcement (element 91, refer to Fig. 47) reaches near yield conditions ( $62000 \text{ lb/in}^2$ ). The stress in the angle strut (element 125) reaches a peak at approximately  $46000 \text{ lb/in}^2$ . Compressive stresses in the reinforcement are negligible.

### 5.2 OPENINGS IN REINFORCED CONCRETE STRUCTURES

Due to the extreme behavior observed in the localized response of concrete directly subjected to a blast loading, adhering to the criteria for strength and serviceability outlined earlier is not feasible. Each parameter for analysis must be looked at individually for failure conditions. If failure occurs at any particular point in the detail, a determination must be made as to its effects on the remainder of the structure and its overall strength and serviceability.

#### 5.2.1 Reinforced Concrete Openings

Width of load distribution is the key factor in the design of opening edge reinforcement. After several preliminary test runs, it was concluded that a detail with a top and bottom plate 12 in wide (STAND, Fig. 52) is required to distribute the load. In Tables 23 and 24, flexural stresses in the reinforcement are within allowable values; but stresses due to direct shear are much higher, which accounts for the large number of bars used in the section. The maximum compressive force experienced by the concrete directly beneath the plate (elements 15 and 16) reaches  $6800 \text{ lb/in}^2$ . This is entirely possible for a confined concrete with

$f'_c = 6000 \text{ lb/in}^2$ ; however, the concrete in this region is expected to experience a large amount of damage. To test this damaged detail, soft elements (to simulate crushed concrete) were inserted between the top plate and the remaining portion of undamaged concrete with the plate anchorages left intact (CRUSH, Fig. 53), and a second blast load was then applied. The most pronounced effect of this second loading is resisted by the vertical plate anchorages (elements 49 and 52). Compressive stresses extend into the strain hardening portion of the bars and reach a peak value of  $95000 \text{ lb/in}^2$ . Bond is lost and buckling occurs. This opening will not resist a third blast load.

### 5.3 SIFCON OPENINGS

The top and bottom plates required for distribution of blast loads to SIFCON may be limited to 6 in (SIFCO, Fig. 54). The stresses due to direct shear and compression are within the allowable ranges with no sign of damaged areas. Note that the area of steel fibers in the SIFCON material was used for the calculation of direct shear capacity. The observed behavior indicates that SIFCON will significantly improve the response of the opening detail.

### 5.4 INSERTS FOR ATTACHMENTS

After several evaluations of the proposed detail, it was found that an attachment consisting of an insert ( $A_{si} = 0.31 \text{ in}$  and  $f_y = 60 \text{ k/in}^2$ ) connected directly to the main flexural reinforcement of the structure showed no signs of failure when a 1000-lb supported weight was subjected to an acceleration of 20 g. The maximum stress in the insert attained a value of  $35000 \text{ lb/in}^2$  which is well below yield. These results indicate that the proposed detail should be adopted for the construction of attachments in hardened facilities. Linear interpolation is recommended for developing attachment details for cases different from the present conditions.

TABLE 23. Results for openings in concrete structures (bar elements).

ELEMENT STAND	ELEMENT CRUSH	ELEMENT SIPCO	STAND	CRUSH	SIPCO
30	30	30	41000	7200	23000
33	33	33	15000	55000	42000
35	35	35	24000	41000	32000
45	45	45	-25000	-34000	16000
57	49	17 shear	-46000	-95000	-2200
60	52	56	-47000	-95000	-65000

TABLE 24. Results for openings in concrete structures (concrete elements).

ELEMENT no.	PARAMETER	STAND	CRUSH	SIPCO
12	Y-stress	-4300	-1600	-3900
15	Y-stress	-6800	-3500	-1450
16	Y-stress	-6800	-3600	-7300
17	Y-stress	-6700	-3200	-10600
18	Y-stress	-4600	-2400	-8100
	shear			
8	direct	-1900	-1750	-2300
9	direct	-1900	-1400	-2200
14	direct	-1900	-1500	-2200

## **6.0 CONCLUSIONS AND RECOMMENDATIONS**

### **6.1 INTRODUCTION**

This study was initiated for the development of design recommendations for structural details of connections, openings and attachments in reinforced concrete protective structures. The urgent need for such recommendations has become evident in recent years, following a significant number of experimental studies that highlighted deficiencies in current design approaches. These deficiencies do not necessarily reflect errors in those documents, but rather lack of specific recommendations on how such structural details should be implemented.

The approach adopted for this study, as presented in Section 3, was to perform "numerical experiments" of typical structural details, and to modify the structural details until a desired behavior was achieved. Prior to these experiments, an extensive review of previous studies on related topics was conducted, and structural details were selected for a closer evaluation. The analyses and the results obtained by this approach were presented and discussed in Sections 4 and 5. Specific conclusions and partial recommendations were presented throughout this report, as they became evident from the study. Nevertheless, the important findings, and the design recommendations are combined in this section.

### **6.2 CONCLUSIONS**

Two types of conclusions were derived from this study. The first were about the accuracy and practicality of the approach, and the second about the structural behavior of specific construction details in protective structures.

"Numerical experiments," or simulations, are an attractive alternative for studying structural responses under various loading conditions, especially those responses to severe explosively induced loads. Performing real experiments is an extremely expensive endeavor, and there are always difficulties that may render specific tests wasted. Furthermore, the time required for preparing, performing and interpreting experiments is significant, a factor that may delay the outcome from a given study. Despite these arguments, one must ensure that numerical simulations of real behavior are accurate and that the results are reliable. An important part of this study was devoted to establishing these requirements. The choice of the numerical method, the computer code, constitutive models for reinforced concrete and SIFCON were discussed in Sections 2 and 3. The combination of these elements were then validated by the analyses of two structures for which experimental data were available. Furthermore, certain components of this approach were used in other studies performed by members of this research group, as discussed in Sections 2 and 3, and the experience gained from such efforts were implemented herein. Therefore, the conclusion derived about the validity of the approach and its practicality is very clear. It is quite acceptable to perform numerical simulations of real structural behavior, as presented in this report, provided that the analysts ensure that the required conditions for performing such "experiments" are met.

The numerical approach adopted for this study provided a large body of reliable data that was used for the evaluation of the structural details under consideration. The continuous evolution of these details highlighted the influence of how changes in the design, or construction, would affect the observed response. The results obtained from this study demonstrate that careful attention to details is critical for any structure, and especially for protective structures. This conclusion is not



new; it has been known for many years (see for example, Park and Paulay, 1975), but it has also been ignored by many designers. The main conclusion derived from this study is that careful practice of current design recommendations for static design should, in most cases, eliminate the simple problems. However, close attention to the dynamic effects is required, and the analyst/designer should implement the recommendations from this study, as presented next.

### 6.3 RECOMMENDATIONS

Several important observations were made during this study, and they are presented next.

#### 6.3.1 General Recommendations

6.3.1.1 Reinforcement ratios ( $A_s/bd$ ) in slab/wall connections shall be limited to a range of between 0.5% to 0.75%. If higher reinforcement ratios are required to resist the applied loads by the adjoining members, the size of the detail should be increased. The reason for this recommendation is to prevent congestion of the steel detail. For beam/column connections, it is appropriate for the reinforcement ratio to exceed 0.75%, but cross-ties (stirrups) must be provided, according to the following recommendations.

6.3.1.2 Stirrups for diagonal shear are required in all beam/column joints in accordance with ACI 318-83 (1986) Type Two connections for shear and confinement (Eqs. 1 and 2 in Section 2). The designer may use the recommendation by Park and Paulay '75 for diagonal splitting (Eqs. 3 and 4 in Section 2).

- 6.3.1.3 Reinforcement terminating in a knee joint should be developed in a 180-deg bend, with the return leg embedded in the opposing force region.
- 6.3.1.4 Reinforcement terminating in a tee joint should be developed in a 90-deg hook with the legs extending through the mid-height of the connection (Eq. 8 in Section 2).
- 6.3.1.5 Minimum clear cover for reinforcement should exceed  $2d_b$  and the minimum bar spacing should exceed  $3d_b$  for limiting the effects of splitting cracks as set forth in the ACI 318-89 code (to appear in early 1990).
- 6.3.1.6 Diagonal haunches or splays (8 in for an 18-in member thickness, and this ratio should be used for other dimensions) should be added to all inside corners.
- 6.3.1.7 Diagonal reinforcement equal to half the area of the main flexural steel is required at the inside corner of all knee joints. Diagonal reinforcement equal to the area of the main flexural steel is required at each inside corner of all tee joints.
- 6.3.1.8 A hinge should not occur in the joint region, and this can be controlled by the amount of diagonal reinforcement.
- 6.3.1.9 Precast connections should be posttensioned to a minimum of  $20 \text{ k/in}^2$  for eliminating the formation of gaps which could allow external contamination to enter the facility.

### 6.3.2 Strength and Serviceability Requirements

- 6.3.2.1 The "ductility factor" ( $\mu$ ) should not exceed 1, and deflections should not exceed approximately  $L/240$  at midspan. The value for deflections may be altered by the designer depending on the structures requirements.
- 6.3.2.2 Average compressive stress due to flexure in the concrete immediately above the compression reinforcement should not exceed  $0.45 * f'_c$ .
- 6.3.2.3 Tensile and compressive stress in the reinforcement located in the elements should not exceed  $2/3 f_y$ .
- 6.3.2.4 Tensile and compressive stress in the reinforcement located in the joint region should not exceed  $1/3 f_y$ .
- 6.3.2.5 Direct shear at any point in the structure should not exceed the Hawkins shear limit  $\tau_m * 0.8$  (Eq. 9 in Section 2).
- 6.3.2.6 Diagonal shear located at the interior of slab/wall joints should not exceed  $[0.85(4)(f'_c)^{1/2}]/\alpha$ . For values of shear higher than this, stirrups must be added in accordance with ACI 318-83 (1986) Type Two connections.
- 6.3.2.7 The opening detail for reinforced concrete protective structures should follow the design concept presented in Fig. 52, as discussed in Section 4.3. The loads from the closure should be distributed onto steel plates having a minimum width of 12 in for concrete openings, and 6 in for SIFCON openings.

- 6.3.2.8 The use of a fiber reinforced concrete material, such as SIFCON, should be considered for connections and opening details that cannot be designed to react according to the above requirements. Although not a requirement for all cases, the results obtained in this study suggest that a significantly superior response can be achieved by such substitution.
- 6.3.2.9 Attachments should be fastened directly to the structural slab/wall reinforcement to insure ductility.
- 6.3.2.9 Connecting precast elements in protective structures has proven to be a difficult task. High stress concentrations located at the discontinuous gap between elements must be properly designed for. Reinforcement used for posttensioning should consist of high strength ( $88 \text{ k/in}^2$ ) coil rods with a ratio ( $A_s/bd$ ) of 0.66% recommended for steel crossing this gap, and an equal amount of steel in the diagonal located at the haunch. An investigation should be performed on the applicability of a cruciform type precast element structure allowing continuity at the joint location with connections between elements occurring at midspan.

### 6.3.3 Recommendations for Further Research

Additional numerical studies should be performed in three-dimensions for a determination of blast load distribution in these type of details.

Due to the difficulties encountered in the precast connection details, a more comprehensive study on their use in protective structures should be completed before final recommendations on their implementation can be given.

As stated earlier, the intent of this study was to determine the best candidates for the structural details in question. These candidates, described by the above design recommendations, have been confirmed numerically. However, for a complete verification of their applicability, actual physical testing should be performed in the laboratory. After the laboratory evaluations, and possible modifications, field tests should be performed for final validation.

## BIBLIOGRAPHY

- Assadi-Lamouki, A., and Krauthammer, T., "Development of Improved Timoshenko Beam and Mindlin Plate Theories For the Analysis of Reinforced Concrete Structures Subjected To Impulsive Loads," Structural Engineering Report No. 88-02, Department of Civil and Mineral Engineering, University of Minnesota, May 1988.
- Balint, P.S., and Taylor, H.P., "Reinforcement detailing of frame corner joints with particular reference to opening corners," Cement and Concrete Association, Technical Report 42.462, London, February 1972.
- Bathe, K.J., "Finite element Procedures in Engineering Analysis," Prentice Hall Inc., Englewood Cliffs, New Jersey, 1982.
- "Building Code Requirements for Reinforced Concrete (ACI 318-83)," American Concrete Institute, Detroit, Michigan, 1983, 111 pp.
- Chen, W.F., and Han, D.J., "Constitutive Modelling in Analysis of Concrete Structures," Report CE-STR-85-38, Purdue University, Lafayette, Indiana, 1985.
- Chen, W.F., "Plasticity in Reinforced Concrete," McGraw-Hill Book Company, New York, New York, 1982.
- Collins, M.P., "Toward a Rational Theory for RC Members in Shear," ASCE Journal of Structural Division, ST4, pp. 649-666, April 1978.
- Coltharp, D.R., Vitayaudom, K.P., and Kiger, S.A., "Semihardened Facility Design Criteria Improvement", ESL-TR-85-32, U.S. Army Waterways Experiment Station, Vicksburg, Miss., Sep. 1985. (Limited Distribution)
- Cook, R. D., "Concepts and Applications of Finite Element Analysis," Second Edition, John Wiley and Sons, New York, 1981.
- Cook, W., and Mitchell, D., "Disturbed Regions in Reinforced Concrete", ACI Structural Journal, Mar.- Apr. 1988, pp. 206-216.
- Crawford, E.R., Higgins, C.J., and Bultmann, E.H., "The Air Force Manual for Design and Analysis of Hardened Structures," AFWL-TR-74-102, Air Force Weapons Laboratory, Kirtland AFB, NM., 1974.

- Feldman, A., and Siess, C.P., "Investigation of Resistance and Behavior of Reinforced Concrete Members Subjected to Dynamic Loading, Part II," Structural Research Series No. 165, University of Illinois, Sep. 1958.
- Frantziskonis G., and Desai, C.S., "Elastoplastic Model with Damage for Strain Softening Geomaterials," Acta Mechanica 68, pp. 151-170, 1987.
- Gefcan, P.R., and Ramey, M.R., "Hoop Spacing In Seismic Joints," ACI Journal, Vol 86, No. 2, March-April 1989, pp.168-172.
- Green, A.E., and Naghdi, P.M., "A Dynamical Theory of Interacting Continua," Int. J. Eng. Sci. 3, pp. 231-244, 1965.
- Hawkins, N.M., "The Strength of Stud Shear Connections," Civil Engineering Transactions, Institute of Engineers, Australia, pp. 39-45, Dec. 1974.
- Hawkins, N.M., "Dynamic Shear Resistance of Reinforced Concrete," Letter Report to U.S. Navy, Aug. 28, 1981.
- Hawkins, N.M., Lin, I., and Ueda, T., "Anchorage of Reinforcing Bars for Seismic Forces," ACI Structural Journal, Sep.- Oct. 1987, pp. 407-418.
- Homrich, J.R., Naaman, A.E., "Stress-Strain Properties of SIFCON in Uniaxial Compression and Tension," AFWL-TR-87-115, Air Force Weapons Laboratory, Kirtland AFB, NM, Aug. 1988.
- Hsu, T.T., Slate, F.O., Sturman, G.M., and Winter, G., "Microcracking of Plain Concrete and the Shape of the Stress-Strain Curve," ACI Journal, Vol. 60, No.2, 1963.
- Jayashankar, V., "An Interior Moment Resistant Precast Connection," M.S. Thesis, University of Minnesota, Oct. 1987.
- Kemp, E.L., and Mukherjee, F.R., "Inelastic Behavior of Concrete Knee Joints," The Consulting Engineer, Oct. 1968, pp 44-48.
- Riger, S.A., Getchell, J.V., Slawson, T.R., and Hyde, D.W., "Vulnerability of Shallow-Buried Flat Roof Structures," Technical Report SL-80-7, six parts, USA-WES, Vicksburg, Miss., Sept. 1980 to Sept. 1984.
- Krajcinovic, D., and Panella, D., "A Micromechanical Damage Model for Concrete," Eng. Fract. Mech., Vol. 25, Nos. 5/6, pp. 585-596, 1986.

- Krauthammer, T., "Reinforced Concrete Arches Under Blast and Shock Environments," The Shock and Vibration Bulletin, No. 57, part 4, January 1987, pp. 19-27.
- Krauthammer, T., and Stevens, D.J., "Development of an Advanced Computational Approach for the Analysis of Buried Reinforced Concrete Structures Subject to Severe Stress Transients," Structural Engineering Report ST-88-05, Department of Civil and Mineral Engineering, University of Minnesota, Sep. 1988.
- Leon, R., "Performance of Interior Joints with Variable Anchorage Lengths," ACI Structural Journal, (to appear).
- Leon, R., "Shear Strength and Hysteretic Behavior of Interior Beam - Column Joints," ACI Structural Journal, (to appear).
- Mattock, A.H., "Effect of Moment and Tension Across the Shear Plane on Single Direction Shear Transfer Strength in Monolithic Concrete," Report No. SM-74-3, Department of Civil Engineering, University of Washington, Oct. 74.
- Mattock, A.H., "Shear Transfer Under Monotonic Loading Across an Interface Between Concrete Cast at Different Times," Report SM76-3, Department of Civil Engineering, University of Washington, Sept. 76.
- Mattock, A.H., "Effect of Reinforcing Bar Size on Shear Transfer Across a Crack in Concrete," Report SM77-2, Department of Civil Engineering, University of Washington, Sept. 77.
- Mattock, A.H. and Hawkins, N.M., "Shear Transfer in Reinforced Concrete-Recent Research," PCI Journal, pp. 55-75, March-April 72.
- Mayfield, B., Kong, F.K., Bennison, A., and Davies, J.C., "Corner Joint Details in Structural Lightweight Concrete," ACI Journal Proceedings, Vol 68, No. 5, Detroit, May 1971, pp. 366-372.
- Mazars, J., "Mechanical Damage and Fracture of Concrete Structures," in Advances in Fracture Research (Fracture 81), Vol. 4, Pergamon Press, pp. 1499-1506, 1982.
- Mitchell, D. and Collins, M.P., "Diagonal Compression Field Theory-A Rational Model for Structural Concrete in Pure Torsion," ACI Journal, Vol. 71, pp. 306-403, Aug. 1974.
- Muller, F.X., Muttoni, A., Thurliman, B., "Durchstanzversuche an Flachdecken mit Aussparungen," Institut für Baustatik und Konstruktion, ETH Zurich, Bericht Nr. 7305-5, Dec. 1984.



- Murtha, R.N., and Holland, T.J., "Analysis of WES FY82 Dynamic Shear Test Structures," Naval Civil Engineering Laboratory, Technical Memorandum No. 51-83-02, Dec., 1982.
- Naeyaert, G.C., "Steel Fibers in Protective Structures, Structures for Enhanced Safety and Physical Security, Proceedings of the Specialty Conference, Structural Division of The American Society of Civil Engineers, March 1989, pp. 270-281.
- Newmark, N.M., and Rosenblueth, E., "Fundamentals of Earthquake Engineering," Prentice-Hall Inc., Englewood Cliffs, NJ, 1971.
- Nilsson, I.H.E., "Reinforced Concrete Corners and Joints Subjected to Bending Moment," National Swedish Building Research, Document D7, 1973.
- Ortiz, M., 1985, "A Constitutive Theory for the Inelastic Behavior of Concrete," Mech. of Mat., No. 4, pp. 67-93.
- Park, R., and Paulay, T., "Reinforced Concrete Structures," John Wiley and Sons, New York, NY, 1975.
- "PCI Design Handbook, Third Edition," Prestressed Concrete Institute, Chicago, Illinois, 1985.
- Read, H.E., and Hegemier, G.A., "Strain Softening of Rock, Soil and Concrete - A Review Article," Mech. of Mat. 3, pp. 271-294, 1984.
- "Recommendations for Design of Beam-Column Joints in Monolithic Reinforced Concrete Structures," reported by ACI-ASCE Committee 352, ACI Journal, May-June 1985, No. 2, V. 82, pp. 266-284.
- Resende, L., "A Damage Mechanics Constitutive Theory for the Inelastic Behaviour of Concrete," Comp. Met. in App. Mech. and Eng., Vol. 60, pp. 57-93, 1987.
- Ross, T.J., "Direct Shear Failure in Reinforced Concrete Beams Under Impulsive Loading," AFWL-TR-83-84, Air Force Weapons Laboratory, Kirtland AFB, NM, Sept. 83.
- Schreyer, H.L., and Bean, J.E., "Third-Invariant Models for Rate-Dependent Soils," J. Geo. Eng., ASCE, Vol. 111, No. 2, pp. 181-192, 1985.
- Schreyer, H.L., Richards, C.G., Bean, J.E., and Durka, G.R., "SAMSON2 Users Manual," AFWL-TN-82-18, Air Force Weapons Laboratory, Kirtland AFB, NM, September 1982 (Revised June 1984).

- Simo, J.C., and Ju, J.W., 1987, "Strain- and Stress-Based Continuum Damage Models--II. Computational Aspects," Int. J. Solids Structures, Vol. 23, No. 7, pp. 841-869.
- Simo, J.C., Ju, J.W., Taylor, R.L., and Pister, K.S., "On Strain-Based Continuum Damage Models: Formulation and Computational Aspects," in Constitutive Laws for Engineering Materials: Theory and Applications, Edited by C.S. Desai et al., Elsevier Science Publishing Co., pp. 233-245, 1987.
- Slawson, T.R., "Dynamic Shear Failure of Shallow-Buried Flat-Roofed Reinforced Concrete Structures Subjected to Blast Loading," Final report No. SL-84-7, U.S. Army Waterways Experiment Station, April 84.
- Soroushian, et al., "Pullout Behavior of Hooked Bars in Exterior Beam - Column Connections," ACI Structural Journal, May-June 1988, pp. 269-276.
- Swann, R.A., "Flexural Strength of Corners of Reinforced Concrete Portal Frames," Cement and Concrete Association, Technical Report TRA 434, London, November 1969.
- Vecchio, F.J. and Collins, M.P., "The Modified Compression-Field Theory for Reinforced Concrete Elements Subjected to Shear," ACI Journal, No. 2, Proceedings V. 83, pp.219-231, March-April 1986.
- Wagner, H., "Ebene Blechwantrager mit sehr Dumen Stegblech," Zeitschrift fur Flugtbchnik uno motorluftschiffahrt," Vol. 20, No. 8 212, Berlin, 1929.

## APPENDIX

### A CONTINUUM DAMAGE/PLASTICITY MODEL FOR CONCRETE

#### A.1 Continuum Damage Mechanics Model

The continuum damage mechanics model that is coupled with the Prager-Drucker model is based on a scalar damage approach. It can rightfully be argued that a complete three-dimensional treatment of microcracking effects on the response of concrete requires a higher order definition of the damage variable, and, first, second, fourth, and even eighth order tensors have been proposed. However, in cases where damage directionality is not a dominant feature, such as in the plane strain or plane stress conditions of beams, frames, and slabs, a scalar parameter is sufficient (Resende '87). The continuum damage model approach developed herein is based loosely on the approach of Frantziskonis and Desai '87.

The key assumption in this approach is that the material behavior can be decomposed into two constituents, a topical portion and a damaged portion. During loading, the topical material is progressively transformed into damaged material, which, in turn, suggests the use of the theory of mixtures or the theory of interacting continua (Frantziskonis and Desai '87). The topical material is treated as elastic/strain hardening plastic (using the modified Prager-Drucker cap model described later) while the damaged material is rigid/plastic. The topical, damaged, and total areas ( $A^t$ ,  $A^o$ , and  $A$ , respectively) and the topical, damaged, and total internal force vectors ( $F^t$ ,  $F^o$ , and  $F$ , respectively) acting on the area  $A$  are shown in Figure 20. The topical, damaged, and average stress tensors are defined as follows:

$$\begin{aligned} F_i^t &= \sigma_{ij}^t n_j \\ F_i^o &= \sigma_{ij}^o n_j \\ F_i &= \sigma_{ij} n_j \end{aligned} \tag{A-1}$$

where

$\sigma_{ij}^t$ ,  $\sigma_{ij}^o$ ,  $\sigma_{ij}$  = topical, damaged, and average stresses,  
respectively

$n_i$  = unit normal vector to the area A.

The average force is the sum of the damaged and topical forces and

$$\sigma_{ij} = (1 - d)\sigma_{ij}^t + d\sigma_{ij}^o \quad (A-2)$$

where

$d = A^o/A$  = damage parameter

Thus, the average stress is the summation of the partial stresses defined on the two components; it follows from the principle of angular momentum balance that the stress  $\sigma_{ij}$  is symmetric (Green and Naghdi '65; Frantziskonis and Desai '87). However, while this does not imply that the stresses  $\sigma_{ij}^t$  and  $\sigma_{ij}^o$  are symmetric, it is assumed herein that the topical and damaged stresses are symmetric. Also, since diffusion processes are absent, the strains in the damaged and topical components can be assumed as equal (Ortiz '85) and

$$\epsilon_{ij} = \epsilon_{ij}^t = \epsilon_{ij}^o \quad (A-3)$$

where

$\epsilon_{ij}$ ,  $\epsilon_{ij}^t$ ,  $\epsilon_{ij}^o$  = average, topical, and damage strain tensors.

At this point, Frantziskonis and Desai '87 assume that the damaged material can sustain only confining pressure and they rewrite Equation A-2 as

$$\sigma_{ij} = (1 - d)\sigma_{ij}^t + \frac{d}{3}\delta_{ij}\sigma_{kk}^t \quad (A-4)$$

where

$$\delta_{ij} = \text{Kronecker delta tensor} = \begin{cases} 1 & \text{if } i = j \\ 0 & \text{if } i \neq j \end{cases}$$

This assumption that the damaged material continues to support normal stresses is debatable since the microcracking that occurs in concrete reduces the area of contact over which both shear and normal stresses may act; this concept of area reduction is the principle upon which many, if not all, continuous damage mechanics theories are based (Krajcinovic '85b, Mazars '82, Ortiz '85). Therefore, an alternative assumption is made herein that the damaged material cannot support shear stresses or confining pressures, i.e.,  $\sigma_{ij}^o = 0$ . Thus, the average stress is now defined to be

$$\sigma_{ij} = (1 - d)\sigma_{ij}^t \quad (\text{A-5})$$

Again, the evolution of the topical stress,  $\sigma_{ij}^t$ , is governed by the modified Prager-Drucker cap model as discussed later.

Equation A-5 obviously determines both the reduction in stiffness of the damaged concrete as well as the development of strain softening or, alternatively, the reduction of stress with increased deformation (damage).

The next issue is the form of the evolution equations for the damage parameter,  $d$ . In view of the significance of tensile extensions in brittle damage processes, the evolution equations in the proposed approach will be parameterized using the concept of equivalent tensile strain (Simo, Ju, Taylor, and Pister '87), which is defined as follows. The spectral decomposition of the strain tensor may be written as

$$\epsilon_{ij} = \sum_{\alpha=1}^3 \epsilon^{(\alpha)} p_i^{(\alpha)} p_j^{(\alpha)} \quad (A-6)$$

where

$\epsilon^{(\alpha)}$  = eigenvalues of  $\epsilon_{ij}$ ,  $\alpha = 1, 2, 3$

$p_j^{(\alpha)}$  = normalized eigenvectors of  $\epsilon_{ij}$ ,  $\alpha = 1, 2, 3$

$$[(p_j^{(\alpha)} p_j^{(\alpha)})^{\frac{1}{2}} = 1]$$

The positive projection of  $\epsilon_{ij}$ ,  $\epsilon_{ij}^+$ , is given by

$$\epsilon_{ij}^+ = \sum_{\alpha=1}^3 \langle \epsilon^{(\alpha)} \rangle p_i^{(\alpha)} p_j^{(\alpha)} \quad (A-7)$$

where

$$\langle x \rangle = (x + |x|)/2 = \text{McAuley bracket}$$

The equivalent tensile strain is then defined as the norm of the positive strain tensor

$$r = (\epsilon_{ij}^+ \epsilon_{ij}^+)^{\frac{1}{2}} \quad (A-8)$$

The state of damage in the material is characterized by a damage criterion  $G = G(r, r) \leq 0$ , formulated in strain space, with the following form (Simo and Ju '87):

$$G = r_t - r_t \leq 0 \quad (A-9)$$

where

$r_t$  = equivalent tensile strain at current time  $t$

$r_t$  = damage threshold at current time  $t$

If  $r_0$  denotes the initial damage threshold before any loading is applied, a property of the material, then  $r_t \geq r_0$ . This damage

criterion,  $G$ , states that damage in the material is initiated when the norm of the tensile strain tensor,  $r$ , exceeds the initial damage threshold  $r_0$ . For the isotropic case, the evolution of the damage variable  $d$  is defined by the following rate-independent equations

$$\dot{d}_t = \dot{\mu} H \quad (A-10)$$

$$\dot{r}_t = \dot{\mu} \quad (A-11)$$

where

$\dot{\mu}$  = damage consistency parameter

$H = H(r_t, d_t, \sigma_{ij}^t)$  = damage accumulation function

$\dot{\mu}$  defines the damage loading/unloading conditions according to the Kuhn-Tucker relations

$$\dot{\mu} \geq 0, \quad G \leq 0, \quad \dot{\mu} G = 0 \quad (A-12)$$

If further damage is taking place, the value of  $\dot{\mu}$  is determined by the damage consistency condition

$$G - \dot{G} = 0 \quad \Rightarrow \quad \dot{\mu} = \dot{r}_t \quad (A-13)$$

The current damage threshold,  $r_t$ , is given by

$$r_t = \max\{r_0, \max r_s, \forall s \in (-\infty, t)\} \quad (A-14)$$

Lastly, it is assumed (Simo and Ju '87) that the function  $H(r_t, d, \sigma_{ij}^t)$  given in the evolution equation for  $d$  is independent of  $d$  and may be written as

$$H(r_t, \sigma_{ij}^t) = \frac{\partial Q}{\partial r_t} \quad (A-15)$$

where

$Q = Q(r_t, \sigma_{ij}^t)$  = damage accumulation function, monotonic  
with respect to  $r$

The following functional form for  $Q$  will be used:

$$Q = \begin{cases} d_u(1 - \exp[-A(r - r_o)^B]) & r_o \leq r \leq Cr_o \\ Q^* + (1 - Q^*) \frac{r - Cr_o}{(D - C)r_o} & Cr_o < r \leq Dr_o \\ 1 & Dr_o < r \end{cases} \quad (A-16)$$

and

$$A = A(\sigma_{ij}^t) = A_{t0} - (A_{t0} - A_{c0})\{1 - \exp[-\eta(P - P_t)]\} \quad (A-17)$$

where

$d_u, B, C, D, \eta$  = material parameters

$A = A(\sigma_{ij}^t)$  = material response function determining rate  
at which damage accumulates

$r_o$  = damage threshold

$Q^*$  =  $Q(Cr_o, \sigma_{ij}^t)$

$A_{t0}, A_{c0}$  = rate at which damage accumulates in  
hydrostatic tension and compression,  
respectively

$P$  =  $-\sigma_{kk}^t/3$  = hydrostatic pressure

$P_t$  = maximum tensile hydrostatic pressure on the  
Prager-Drucker failure surface (described  
later)



The functional form of  $Q$  for the region of damage  $r_0 \leq r \leq Cr_0$  was suggested by Frantziskonis and Desai '87. Note that Frantziskonis and Desai '87 do not include the pressure dependency of the damage accumulation rate and, more importantly, they use the trajectory of the plastic deviatoric strain tensor, rather than the equivalent tensile strain, to parameterize the damage accumulation function.

## A.2 Plasticity Model

The plasticity model, which determines the response of the topical material, is based on a strain-hardening Drucker-Prager failure surface combined with a strain-hardening cap (Schreyer and Bean '87). As opposed to the typical Drucker-Prager Cap model, this yield surface is smooth and continuous in stress space and it is described as follows:

$$f^{PD} = J_2 - \frac{\hat{H}^2}{3} = 0 \quad (A-18)$$

and

$$\hat{H} = HH_c \quad (A-19)$$

where

$f^{PD} = f^{PD}(\sigma_{ij}^t, \epsilon_{ij}^p)$  = the Prager-Drucker cap model surface

$J_2 = s_{ij}^t s_{ij}^t / 2$  = second invariant of the deviatoric

topical stress tensor ( $s_{ij}^t = \sigma_{ij}^t - \delta_{ij} \sigma_{kk}^t / 3$ )

$H = H(\sigma_{ij}^t, \epsilon_{ij}^p)$  = hardening function

$H_c = H_c(\sigma_{ij}^t, \epsilon_{ij}^p)$  = cap function

The hardening function is given by

$$H = \begin{cases} H_L \left( h_0 + (1 - h_0) \sin \left[ - \left( \frac{\pi \epsilon^p}{2 \epsilon_L^p} \right)^n \right] \right) & \text{for } 0 \leq \epsilon^p \leq \epsilon_L^p \\ H_L & \text{for } \epsilon^p > \epsilon_L^p \end{cases} \quad (A-20)$$

and

$$H_L = (1 - e^{-\kappa})(\alpha f'_c + \beta P(1 - e^{-\gamma})) \quad (A-21)$$

$$\kappa = \left(1 - \frac{P}{P_t}\right)^m \quad (A-22)$$

$$\gamma = \frac{S_m}{\beta(P - P_t)} \quad (A-23)$$

where

- $h_0$  = constant defining the onset of plastic behavior
- $\epsilon^P$  = plastic strain invariant defined below
- $\epsilon_L^P$  = strain at which all hardening has been exhausted
- $P = -\sigma_{kk}^t/3$  = mean pressure
- $P_t$  = limiting hydrostatic tension stress
- $S_m$  = maximum value of  $J_2$  for large  $P$
- $\alpha$  = constant related to the cohesive strength
- $f'_c$  = maximum uniaxial strength
- $\beta$  = constant related to the frictional strength
- $m$  = constant defining the shape of the surface
- $n$  = rate at which hardening accumulates

The cap function is described by

$$H_c = \begin{cases} \left| 1 - \frac{(P - sP_0)^2}{(P_c - sP_0)^2} \right|^q \text{sign}(P_c - P) & \text{for } P > sP_0 \\ 1 & \text{for } P \leq sP_0 \end{cases} \quad (A-24)$$

and

$$s = c_1 + (c_{cap} - c_1) \frac{\epsilon_1^p}{\epsilon_L^p} \quad (A-25)$$

$$P_o = P_{co} \exp(c_3 \frac{\epsilon_2^p}{\epsilon_L^p}) \quad (A-26)$$

where

- q = constant governing the growth of the cap
- $c_1, c_{cap}$  = constants determining cap shape during strain hardening
- $P_{co}$  = hydrostatic stress at initial plastic flow
- $c_3$  = constant determining the shape of the volumetric-stress/volumetric-strain curve
- $\epsilon_1^p, \epsilon_2^p$  = plastic strain invariants defined below

The three invariants given above are calculated by integrating the following differentials over the course of the loading history:

$$\begin{aligned} d\epsilon_V^p &= d\epsilon_{11}^p \\ d\epsilon_{1j}^{pd} &= d\epsilon_{1j}^p - d\epsilon_V^p \delta_{1j}/3 \\ d\epsilon^p &= (d\epsilon_{1j}^{pd} d\epsilon_{1j}^{pd})^{1/2} \\ d\epsilon_1^p &= \frac{P_o}{P+P_o} d\epsilon^p \\ d\epsilon_2^p &= \langle -d\epsilon_V^p - c_2 d\epsilon^p \rangle \end{aligned}$$

where

$P_0$  = constant controlling the ductility

$c_2$  = constant determining the amount of shear  
enhanced compaction

$\langle x \rangle = (x + |x|)/2$  = McAuley's bracket

Figure 2.1 shows the Prager-Drucker yield surface in the  $J_2$ ,  $P$  space, for the material constants presented in Table 3.

Over the major portion of the yield surface, the plastic strain tensor evolves through use of an associated flow rule; in the tensile and low compressive hydrostatic stress regions, a nonassociated flow rule is used, as discussed in the next section. The associated flow rule is expressed as

$$d\epsilon_{ij}^p = d\lambda \frac{\partial f^{PD}}{\partial \sigma_{ij}^t} \quad (A-27)$$

and

$$d\lambda \geq 0 \quad \text{if } f^{PD} = 0 \text{ and } \dot{f}^{PD} = 0 \quad (A-28)$$

or

$$d\lambda = 0 \quad \text{if } f^{PD} = 0 \text{ and } \dot{f}^{PD} < 0 \quad \text{or} \quad f^{PD} < 0 \quad (A-29)$$

where

$d\lambda$  = positive factor of proportionality

$f^{PD}$  = Prager-Drucker cap model function

The factor of proportionality may be found using the "consistency" condition during loading, which is

$$df^{PD} = 0 \quad (A-30)$$

where

$df^{PD}$  = the total derivative of the yield function

As Schreyer and Bean '87 point out, this model has the following advantages: (1) strain hardening is predicted for all paths, (2) more ductility is predicted for paths associated with large mean pressures, (3) the yield surface intersects the hydrostatic axis at right angles for both positive and negative mean pressures so no special algorithm is needed at these intersection points, and (4) the flow surface is continuous and has a continuous derivative everywhere so a corner algorithm is not required. And, although the number of required material constants is large, the values may be deduced directly from conventional uniaxial and triaxial test results; also, Schreyer and Bean present representative values for low and high strength concretes. One shortcoming of this model is the circular cross section on the  $\pi$  plane; experimentally, a rounded triangular shape is seen at the lower hydrostatic pressures. However, since an accurate response at low hydrostatic pressures is not critical, this deficiency is tolerable.

### A.3 Concrete Modelling in Tension (Nonassociated Flow Rule)

The main shortcoming of this continuum damage/plasticity model lies in its inability to accurately predict strains when the hydrostatic pressure is either tensile or small (less than approximately  $0.1 f'_c$ ) due to the use of an associated flow rule; this is a common characteristic of almost all plasticity-based concrete models, which are generally developed using test results of stress paths that stay in the compressive hydrostatic pressure region of the yield surface. Thus, the predictions of these models are usually quite poor for stress paths in the region of low compressive or tensile hydrostatic pressures.

In order to overcome these shortcomings, the concrete model proposed herein uses a nonassociated flow rule in regions of tensile or low compressive (less than  $0.1 f'_c$ ) hydrostatic pressure; the use of a nonassociated flow rule reduces the dilational strain

predictions, while at the same time allowing reasonable predictions of strength for stress states of tension and shear. The nonassociated flow rule is based on the assumptions that the yield surface and the plastic potential are distinct and that the plastic strains may be calculated as

$$d\epsilon_{ij}^p = d\lambda \frac{1}{M} \frac{\partial g}{\partial \sigma_{ij}^t} \quad (A-31)$$

and

$$M = \left\{ \frac{\partial g}{\partial \sigma_{ij}^t} \frac{\partial g}{\partial \sigma_{ij}^t} \right\}^{1/2} \quad (A-32)$$

where

$$g = g(\sigma_{ij}^t, \epsilon_{ij}^p) = \text{plastic potential}$$

For this model, the plastic potential is chosen as another modified Drucker-Prager surface, given as

$$g = \begin{cases} J_2 - (\alpha F_c + \theta P)^2 \left[ 1 - \Omega \left( 1 - \frac{P}{\phi P_{co}} \right) \omega \right]^2 = 0 & \text{for } P < \phi P_{co} \\ f^{PD} = 0 & \text{for } P \geq \phi P_{co} \end{cases} \quad (A-33)$$

where

$\theta$  = initial slope of surface at  $P = \phi P_{co}$

$\phi$  = fraction of the hydrostatic compression stress

below which the nonassociated flow rule becomes effective

$\Omega, \omega$  = material constants

The other terms in Equation A-33 have been defined previously.

The potential for spontaneous energy generation is one criticism

leveled against the use of nonassociated flow rules. The following modification to the model was made to ensure that energy generation does not occur: during loading from the yield surface and for any predicted elastic state that falls into the "wedge," the associated flow rule will be used. Assuming that the elastic predictor stress has violated the yield surface, this condition may be summarized as

$$d\epsilon_{ij}^p = d\lambda \frac{1}{M} \frac{\partial T}{\partial \sigma_{ij}^t} \quad (A-34)$$

and

$$M = \left\{ \frac{\partial T}{\partial \sigma_{ij}^t} \frac{\partial T}{\partial \sigma_{ij}^t} \right\}^{1/2} \quad (A-35)$$

where

$$T = \begin{cases} g & \text{if } P \leq \phi P_{co} \text{ and } n_{ij}^E n_{ij}^t > 0 \\ f^{PD} & \text{if } P > \phi P_{co} \text{ or } P \leq \phi P_{co} \text{ and } n_{ij}^E n_{ij}^t < 0 \end{cases} \quad (A-36)$$

As Figure A-1 shows, the associated flow rule is invoked when the increment in predicted elastic stress simultaneously decreases  $P$  and  $J_2^{1/2}$  while violating the yield surface. The use of an associated flow rule for this situation results in a dilational increment in volumetric plastic strain, which is reasonable since the stress state is moving further into the tensile hydrostatic region.

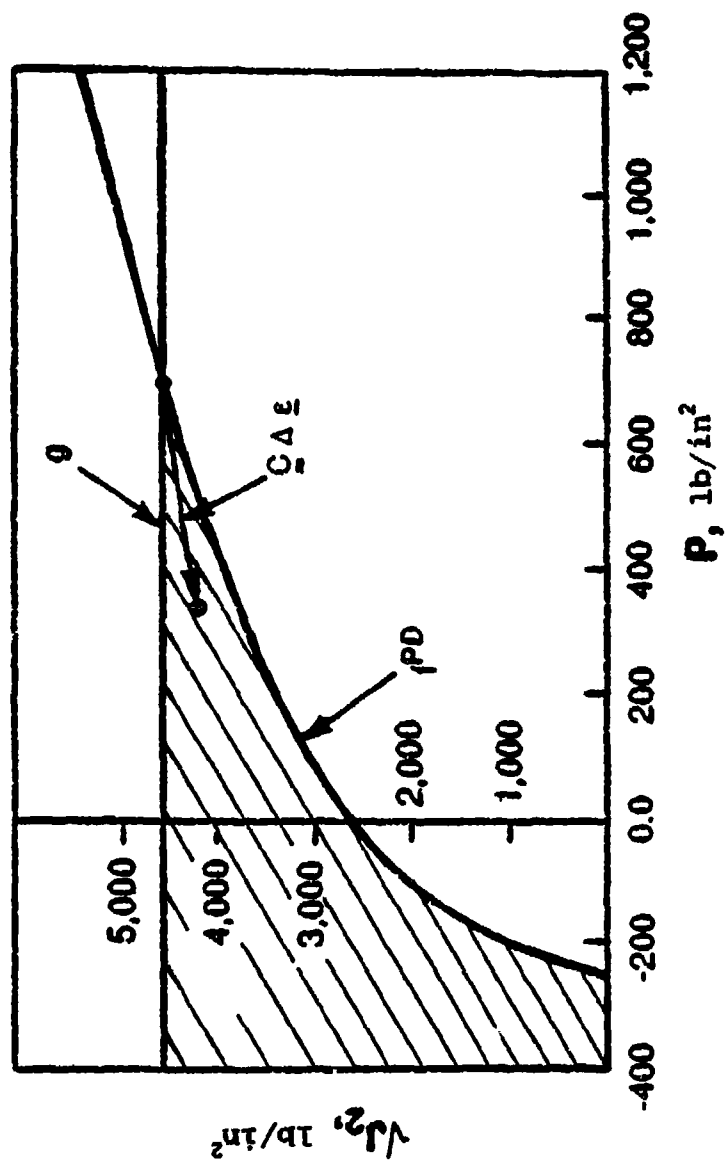


Figure A-1 Elastic predictor stress state inside the "wedge".  
(Stevens and Krauthammer '88)